RadioNuclide (RN) Package
Reference Manual

The RadioNuclide (RN) package models the behavior of fission product aerosols and vapors and other trace species, including release from fuel and debris, aerosol dynamics with vapor condensation and revaporization, deposition on structure surfaces, transport through flow paths, and removal by engineered safety features. The package also allows for simplified chemistry controlled by the user.

Boundary conditions for the various models are obtained from other MELCOR packages: fluid conditions are obtained from the Control Volume Hydrodynamics (CVH) package, fuel and debris temperatures are obtained from the Core (COR) and Cavity (CAV) packages, and structure surface temperatures are obtained from the Heat Structures (HS) package. The COR and CAV packages also provide information regarding bulk debris relocation, allowing the RN package to perform relocation of unreleased fission products in parallel. Likewise, advection of radionuclides between control volumes is done using CVH flows, and wash-off of radionuclides deposited on heat structures is determined from drainage of water films calculated by the HS package. The RN package determines decay heat power for current radionuclide inventories from the Decay Heat (DCH) package when requested by each of these packages.

This document describes in detail the various models incorporated in the RN package in MELCOR. Details on input to the RN package can be found in the RN Users' Guide.

Contents

List of Figures

List of Tables

1. Introduction

Since MELCOR is intended as a tool for probabilistic risk assessment (PRA), it must account for the release and transport of radioactive fission products that upon release to the environment become the *source term*, which is one major product of the overall accident calculation in MELCOR. Source terms are then used to calculate consequences as the end product of the PRA. Such processes as thermal-hydraulics and core degradation are calculated in MELCOR to support calculation of the source term.

The RadioNuclide (RN) package in MELCOR calculates the release and transport behavior of fission product vapors and aerosols. Most of the models and concepts included in the RN package are discussed in detail in the fission product phenomena assessment report prepared at the beginning of MELCOR development [1]. Only a brief overview of the concepts and models is included in this section; Section 2 contains detailed descriptions of the models used in the RN package.

As a source term code, MELCOR is especially concerned with those fission products (and daughters) released during an accident, which are particularly important for determining consequences and risks. However, to model the transport of these important fission products properly, it is necessary to model the transport of other mass that affects the transport of radionuclide mass. For example, radiocesium will exist as CsOH, so the mass of the hydroxide must be modeled, and if the CsOH aerosol interacts with concrete or water aerosols, the transport and thus the mass of the latter must also be modeled. Accordingly, MELCOR treats the molecular forms of all important fission products and also models the transport of all nonradioactive masses (water and concrete or other structural aerosols) with which fission products may interact. Therefore, in this manual the term *radionuclide* is generally taken to mean all masses, both radioactive and nonradioactive masses, that affect fission product transport.

Rather than tracking all fission product isotopes, the masses of all the isotopes of an element are modeled as a sum; that is, the total element mass, not its individual isotopes, is modeled. Furthermore, elements are combined into material *classes*, groups of elements with similar chemical behavior. Fifteen material classes are typically used, thirteen containing fission products, plus water, and concrete oxides. Combination of classes to form new classes upon release, such as Cs + I to CsI, is permitted. The decay heat power per unit initial mass for each class is determined by the Decay Heat (DCH) package based on the class compositions.

Initial radionuclide inventories for each class are generally based on whole-core inventories calculated using the ORIGEN code [2, 3], and distributions may be specified for the fuel in the core, the fuel-cladding gap, any initial cavity debris, and the atmosphere and pool of any control volume. Until released as vapors or aerosols, fission products within the fuel are transported with the fuel as it relocates from core cell to core cell or is ejected to the reactor cavity. The decay heat power from radionuclides contained in a control volume,

both those that are gas borne and those deposited on heat structure surfaces or contained in water pools, can be apportioned among the atmosphere, surfaces, and pools according to specifications supplied by the user, thus allowing the different penetrating powers of α, β, and γ radiation to be modeled appropriately. Radiation is allocated to various surfaces in the control volume on the basis of area.

Release of radionuclides can occur from the fuel-cladding gap by exceeding a failure temperature criterion or losing intact geometry, from material in the core using the various CORSOR empirical release correlations [4,5] based on fuel temperatures, and during core-concrete interactions in the reactor cavity using the VANESA [6] release model. After release to a control volume, masses may exist as aerosols and/or vapors, depending on the vapor pressure of the radionuclide class and the volume temperature.

Aerosol dynamic processes and the condensation and evaporation of fission product vapors after release from fuel are considered within each MELCOR control volume. The aerosol dynamics models are based on MAEROS [7], a multisection, multicomponent aerosol dynamics code, but without calculation of condensation. Aerosols can deposit directly on surfaces such as heat structures and water pools, or can agglomerate and eventually fall out once they exceed the largest size specified by the user for the aerosol size distribution. Aerosols deposited on surfaces cannot currently be resuspended.

The condensation and evaporation of radionuclide vapors at the aerosol surfaces, pool surfaces, and heat structure surfaces are decoupled from MAEROS. These processes are evaluated by the rate equations from the TRAP-MELT2 code [8], which are based on the surface area, mass transfer coefficients, and the difference between the present surface concentration and the saturation surface concentration.

The steam condensation/evaporation is also decoupled from the MAEROS solution for agglomeration and deposition in order to reduce the stiffness of the differential equation set. The amount of steam condensed or aerosol water evaporated is calculated by thermodynamics routines called by the Control Volume Hydrodynamics (CVH) package.

Water droplets are transported as *fog* by the CVH package and treated as water-class aerosol by the RN package. (Water in pools or condensed on surfaces is not treated by the RN package.) Other radionuclide aerosols and vapors are transported between control volumes by bulk fluid flow of the atmosphere and the pool, assuming zero slip between the radionuclides and the host medium (steam, water, etc.). In addition, in the absence of bulk flow, aerosols may move by Brownian motion or by gravitational settling through openings between control volumes.

The difference between CVH fog and RN water-class masses in a control volume at the end of the CVH advancement represents net condensation of water onto or evaporation from the aerosols in that volume. The net change in water mass is imposed on the water-class inventory in the RN package, which then uses the Mason equation [9] to distribute the mass change over the aerosol size distribution in the control volume.

Models are available for the removal of radionuclides by pool scrubbing, filter trapping, and containment spray scrubbing. The pool scrubbing model is based on the SPARC code [10], and treats both spherical and elliptical bubbles. The model includes condensation at the pool entrance, Brownian diffusion, gravitational setting, inertial impaction, and evaporative forces for the rising bubble. Currently, only aerosols are removed by pool scrubbing in the RN package. Water condensation and evaporation are calculated within the CVH package using its own implementation of SPARC modeling (see the CVH Reference Manual). The filter model can remove aerosols and fission product vapors with a specified maximum mass loading. The containment spray model is based on the model in HECTR 1.5 [11] and removes both vapors and aerosols from the atmosphere.

Chemistry effects can be simulated in MELCOR through the *class reaction* and *class transfer* models, which are controlled entirely by user-specified parameters. The class reaction process uses a first-order reaction equation to simulate reversible chemical reactions. The class transfer process, which can instantly change the material class or location of a radionuclide mass, can be used to simulate fast, irreversible chemical reactions. With these two processes, phenomena including adsorption, chemisorption and other important chemical reactions can be simulated. Only fission product vapors are currently treated with these mechanisms. In addition, chemisorption of radionuclides on surfaces can be simulated with the chemisorption model.

Most intravolume processes involving radionuclides are calculated first in the RN package, including fission product release, aerosol agglomeration and deposition, fission product condensation and evaporation, distribution of decay heat, and chemical interactions. The effects of these processes are included in the hydrodynamic transport and thermodynamic calculations performed in the CVH package, executed subsequently.

The transport of fission products is inferred from the transport of hydrodynamic materials, but the CVH package may subcycle during a MELCOR timestep. Since radionuclide advection must also abide by the Courant limit, the transport calculations are performed by RN package utility routines called from within the CVH subcycle loop. Part of this transport process includes removal of fission product aerosols and vapors, for example, by filters.

After CVH has advanced through the full MELCOR system timestep, the additional intervolume process of pool scrubbing is calculated. While water condensation/ evaporation is an intravolume process, it also is calculated after the CVH package thermodynamics calculations have been performed so that the mass of water condensed in a control volume during the timestep is known.

2. Detailed Models

2.1 General Framework

The RN package operates on the principle of material classes, which are groups of elements that have similar chemical properties. The number of classes is specified on the RN1001 input record, with a default of 15 classes. Classes are generally referred to by their class name or representative element. Combination of masses in these classes upon release to form compounds in other classes, such as Cs + I to CsI, is permitted subject to stoichiometric constraints (e.g., excess Cs is retained in the Cs class). For the RN package, the classes must be in numerical order without any gaps. A maximum of 30 classes can presently be employed.

Each class is described by the following set of properties for use in various models:

1	release rates in core	(see Section 2.3)
2	molecular weights	(see Section 2.3)
3	vapor pressure	(see Section 2.5)
4	vapor diffusivity	(see Section 2.5)
5	decay heat power	(see DCH Package Users' Guide)

Two molecular weight values are used for each class, the *elemental* molecular weight (i.e., the element's atomic weight) and the *compound* molecular weight, which are specified in sensitivity coefficient array 7120 (see Appendix A). The elemental molecular weight is used to determine the number of moles of *radioactive* material that are released and available for combination with other RN classes. The compound molecular weight is used to increase the released mass due to combination upon release with *nonradioactive* materials if that is expected to occur (e.g., Cs with H_2O to form CsOH). *Total* class masses after release therefore include both radioactive and nonradioactive masses. In addition, nonradioactive masses from bulk materials in the Core or Cavity package (e.g., cladding Zircaloy, structural steel, control poison, or concrete) may be released as vapors or aerosols and added to the total class masses but not to the radioactive masses of the class to which the materials are assigned.

Some models in the RN package use groupings of elements different from the groupings defined in Table 2.1. Transfers of masses between various models must therefore use *mapping* strategies.

For the transfer of bulk, nonradioactive, Core package structural masses released by the CORSOR models to the RN classes (see Section 2.3), the default mapping defined in Table 2.2 is employed. This mapping may be changed with input records RNCRCLXX, but this practice is discouraged. Note from Table 2.2 that B_4C control poison in BWRs is

mapped totally into the boron class, whereas Ag-In-Cd control poison in PWRs is split between the Cd and Sn classes using the percentages shown.

The VANESA model for radionuclide releases from debris in the cavity (see Section 2.3) recognizes 25 different species groups (for most, several different compounds of one element), and mapping must be used both to transfer RN class masses in the debris (as initially specified and as transferred from the COR and/or Fuel Dispersal Interactions [FDI] packages) to the VANESA groups and also to transfer them back again into the RN classes as VANESA calculates releases. The default mappings for to-VANESA and from-VANESA transfers are defined in Table 2.3 and Table 2.4, respectively. These mappings may be changed with input records RNCLVNXX and RNVNCLXX.

Table 2.1 RN Class Compositions

Class Name	Representative	Member Elements
1. Noble Gases	Xe	He, Ne, Ar, Kr, Xe, Rn, H, N
2. Alkali Metals	Cs	Li, Na, K, Rb, Cs, Fr, Cu
3. Alkaline Earths	Ba	Be, Mg, Ca, Sr, Ba, Ra, Es, Fm
4. Halogens	I	F, Cl, Br, I, At
5. Chalcogens	Te	O, S, Se, Te, Po
6. Platinoids	Ru	Ru, Rh, Pd, Re, Os, Ir, Pt, Au, Ni
7. Early Transition Elements	Mo	V, Cr, Fe, Co, Mn, Nb, Mo, Tc, Ta, W
8. Tetravalent	Ce	Ti, Zr, Hf, Ce, Th, Pa, Np, Pu, C
9. Trivalents	La	Al, Sc, Y, La, Ac, Pr, Nd, Pm, Sm, Eu, Gd, Tb, Dy, Ho, Er, Tm, Yb, Lu, Am, Cm, Bk, Cf
10. Uranium	U	U
11. More Volatile Main Group	Cd	Cd, Hg, Zn, As, Sb, Pb, Tl, Bi
12. Less Volatile Main Group	Sn	Ga, Ge, In, Sn, Ag
13. Boron	B	B, Si, P
14. Water	H_2O	H_2O
15. Concrete	- -	- -

In addition to the 25 VANESA groups, two additional groups can be transferred to VANESA but are changed before VANESA uses them. They are I (VANESA group 26), which is combined automatically with Cs, and Xe (VANESA group 27), which VANESA releases immediately. VANESA assumes that Cs is in excess so that no elemental I remains as debris is added to the cavity. Also, aerosol products from concrete ablation (VANESA groups 12 through 16) are automatically transferred to the RN concrete class, and bulk gases (VANESA group 1) are transferred directly to the CVH package. The user should not specify mapping values for any of these VANESA groups.

Table 2.2 COR Material to RN Class Mapping

COR Material		RN Class (Rep. Element)		
1	UO2	10	U	
2	Zr	8	Ce	
3	ZrO2	8	Ce	
4	Steel	7	Mo	
5	Steel Oxide	7	Mo	
6	Control Rod Poison	13	B	100% BWR / 0% PWR
		11	Cd	0% BWR / 5% PWR
		12	Sn	0% BWR / 95% PWR

Table 2.3 RN Class to VANESA Species Mapping

RN Class		VANESA Species	
1	Xe	27	Xe (released instantaneously)
2	Cs	19	Cs
3	Ba	20	Ba
4	I	26	I (immediately forms CsI)
5	Te	9	Te
6	Ru	6	Ru
7	Mo	5	Mo
8	Ce	23	Ce
9	La	22	La
10	U	17	U
11	Cd	8	Sb
12	Sn	7	Sn
13	B	0	(RN class not present in fuel)
14	H2O	0	(RN class not present in fuel)
15	Concrete	0	(RN class not present in fuel)

Warning: If a class is redefined from the default values, or if a new class is added, all of the properties, including mappings, should be evaluated and possibly redefined through the RN sensitivity coefficients. Default values for these properties are defined based on the elements in each class. Whether default values are appropriate when classes are modified must be determined by the user. Note that the DCH package might also have to be redefined in a consistent manner.

Table 2.4 VANESA Species to RN Class Mapping

VANESA Species		RN Class	
1	bulk gases (from CORCON)	(released by CAV pkg to CVH)	
2	Fe	7	Mo

VANESA Species		RN Class	
3	Cr	7	Mo
4	Ni	6	Ru
5	Mo	7	Mo
6	Ru	6	Ru
7	Sn	12	Sn
8	Sb	11	Cd
9	Te	5	Te
10	Ag	12	Sn
11	Mn	7	Mo
12	Ca (from concrete ablation)	15	Concrete
13	Al (from concrete ablation)	15	Concrete
14	Na (from concrete ablation)	15	Concrete
15	K (from concrete ablation)	15	Concrete
16	Si (from concrete ablation)	15	Concrete
17	U	10	U
18	Zr	8	Ce
19	Cs	2	Cs
20	Ba	3	Ba
21	Sr	3	Ba
22	La	9	La
23	Ce	8	Ce
24	Nb	7	Mo
25	CsI	2	Cs and 4 I
26	I	(combined with Cs by VANESA)	
27	Xe	(released by VANESA)	

2.2 Initial Radionuclide Inventories

Initial inventories and distributions of radionuclides must be specified for the core, for the cavity, and for control volume pools and atmospheres. (Inventories for some locations may be zero initially.) Masses can be distributed among core cells according to radial and axial decay heat power profiles in the core. In addition, a fraction of the radionuclides in a core cell can be designated as residing in the fuel-cladding gap.

Total radioactive class masses are normally determined by the DCH package from the operating power of the reactor and the mass of each element in the class per unit of operating power (see the DCH Package Reference Manual and Users' Guide). RN package input generally defines only the initial distribution of these masses in the core and cavity through reference values and multipliers specified on the RNFPNijjXX input records. However, options are provided to use these records to specify the class masses directly. These options are useful for analysis of experiments.

The total mass inventories for all RN classes in a particular core cell or in a cavity are normally calculated from user-specified multipliers r_1 and r_2 as

$$M_x = r_1 \ r_2 M_{x,ref} \tag{2.1}$$

where $M_{x,ref}$ is a reference value for class x that may be taken as the total class mass defined by the DCH package or as the inventory in some other core cell or cavity location, depending on the option chosen. For core cells, r_1 and r_2 typically represent axial and radial multipliers to specify the decay heat power profile in the core, while for cavities they are arbitrary. If the DCH package option is chosen, however, the mass of the uranium class (default class 10) is calculated by decrementing the total uranium mass in the Core package, $M_{U,COR}$ by the sum of the masses in the remaining classes, i.e.,

$$M_{U,RN} = M_{U,COR} - \sum_{i \neq U} M_i \ \text{(Uranium class only)} \tag{2.2}$$

Optionally, as specified on the RNFPNijjXX records, the mass for a specified class in a particular core cell or cavity location may be input directly as

$$M_x = r_1 \ r_2 \tag{2.3}$$

where r_1 is typically chosen as the total mass, with r_2 defined as the fraction of that mass in the core cell or cavity location. The various options are additive and may be combined as convenient. Note that masses can also be reduced if a negative multiplier is used.

The masses given by Equations (2.1) through (2.3) determine the total radioactive mass of radionuclides in a particular core cell, including the fuel-cladding gap. The fraction of radioactive mass that resides in the gap is determined by the parameter r_1 input on the RNGAPijjXX input record series (different from r_1 input on RNFPNijjXX). Depending on the input option chosen, the gap fraction F_x may be specified directly for each class as

$$F_x = r_1 \tag{2.4}$$

or it may be calculated as a proportion of the gap fraction $F_{x,ref}$ at some other location,

$$F_x = r_1 F_{x,ref} \tag{2.5}$$

For a core cell, the radioactive masses residing in the fuel and gap, $M_{x,fuel}$ and $M_{x,gap,R}$, respectively, are thus given by

$$M_{x,fuel} = (1 - F_x) M_x \tag{2.6}$$

$$M_{x,gap,R} = F_x M_x \tag{2.7}$$

The total masses residing in the gap must be calculated to account for the addition of nonradioactive material from presumed chemical reactions following release from the fuel. (See the discussion of total vs. radioactive masses in Section 2.1.) If the gap fraction has been specified directly from Equation (2.4), the total gap mass $M_{x,gap,T}$ is given by

$$M_{x,gap,T} = r_2 M_{x,gap,R} \tag{2.8}$$

where r_2 is the ratio of total mass to radioactive mass (usually the ratio of compound to elemental molecular weights, matching the values in sensitivity coefficient array 7120; see Appendix A), whereas if the gap fraction has been specified as a proportion r_1 of the gap fraction at some other location with Equation (2.6), the total gap mass is that same fraction of the total gap mass $M_{x,gap,T,ref}$ at the other location,

$$M_{x,gap,T} = r_1 M_{x,gap,T,ref} \tag{2.9}$$

in which case no value is needed for r_2 since it is already reflected in $M_{x,gap,T,ref}$ (any value input for r_2 is ignored).

The distribution of radionuclide masses between fuel and gap in a core cell will change with time due to release and the relocation of fuel. When fuel is relocated by the COR package, the radionuclides still residing in the fuel are transported with it. Relocation of the gap radionuclide mass is not necessary since cladding failure and gap release will always occur before fuel relocates (see Section 2.3.2).

In addition to the radioactive masses initially residing in the fuel or fuel-cladding gap, nonradioactive bulk masses in other packages, such as Zircaloy fuel rod cladding, may be released as vapors or aerosols by the RN package release models. Initial inventories for these bulk masses are already available in the appropriate package database and no additional input is needed for the RN package. Release of core or cavity masses by the RN package does not change the mass values in the other packages. For example, the mass of Zircaloy in the COR package is not modified by release of Zircaloy aerosols in the RN package. The errors introduced by this assumption should be very small since the fractions of core and cavity materials that are released as vapors and aerosols are very small. Nevertheless, the user should be aware that mass is not explicitly conserved in this modeling.

The user may also directly specify the initial radionuclide aerosol and/or vapor inventory for any class in any control volume by using the RNAGXXX, RNALXXX, RNVGXXX, and RNVLXXX input record series.

2.3 Release of Radionuclides

Release of radionuclides can occur from the core fuel (with nonradioactive releases from other core structures), from the fuel-cladding gap, and from material in the cavity. At present, no material can be released from the reactions treated in the FDI package. The release models used in each of these areas are discussed below.

2.3.1 Core Release

Radioactive and nonradioactive material may be released from the core. As described in Sections 2.1 and 2.2, the radionuclides residing in the COR package fuel are assumed to be in elemental form and therefore to have only radioactive mass (no associated molecular mass). Upon release from fuel, the total class masses are converted to compound form with a corresponding increase in mass from the added nonradioactive material (e.g., the hydroxide mass in CsOH). By default the release models are used to calculate the release of radioactive radionuclides from core fuel material (i.e. UO_2) only, which exists in the intact fuel component, in refrozen fuel material on other components and in particulate debris.

In order to apply the release models to core materials other than fuel, such as the fuel rod cladding, the user must change the default values of the core material release multipliers contained in sensitivity coefficient array 7100. For these other core materials, the mapping scheme described in Section 2.1 (with defaults in Table 2.2) determines the apportioning of the core masses among the RN classes, and the entire masses are considered nonradioactive. Hence, by changing the release multiplier for Zr from 0.0 to 0.5, for example, the user will obtain half the fractional release rates calculated by the release correlations for Zr in the cladding, canisters and particulate debris. However, because the mass of structural Zr in the cladding component is enormous compared to the mass of Zr class fission products in the fuel component, the actual release rate (fractional rate times the available mass) from the cladding may be quite large. Because the core release models were developed for fuel releases, their use to calculate the release of structural materials in other components is questionable.

Before cladding failure has occurred, radionuclides released from the fuel in the core are transferred to the gap inventory and are released to the surrounding atmosphere of control volume only upon cladding failure. (However, they are reported by RN output as “released.”) After cladding failure, radionuclides released from the core are transferred to the atmosphere of control volumes as specified in the Core package input, which defines channel and bypass control volumes for each core cell. These volumes are used by the RN package as follows:

Core Component	RN Release Volume
Intact:	
Fuel	Channel
Cladding	Channel
Control Rods	Bypass
Canisters	Split Equally Between Channel and Bypass
Conglomerate Debris:	
Refrozen on Cladding	Channel
Refrozen on Control Rods	Bypass
Refrozen on Canisters	Channel
Particulate Debris:	
All	Channel

In addition to releases in the core calculated by the RN package, the reaction modeled in the Core package of B_4C in control rods with steam can release B_2O_3 to the RN package. The class specified on the RN1001 input record for B_2O_3 receives this mass in the bypass control volume defined for that core cell.

Three options are currently available for the release of radionuclides from the core fuel component; the CORSOR, CORSOR-M [4] or CORSOR-Booth [5] model may be specified on Input Record RNFP000. The CORSOR-BOOTH model contains low and high burn-up options. In addition, the CORSOR and CORSOR-M release rates can be modified to be a function of the component surface-to-volume ratio as compared to a base value, derived from the experimental data on which CORSOR is based. The surface areas, volumes, and temperatures of the components used in the calculation are obtained from the COR package database. Because none of these radionuclide release models can be considered truly general or universally applicable, it is recommended that concerned users refer to the release model references [4, 5] for a more complete description of modeling assumptions and limitations.

The reduction in release rate of the tellurium class by the presence of unoxidized zirconium can be modeled if desired. The parameters affecting this option are controlled by sensitivity coefficient array 7105 for CORSOR and CORSOR-M and within array 7107 for CORSOR-Booth (see Appendix A). The release rate of Te is reduced by a release rate multiplier (with a default value of 1/40 = 0.025) until the mass of unoxidized intact metal cladding falls below a cut-off fraction (default value of 0.7) of the total mass of intact cladding (including the oxide mass). The default values are based on discussion in Reference [12].

Note that for each core component, the same correlation is used to calculate the release rate for a given class using the individual temperature of that component. That is, the calculation of release of radionuclides from fuel, cladding, canisters, control rods, and particulate debris differs only in the temperature used. Separate correlations for these

components are not employed since their form is not compatible with the MELCOR structure.

2.3.1.1 CORSOR

The original CORSOR model correlates the fractional release rate in exponential form,

$$\dot{f} = A \ \exp(B\,T) \qquad \text{for } T \geq T_i \tag{2.10}$$

where $\dot{f}$ is the release rate (fraction per minute), A and B are empirical coefficients based on experimental data, and T is the core cell component temperature in degrees Kelvin. Different values for A and B are specified for three separate temperature ranges. The lower temperature limit T_i for each temperature range and the A and B values for that range are defined for each class in sensitivity coefficient array 7101 (see Appendix A). If the cell temperature is below the lowest temperature limit specified, no release is calculated.

2.3.1.2 CORSOR-M

The CORSOR-M model correlates the same release data used for the CORSOR model using an Arrhenius form,

$$\dot{f} = k_o \exp(-Q/RT) \tag{2.11}$$

The values of k_o, Q, and T are in units of min^{-1}, kcal/mole, and K, respectively. The value of R is 1.987 x 10^{-3} in (kcal/mole)K^{-1}. The values of k_o and Q for each class are implemented in sensitivity coefficient array 7102 (see Appendix A).

2.3.1.3 CORSOR-Booth

The CORSOR-Booth model considers mass transport limitations to radionuclide releases and uses the Booth model for diffusion with empirical diffusion coefficients for cesium releases. Release fractions for other classes are calculated relative to that for cesium. The classical or effective diffusion coefficient for cesium in the fuel matrix is given by

$$D = D_o \exp(-Q/RT) \tag{2.12}$$

where R is the universal gas constant, T is the temperature, Q is the activation energy, and the pre-exponential factor D_0 is a function of the fuel burn-up. For fuel with burn-up in excess of 30,000 MWD/MTU the model uses a value for D_0 five times larger than the value it uses for fuels with lower burn-up. The two default values for D_0, the transition burn-up value, and the activation energy Q, based on experimental data for the release of fission gases from fuel test samples [13], are all given in sensitivity coefficient array 7106 (see Appendix A).

The cesium release fraction at time t is calculated from an approximate solution of Fick's law for fuel grains of spherical geometry [14],

$$f = 6\sqrt{\frac{D't}{\pi}} - 3\,D't \qquad \text{for } D't < 1/\pi^2 \tag{2.13}$$

$$f = 1 - \frac{6}{\pi^2}\exp(-\pi^2 D't) \qquad \text{for } D't > 1/\pi^2 \tag{2.14}$$

where

$D't$ = Dt/a^2 (dimensionless)

a = equivalent sphere radius for the fuel grain

The release rate of Cs during a time interval t to $t+\Delta t$ from the fuel grain is calculated as

$$\text{Release rate}_{Cs} = \frac{\left[f\left(\sum D'\Delta t\right)_{t+\Delta t} - f\left(\sum D'\Delta t\right)_t\right]V\rho}{F\Delta t} \tag{2.15}$$

where ρ is the molar density in the fuel, V is the fuel volume, F is the fraction of the Cs inventory remaining in the fuel grain, and the summations are done over the timesteps up to time $(t+\Delta t)$ and t, respectively.

The release rate formulation in the CORSOR-Booth model is also limited by mass transfer through the gas-phase. The gas-phase mass transport release rate from the fuel rod for species k, $\dot{m}_k$, is calculated using an analogy from heat transfer as

$$\frac{1}{\dot{m}_k} = \frac{D_{fuel}RT}{A_{fuel}Nu\,D_{k,gas}P_{k,eq}} \tag{2.16}$$

where

D_{fuel} = diameter of fuel pellet

A_{fuel} = fuel rod flow contact area

$D_{k,gas}$ = diffusivity of class k in the gas mixture

Nu = Nusselt number

$P_{k,eq}$ = equilibrium vapor pressure of class k at temperature T

The effective release rate for Cs given by Equation (2.16) is a combination of the rates given by diffusion and by gas-phase mass transport. Therefore, the contribution from diffusion only is taken as

$$DIFF_{Cs} = \left[\frac{1}{\text{Release rate}_{Cs}} - \frac{1}{\dot{m}_{Cs}} \right]^{-1} \tag{2.17}$$

The diffusion release rate for species other than cesium is given by multiplying the cesium release rate by an appropriate scaling factor S_k for each *RN* class k:

$$DIFF_k = DIFF_{Cs} S_k \tag{2.18}$$

Nominal values for S_k are given in sensitivity coefficient array 7103. For certain conditions of cladding oxidation and temperature, the scaling factors must be modified for some classes. When the oxide mass fraction exceeds a critical value F_{k1} and the temperature exceeds a critical value T_{k1}, the class scaling factor is given by

$$S_k = S_{k1} \exp(C_k T) \tag{2.19}$$

where T is not allowed to exceed a maximum value T_{max}. When the oxide mass fraction is below a minimum value F_{k2}, the class scaling factor is given by

$$S_k = S_{k2} \tag{2.20}$$

Values for F_{k1}, T_{k1}, S_{k1}, C_k, T_{max}, F_{k2}, and S_{k2} are all contained within sensitivity coefficient array 7107.

The combined mass transport and diffusion release rate $\dot{m}_{tot,k}$ for class k is then

$$\dot{m}_{tot,k} = \frac{1}{DIFF_k^{-1} + \dot{m}_k^{-1}} \tag{2.21}$$

The fractional release rate for the inventory of class *k* is calculated as

$$\dot{f}_k \text{ (fraction/s)} = \frac{\dot{m}_{tot,k}}{\rho V}\left[F - \frac{P_{k,bulk}}{P_{k,eq}}\right] \tag{2.22}$$

2.3.1.4 Surface-to-Volume Ratio

In the CORSOR and CORSOR-M release expressions, the effect on the release rate of the surface-to-volume ratio of the material from which release occurs is not treated. An option has been added to include the effect of this ratio as follows:

$$\dot{f} = \dot{f}_{CORSOR(-M)} \left(S/V\right)_{structure} / \left(S/V\right)_{base} \tag{2.23}$$

where the $(S/V)_{base}$ value has been derived from the original CORSOR data with a value of 422.5 m^{-1} that is stored in sensitivity coefficient array 7104 (see Appendix A). Values for $(S/V)_{structure}$ are calculated from component surfaces and volumes in the Core package (see Section 3 of the COR Package Reference Manual) and thus reflect the effects of core degradation on the surface-to-volume ratios of core components.

2.3.1.5 Class Combination at Release

The release model also can provide for the combination of different donor classes into a new class based on the elemental molecular weights. An example is the combination upon release of Cs and I atoms to form CsI molecules, which is modeled by moving stoichiometric amounts of Cs and I mass from the Cs and I classes into a new CsI class. The number of moles of each class that combine is defined by RNCLSNNXX input data. This combination occurs instantaneously upon release and is only limited by the availability of the released mass during that timestep. If there is an excess of any donor class during the timestep, that excess material stays in the original class. Chemical reactions that take place once release has been completed can be approximated using the models discussed in Section 2.8.

Note: The class combination model is only used for release from the fuel in the core and not for tabular or control function input sources defined using the RNASXXX or RNVSXXX records.

2.3.2 Fuel-Cladding Gap

Release of the radionuclides in the fuel-cladding gap (initial inventory plus masses from fuel release) occurs on cladding failure. Cladding failure is assumed to occur if either a temperature criterion is exceeded or if the intact cladding geometry has been lost due to candling or oxidation. It is assumed that the gaps in each radial ring can communicate axially between core cells, so when cladding in one axial level in a radial ring fails, the gap inventory for that entire ring is released. The cladding failure temperature for each core cell is specified on the RNGAPijj00 input record, with a default value of 1173 K (900° C) [15]. The control volume that receives the gap release is the channel control volume associated with the core cell where failure occurs, as defined by the CORijj01 input records (see the COR Package Users' Guide).

2.3.3 Cavity Release

For release of radionuclides from the cavity due to core-concrete interactions, the VANESA model [6] has been implemented in MELCOR and is coupled to CORCON [16] during every timestep. The control volume for cavity releases is specified in the Cavity package input. If a water pool is present, pool scrubbing calculations are performed to apportion the released mass between the pool and the atmosphere.

A number of changes have been made to the stand-alone VANESA program to allow it to function within the MELCOR framework. The major changes are:

(1) The concrete composition used in VANESA is converted from CORCON input using the following mapping, rather than input independently:

CORCON Mass Fraction	VANESA Mass Fraction
CaO + MgO	CaO
Al_2O_3	Al_2O_3
Na_2O	Na_2O
K_2O	K_2O
SiO_2	SiO_2
Fe_2O_3 (converted to FeO) + MnO	FeO
Ti_2O	Ti_2O
Cr_2O_3	Cr_2O_3
Rebar	Fe

(2) To ensure conservation of mass in the calculations, the rate of addition of concrete decomposition products (gases and condensed-phase oxides) is now derived from CORCON results by forward differences, rather than the central difference scheme originally in VANESA.

(3) Core debris masses (and associated radionuclides) may be added as a function of time throughout the transient.

(4) Both radioactive and total masses are tracked. The fraction of the radioactive mass released is assumed to be the same as the fraction of total mass released.

(5) The radioactive inventory is used (by default) to calculate the decay heat in the Cavity package. It is partitioned between the metallic and oxidic phases according to the assumed chemical state of the VANESA class. This partitioning accounts for the difference between elemental mass (e.g., Ba) and compound mass (e.g., BaO) and the mapping of released structural materials (e.g., Fe) into the nonradioactive portions of RN inventories.

(6) Pool scrubbing calculations are done by the RN package rather than the model in stand-alone VANESA.

2.4 Aerosol Dynamics

This section describes the models used in the RN package to predict the behavior of aerosols during an accident in a LWR. Fission products may be aerosolized as they are released from fuel early in a LWR accident and later expelled from the reactor coolant system. Other events and processes that occur late in the accident, such as core-concrete interactions, pool boiling, direct containment heating, and deflagrations, may also generate (or resuspend) aerosols. High structural temperatures may also result in aerosolization of nonradioactive materials.

The principal aerosol quantities of interest are the mass and composition of aerosol particles and their distribution throughout the reactor coolant system and containment. The calculation of aerosol agglomeration and deposition processes is based on the MAEROS [7] computer code, but without direct inclusion of condensation or evaporation within the MAEROS solution framework. Vapor condensation on and evaporation from aerosol particles are handled separately to reduce the stiffness of the differential equation set and to ensure consistency with the calculation of these processes by other models and packages, as described later.

MAEROS is a multisectional, multicomponent aerosol dynamics code that evaluates the size distribution of each type of aerosol mass, or *component*, as a function of time. This size distribution is described by the mass in each size bin, or *section*. Each section may have a different chemical composition as described by the masses of various components for that section. In other words, a section is an aerosol size group and a component is a particular type of aerosol material. Since MELCOR operates on a radionuclide class structure, as discussed earlier, a mapping between RN classes and MAEROS aerosol components must be specified by the user.

Figure 2.1 illustrates the sectional representation of a two-component aerosol with 5 sections. The mass concentrations of component 1 in the five sections are given by the stair-stepped line that bounds the lower crosshatched region. The total aerosol mass concentrations in the five sections are given by the uppermost stair-stepped line. Therefore, the mass concentrations of component 2 in the five sections are given by the upper shaded region.

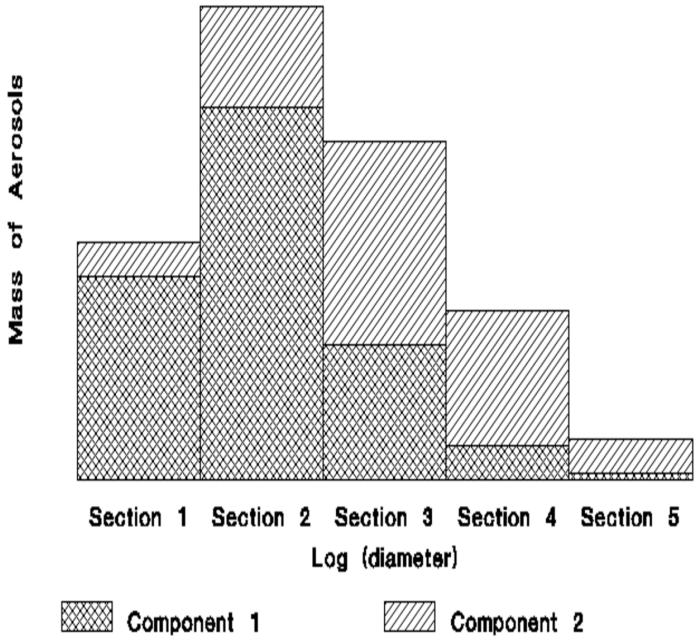

Figure 2.1 MAEROS Aerosol Model

One powerful feature of MELCOR is that water condensation on and evaporation from aerosols is modeled in a manner consistent with the thermal/hydraulic calculations in the CVH and HS packages. That is, the latent heat associated with the coolant mass transfer between the atmosphere and aerosol surfaces is incorporated in the total internal energy transfer to and from the atmosphere. In addition, condensation and evaporation of fission product vapors on aerosols is calculated in parallel with condensation on and evaporation from heat structure surfaces, but without consideration of the latent heat of condensation of the vapor, since it is negligible compared to the energy of the atmosphere and the heat structure.

The MELCOR calculation of changes in aerosol distribution and location within a plant considers the following general processes:

(1) aerosol phenomenological sources from other packages, such as release from fuel rods or during core-concrete interactions, and/or arbitrary user-specified sources;

(2) condensation and evaporation of water and fission products to and from aerosol particles;

(3) particle agglomeration (or coagulation), whereby two particles collide and form one larger particle;

(4) particle deposition onto surfaces or settling through flow paths into lower control volumes;

(5) advection of aerosols between control volumes by bulk fluid flows; and

(6) removal of aerosol particles by engineered safety features (ESFs), such as filter trapping, pool scrubbing, and spray washout.

The RN package includes models to simulate each of these processes, but only user-defined aerosol sources and agglomeration and deposition processes are formally coupled in the MAEROS integrated solution framework. Aerosol sources from other phenomenological packages in MELCOR and condensation on and evaporation from aerosols are decoupled and treated outside the MAEROS solution. This section describes principally the details of the implementation of MAEROS within MELCOR. Section 2.4.1 describes in more detail how the component/class mapping scheme works and how the particle size distribution is represented in MELCOR. The general MAEROS equations and the specific models for aerosol agglomeration and deposition are described in Section 2.4.2. Section 2.4.3 provides information on how various aerosol sources are treated, and Section 2.4.4 discusses the MELCOR aerosol resuspension model (not yet implemented).

Condensation and evaporation processes for both aerosols and heat structure surfaces are described later in Section 2.5, and Section 2.6 describes the modeling for advection of aerosols between control volumes. Section 2.7 describes the removal of aerosols by ESFs.

2.4.1 Aerosol Mass and Size Distributions

In MELCOR, one or more RN classes can be assigned to a component, as specified on the RNCCXXX input records, but a particular class cannot be assigned to more than one component. For each control volume, the fractions within a particular component of each class assigned to that component are determined before the aerosol dynamics calculation is performed to determine the new size distribution. These fractions necessarily sum to unity. After the aerosol dynamics calculation, the masses for each aerosol size, the deposited masses, and the fallout masses for each class are determined by multiplying the appropriate component mass values by the previously calculated class mass fraction. In effect, all classes assigned to the same component are assumed to have the same size distribution.

The aerosol particle size distribution is discretized into particle size bins called *sections*. The distribution of aerosol mass within a section is treated as constant with respect to the logarithm of particle mass. The user may input any arbitrary initial aerosol size distribution for any fission product class by specifying the mass in each size section at the initial time (see the RNAGXXX and RNALXXX input records). The initial aerosol water mass (fog) is determined from the CVH package input data only and is put in the smallest aerosol section; an error message is generated if an attempt is made to initialize water aerosol mass through RN input.

The number of sections and components to be used in the aerosol calculations, as well as the minimum and maximum aerosol diameters, are specified by the user (see input records RN1001 and RN1100). Individual section boundaries are calculated from these values so that the ratio of the upper and lower bound diameter of each section is the same. A check is also made that the ratio of the upper to lower mass boundary for each section is greater than or equal to two to assure that the calculations will conform to the assumptions made in the derivation of the MAEROS equations. If this constraint is not met, an error message is generated and the calculation terminates.

Although the aerosol component distributions from the MAEROS calculation are not stored permanently, the class distributions are used to calculate the mass median diameter and geometric standard deviation for the wet, dry and component distributions in each control volume for editing. The wet distribution is the sum over all classes including water; the dry distribution, which is commonly determined experimentally, is the sum over all classes excluding water; and the component distribution is the sum over all classes assigned to the particular component. The mass median diameter is defined to be the diameter above and below which half the total mass (wet, dry or component mass) in the distribution occurs,

$$0.5 \times \int_0^{\infty} f_m(D)\,dD = \int_0^{D'} f_m(D)\,dD \tag{2.24}$$

where D' is the mass median diameter and $f_m(D)\ dD$ is the mass in the distribution between diameter D and $D + dD$. The geometric standard deviation, σ_G, is defined as

$$(\ln \sigma_G)^2 = \frac{\int_0^{\infty} \ln^2\left(D / \overline{D}\right) f_m(D)\,dD}{\int_0^{\infty} f_m(D)\,dD} \tag{2.25}$$

where $\overline{D}$ is the logarithmic mass mean diameter defined by

$$\ln\left(\overline{D}\right) = \frac{\int_0^\infty \ln(D) f_m(D)\, dD}{\int_0^\infty f_m(D)\, dD} \tag{2.26}$$

In MELCOR, any aerosol particles that are calculated to grow larger (by agglomeration or condensation) than the maximum size section, are assumed to *fall out* onto either floor-type heat structures or into adjacent lower control volumes. Aerosols that fall out into a lower control volume are put in the largest size section of the aerosol distribution in that control volume and thus should quickly deposit or fall out onto floor structures. This is described in more detail in Section 2.4.2.2.

2.4.2 MAEROS Equations

The aerosol agglomeration and deposition models from MAEROS are used to calculate the changing aerosol size distributions as these processes affect the aerosol in each control volume at each timestep. Particle agglomeration, deposition onto heat structure surfaces, fallout onto floors or into lower control volumes, and the effects of user-defined aerosol sources are all integrated in the MAEROS calculation.

The modeling of the aerosol size distribution is governed by a complex integro-differential equation. MAEROS was developed as a method of discretizing this equation into a form that can be solved numerically. In their method (and using their notation), the full range of aerosol masses is divided into *m* contiguous arbitrarily sized sections, and Q_ℓ is defined as the total mass of aerosol per unit volume of fluid in section ℓ at time *t*. Thus,

$$Q_\ell(t) = \sum_{k=1}^{s} Q_{\ell,k}(t) \tag{2.27}$$

where $Q_{\ell,k}(t)$ is the mass of component *k* in section ℓ, and *s* is the total number of components. The upper bound of section $\ell - 1$ is equal to the lower bound of section ℓ for ℓ = 2, 3, ... *m*. These equations can be written

$$\begin{aligned}\frac{dQ_{\ell,k}}{dt} &= \tfrac{1}{2}\sum_{i=1}^{\ell-1}\sum_{j=1}^{\ell-1}\left[{}^{1a}\overline{\beta}_{i,j,\ell}\,Q_{j,k}Q_i + {}^{1b}\overline{\beta}_{i,j,\ell}\,Q_{i,k}Q_j \right] \\ &\quad -\sum_{i=1}^{\ell-1}\left[{}^{2a}\overline{\beta}_{i,\ell}\,Q_iQ_{\ell,k} - {}^{2b}\overline{\beta}_{i,\ell}\,Q_\ell Q_{i,k} \right] \\ &\quad -\tfrac{1}{2}{}^{3}\overline{\beta}_{\ell,\ell}\,Q_\ell Q_{\ell,k} - Q_{\ell,k}\sum_{i=\ell+1}^{m} {}^{4}\overline{\beta}_{i,\ell}\,Q_i + {}^{1}\overline{G}_{\ell,k}Q_\ell \\ &\quad -\sum_{i=1}^{N_a}\left[{}^{2}\overline{G}_{\ell,k}Q_{\ell,k} - {}^{2}\overline{G}_{\ell\pm1,i}\,Q_{\ell\pm1,k}\right] + {}^{3}\overline{G}_{\ell\pm1,k}\,Q_{\ell\pm1} + \overline{S}_{\ell,k} - \overline{\Re}_{\ell,k}\end{aligned} \tag{2.28}$$

where

$dQ_{\ell,k}(t)/dt$ = time rate of change of aerosol mass of component k (per unit volume) in section ℓ at time t

k = aerosol component (for example, water or a specific FP) = 1, 2,...N_a

ℓ = discretized section (or physical size range) of the aerosol = 1, 2, 3,...m

$\ell \pm 1$ = $\ell - 1$ for condensation, or ℓ + 1 for evaporation

Each term in Equation (2.28) represents a distinct mechanism for changes in mass concentration of component k in a particular section. Time integration of Equation (2.28) requires that the coefficients used in each term be known on a sectional basis. These sectional coefficients correspond to the following mechanisms:

$\overline{\beta}$ = agglomeration (or coagulation), m^3/s-kg

$\overline{G}$ = gas-to-particle conversion (condensation/evaporation), s^{-1}

$\overline{S}$ = sources, kg/m^3-s

$\overline{\Re}$ = removal (deposition) kg/m^3-s

The $\overline{\beta}$'s are called sectional coagulation coefficients, and they can be evaluated by using a variety of formulas that incorporate the effects of the different physical processes. These processes include gravitational agglomeration (a larger particle overtakes a smaller one as they both fall) and agglomeration through diffusion (either Brownian or turbulent), and are described in more detail in Section 2.4.2.1. The six agglomeration terms in the Gelbard-Seinfeld approach refer respectively to the following processes:

$^{1a}\overline{\beta}_{i,j,\ell}$	addition of component *k* in section ℓ, by removal of component *k* in section *j* when a particle in section *j* coagulates with a particle in section *i* to form a particle in section ℓ.
$^{1b}\overline{\beta}_{i,j,\ell}$	addition of component *k* in section ℓ, by removal of component *k* in section *i* when a particle in section *i* coagulates with a particle in section *j* to form a particle in section ℓ.
$^{2a}\overline{\beta}_{i,\ell}$	removal of component *k* in section ℓ, resulting from a particle in section *i* coagulating with a particle in section ℓ.
$^{2b}\overline{\beta}_{i,\ell}$	addition of component *k* in section ℓ, resulting from a particle in section *i* coagulating with a particle in section ℓ, with the resulting particle remaining in section ℓ.
$^{3}\overline{\beta}_{\ell,\ell}$	removal of component *k* in section ℓ, by two particles in section ℓ coagulating and the resulting particle is in a section higher than ℓ.
$^{4}\overline{\beta}_{i,\ell}$	removal of component *k* in section ℓ, by a particle in section ℓ coagulating with a particle in section *i*, where i > ℓ.

The four condensation terms represented by the $\overline{G}$ coefficients correspond to the following processes:

$^{1}\overline{G}_{\ell,k}$	addition (removal) of component *k* within section ℓ by condensation (evaporation) of component *k* onto (from) particles in that section;
$2\overline{G}_{\ell,j}$	transfer of existing component *k* from section ℓ to section ℓ + 1 (ℓ – 1) by condensation (evaporation) of component *i* onto (from) particles in section ℓ;
$^{2}\overline{G}_{\ell\pm1,j}$	transfer of existing component *k* from section ℓ – 1 (ℓ + 1) to section ℓ by condensation (evaporation) of component *i* onto (from) particles in section ℓ – 1 (ℓ + 1); and
$^{3}\overline{G}_{\ell\pm1,k}$	transfer of changed mass of component *k* from section ℓ – 1 (ℓ + 1) to section ℓ by condensation (evaporation) of component *k* onto (from) particles in section ℓ – 1 (ℓ + 1). This term vanishes in the limit that aerosol masses are large compared to molecular masses.

Water condensation on and evaporation from aerosol particles are the principal couplings between thermal-hydraulics and aerosol behavior. However, these terms are not used directly in the MELCOR implementation of MAEROS. As described in Section 2.5.1, water condensation and evaporation are treated separately (but still using the MAEROS-calculated coefficients for water, as discussed in Section 2.5.1) for consistency with the water thermodynamics calculated in the CVH package.

Furthermore, fission product condensation onto and evaporation from aerosols are also integrated with the calculation of fission product condensation and evaporation on heat structure surfaces by the TRAP-MELT model, as described in Section 2.5.2, and are thus treated outside the MAEROS framework as well.

In Equation (2.28), particle removal (or deposition) is addressed by the $\overline{\mathfrak{R}}$ term. Deposition occurs through a number of processes, including gravitational settling, diffusion to surfaces, thermophoresis (a Brownian process causing migration of particles toward lower temperatures), and diffusiophoresis (deposition induced by condensation of water vapor onto structural surfaces). The sectional deposition coefficients are described in more detail in Section 2.4.2.2.

Aerosol sources are included by the $\overline{S}$ term in Equation (2.28). Currently, only sources defined by the user as tabular functions of time are directly included in the MAEROS equations. Sources from phenomenological models are added directly to the aerosol sectional distributions as described later in Section 2.4.3.

Intraparticle chemical reactions can occur between constituents of the aerosol. The modeling of aerosol size/composition changes resulting from chemical reactions is not currently implemented in MELCOR, but this phenomenon could easily be included in the sectional model.

Simplifications in the coefficients and in Equation (2.28) occur if the geometric constraint

$$m_{i+1}/m_i > 2 \qquad (2.29)$$

is satisfied, where m_i is the particle mass at the lower boundary of section i. The geometric constraint ensures that the agglomeration of two particles results in a new particle that will fit into either the section that contains the larger of the two original particles or the section just above it. This constraint thus reduces the number of sectional agglomeration coefficients. As stated earlier in Section 2.4.1, input specifying the section boundaries is checked to verify that this constraint is met.

Equation (2.28) is used in MELCOR to describe the evolution of the aerosol size and composition distributions within each control volume. Each control volume has its own particle size and chemical composition distributions, and the aerosols are carried from one control volume to another by gas flow and may be removed by ESFs, as described in Section 2.7.

2.4.2.1 Agglomeration

When two aerosol particles collide, they can combine to form a larger particle. This process is known as agglomeration or coagulation. The sectional method used in MAEROS treats four agglomeration processes: Brownian diffusion, differential gravitational settling, and turbulent agglomeration by shear and inertial forces. A basic assumption about these processes is that simultaneous agglomeration of three or more particles is negligible.

The full dependence of the agglomeration coefficients β (m^3/s) upon the aerosol and atmosphere properties as implemented in MELCOR is given in the equations in Appendix B. The dependence on atmosphere properties is not considered to be a major source of uncertainty in the aerosol calculations. The dependence on particle diameter and key modeling parameters can be summarized as follows:

Brownian:	$\beta_B \propto \gamma\, \chi^{-1}\ f\left(d_i, d_j\right)$
Gravitational:	$\beta_{grav} \propto \varepsilon_g\ \gamma^2\, \chi^{-1} \left(d_i + d_j\right)^2 \left(d_i^2 - d_j^2\right)$
Turbulent, Shear:	$\beta_{Tl} \propto \gamma^3\, \varepsilon^{1/2} \left(d_i + d_j\right)^3$
Turbulent, Inertial:	$\beta_{T2} \propto \gamma^2\, \chi^{-1}\, \varepsilon^{3/4} \left(d_i + d_j\right)^2 \left(d_i^2 - d_j^2\right)$

In these proportionalities, γ and χ are the agglomeration and dynamic shape factors, respectively, and ε is the turbulent energy dissipation density, all of which are specified on user Input Record RNMS000. Variables d_i and d_j are the diameters of the two interacting particles, with $d_i > d_j$. The collision efficiency for gravitational agglomeration is represented by ε_g, with a specific value (discussed below) calculated in the code. The magnitude of the Brownian kernel increases with increasing values of the size ratio d_i/d_j. The role of the various parameters appearing in the kernels is also discussed below.

Except when they include significant amounts of liquid, aerosol particles are not usually assumed to be spherical, and the effective aerosol densities may be significantly less than the bulk density of the materials of which the aerosols are composed. In aerosol codes, these effects may be taken into account by using a formalism based on fully dense spherical aerosols modified through the use of the agglomeration shape factor γ and the dynamic shape factor χ. The shape factors γ and χ are input by the user to represent the effect of nonspherical shape upon aerosol collision cross sections and aerosol-atmosphere drag forces, respectively. Unit values of the shape factors correspond to dense aerosol of spherical shape, while porous spherical agglomerates lead, in theory, to values somewhat greater than unity. Highly irregular aerosols and agglomerates can have shape factors substantially greater than unity, often with γ and χ being quite unequal.

Given experimental data for aerosol shapes and densities applicable to LWR accidents, shape factors could, in principle, be derived theoretically. Because this is not practical, empirical values are obtained by fitting code calculations to the results of aerosol experiments. The values obtained may be sensitive to aerosol composition and to atmospheric conditions, especially to relative humidity. Humid conditions tend to produce more nearly spherical aerosols due to condensation of water on aerosol agglomerates. Only limited information is available concerning the dependence of shape factors upon the relevant parameters (for example, particle characteristics and atmospheric conditions), and these parameters are themselves quite uncertain under accident conditions. Default values of unity are set for both factors in MELCOR.

Agglomeration rates can be enhanced by turbulence in the atmosphere. In the past, very little attention has been given to estimating values of turbulent energy dissipation density ε appropriate for accident conditions, and uncertainty in its value may contribute to uncertainty in the aerosol agglomeration rates. In MELCOR, the user can input the value of ε or use the default value of 0.001 m^2/s^3.

The gravitational collision efficiency ε_g of unity corresponds to the assumption that collision cross sections are equal to the geometric cross sections. It is well known that hydrodynamic interactions between particles (i.e., the tendency of a particle to follow streamlines in flow around another particle) can yield collision efficiencies much less than unity, especially for particles that are unequal in size. The problem of collisions between falling (spherical) aerosols has been the object of much detailed theoretical and experimental study, and may be more complex than can be represented by the simple expressions normally used in aerosol codes. In MELCOR, the value of ε_g is given by

$$\varepsilon_g = 1.5 d_j^2 / \left(d_i + d_j\right)^2 \tag{2.30}$$

where d_j is the smaller of the two aerosol particle diameters. It has been argued [17, 18] that using 0.5 instead of 1.5 as the coefficient in Equation (2.30) gives a better representation and that other corrections are needed when the size ratio d_i/d_j is less than about 2 and/or d_i is greater than about $20 \mu m$. However, more recent experimental measurements of collision efficiencies by Gelbard et al. [19] do not support these proposed revisions and, instead, gave collision efficiencies in reasonable agreement with Equation (2.30). These measurements involved studying the collisions of spheres at higher Reynolds numbers than those typical of aerosols and the results therefore may not be totally conclusive; however, arguments for modifying Equation (2.30) are not judged to be any more convincing.

The agglomeration model used in MELCOR receives temperature, pressure, and mass flow rate information from the CVH package. The turbulent agglomeration kernels are combined as

$$\beta_{TT} = c_s \left(\beta_{T1} + \beta_{T2}\right)^{1/2} \tag{2.31}$$

where c_s is a particle sticking coefficient (default value of unity), which may be specified on Input Record RNMS000. (This sticking coefficient also appears in the other Brownian and gravitational agglomeration kernels.) The total turbulent kernel is added to the Brownian and gravitational kernels to obtain a total agglomeration kernel β_T which is then integrated over sections for use in Equation (2.28):

$$\beta_T = \beta_B + \beta_{grav} + \beta_{TT} \tag{2.32}$$

Examination of the relations for the agglomeration kernels in the proportionalities given above shows that the effects of gravitational collision efficiency, aerosol shape factors, and turbulence are coupled together in a highly nonlinear fashion. The dependence upon the various parameters differs among the different agglomeration mechanisms, and the net effects are strongly size-dependent. Hence, it is possible to give only a few generalizations.

All the agglomeration processes are enhanced by large values of the agglomeration shape factor γ, with the effect being largest for turbulent shear agglomeration and smallest for Brownian agglomeration. Large values of the dynamic shape factor reduce all the kernels (calculational coefficients) except the turbulent shear kernel, which is unaffected. Hence, large values of the shape factors enhance the relative importance of turbulence, especially for the turbulent shear effect. Reference [18] includes sensitivity studies examining the implications of uncertainties in these shape factors as well as in the turbulent energy dissipation density ε.

2.4.2.2 Deposition, Settling, and Fallout

Aerosols can directly deposit onto heat structure and water pool surfaces through four processes calculated within MAEROS. All heat structure surfaces are automatically designated as deposition surfaces for aerosols using information from the HS package, unless made inactive through user input. The parameters obtained from the HS package are:

(1) Geometric orientation

(2) Surface area in the atmosphere

(3) Surface heat flux

(4) Mass transfer coefficient

(5) Water condensation mass flux

Each surface of a MELCOR heat structure must be designated as a ceiling, a floor, or a wall, since MAEROS only calculates deposition kernels for these orientations. The default treatment is:

> The upper surface of a rectangular heat structure with an angle of inclination less than 45 degrees is considered to be a floor, and the lower surface a ceiling. The heat structure orientation parameter ALPHA on HS Input Record HSCCCCC002

determines both the inclination and whether the “left” surface is the upper or the lower surface.

Both surfaces of a rectangular heat structure with an angle of inclination greater than 45 degrees, and both surfaces of cylinders and spheres are treated as walls.

The inner (left) surface of a bottom-half hemisphere is treated as a floor and the outer (right) surface as a ceiling. For a top-half hemisphere, the treatment is reversed.

The user can override these default orientations or deactivate a surface for aerosol deposition through the RNDSXXX input records. However, if the surface of a structure is deactivated for the purposes of deposition, it is also removed from consideration in the calculation of condensation and evaporation of fission product vapors, as discussed in Section 2.5. (Note that the orientation of a structure does not otherwise affect the rate of condensation or evaporation.)

If a control volume contains a water pool, the pool surface is treated as a floor for the purposes of deposition. The area of the water pool is extracted from the CVH database.

Aerosols can also *settle* from one control volume to another through *flowthrough areas* (i.e., the gravitational settling and Brownian diffusion kernels in MAEROS described below are applied to flowthrough areas in addition to HS and pool surfaces). Such areas will ordinarily correspond to open flow paths between the control volumes, through which aerosols and radionuclide vapors are also advected. The appropriate flow areas, path elevations, etc., are specified in the RNSETXXX input records. Aerosols are not transported through these areas if the flow path is blocked by a water pool.

Finally, aerosols can agglomerate and become larger than the user-specified maximum diameter. These aerosols are assumed to immediately deposit onto water pools or horizontal heat structure surfaces or to settle from one control volume to another through *flowthrough areas* defined as part of RN input. The term *fallout* in MELCOR is used exclusively for this immediate deposition or settling of aerosols larger than the maximum user-specified diameter. All control volumes must have at least one upward-facing deposition surface (floor) or flowthrough area defined to receive fallout aerosols generated by this mechanism. During MELGEN a check is made for the existence of at least one such area; if none is present, an error message is generated and no restart file is written.

The MAEROS deposition kernel for each type of surface is made up of four contributions: gravitational deposition, Brownian diffusion to surfaces, thermophoresis, and diffusiophoresis. Of these natural depletion processes, gravitational deposition is often the dominant mechanism for large control volumes such as those typically used to simulate the containment, although phoretic effects may be significant in some cases (e.g., diffusiophoresis during water condensation). Particle diffusion is generally considered to be a relatively unimportant deposition process. The contribution of each of these

processes to the deposition kernel for each type of heat structure surface and for pools and flowthrough areas in MELCOR is summarized below:

Surface	Deposition Kernel[1]			
	grav	BD	therm	diffus
Heat Structure				
Floor	+	+	+	+
Wall	0	+	+	+
Ceiling	-	+	+	+
Pool	+	+	+[2]	+[2]
Flowthrough Area	+	+	0	0

[1] The symbols +, 0, and - mean a positive contribution, no contribution, and a negative contribution, respectively. Of course, the total deposition kernel for any surface can not be less than zero.

[2] Included in the general formulation but currently zeroed out internally.

The velocities calculated for each of these deposition processes are defined below.

Gravitational Deposition

Gravitational deposition is effective only for upward-facing surfaces (i.e., floors and water pools) and flowthroughs to lower control volumes; for downward-facing surfaces (i.e., ceilings), this mechanism works to oppose other deposition processes. The gravitational deposition velocity is given by

$$v_{grav} = \frac{d_p^2 \rho_p g C_m}{18 \mu \chi} \tag{2.33}$$

where

v_{grav} = the downward terminal velocity (m/s)

d_p = the particle diameter (m)

ρ_p = the particle density (kg/m^3)

g = acceleration of gravity = 9.8 m/s^2

C_m = the particle mobility, or Cunningham slip correction factor, which reduces the Stokes drag force to account for noncontinuum effects

The particle mobility, or Cunningham slip correction factor, in the equation above is expressed as

$$C_m = 1 + \frac{2\lambda}{d_p}\left[F_{slip} + 0.4\exp\left(-1.1 d_p / 2\lambda\right)\right] \qquad (2.34)$$

where

λ = mean free path of air at 298 K (~ $0.069 \bullet 10^{-6}$m)

F_{slip} = slip factor specified on Input Record RNMS000 (default value of 1.257)

μ = viscosity of air at 298 K [~ $1.8 \bullet 10^{5}$(N • s/m^2)]

χ = dynamic shape factor

This model assumes that the aerosol particle Reynolds number Re, based on particle diameter and net deposition velocity, is much less than 1. This physically means that inertial effects of the flow may be neglected. This Reynolds number is not to be confused with the bulk mass flow (air, steam, aerosol particles) Reynolds number based on the dimensions and velocities calculated by the CVH package, which is typically much greater than 1.

Brownian Diffusion

Deposition can also result from diffusion of aerosols in a concentration gradient from a higher to a lower concentration region. The diffusive deposition velocity is given by

$$v_{diff} = \frac{\sigma T C_m}{3\pi \mu \chi d_p \Delta} \qquad (2.35)$$

where

v_{diff} = diffusion deposition velocity (m/s)

σ = Boltzmann constant = $1.38 \bullet 10^{-23}$ (J/s-m^{2}K^4)

T = atmosphere temperature (K)

μ = viscosity (N • s/m^2)

χ = dynamic shape factor

Δ = user-specified diffusion boundary layer thickness specified on Input Record RNMS000 (default value of 10^{-5} m)

under the assumption that there is no gas velocity perpendicular to the deposition surface. This impaction mechanism is most effective for larger aerosol particle sizes.

Thermophoresis

This aerosol deposition mechanism results from the force exerted on aerosol particles by temperature gradients in the bulk gas. The thermophoretic deposition velocity v_{therm} is given by

$$v_{therm} = \frac{3\,\mu\,C_m\left(c_t\,Kn + k_{gas}/k_p\right)}{2\;\chi\;\rho_{gas}\,T\left(1+3\,F_{slip}Kn\right)\left(1+2\,c_t\;Kn + k_{gas}/k_p\right)}\;\nabla T \qquad (2.36)$$

where

Kn = $2\lambda / d_p$ (Knudsen number)

k_{gas}/k_p = ratio of thermal conductivity of gas over that for aerosol particle k_p, and is user-specified (on Input Record RNMS000)

∇T = structure surface temperature gradient (K/m)

ρ_{gas} = gas density (kg/m^3)

T = wall temperature (K)

F_{slip} = slip factor

c_t = constant associated with the thermal accommodation coefficients (specified on Input Record RNMS000 with default value of 2.25)

The coefficient of ∇T in Equation (2.36) is calculated for each of the four aerosol coefficient sets at minimum/maximum temperature and pressure and stored as described in Section 2.4.2.3. The actual temperature gradient at each heat structure surface, calculated from the heat flux q'' obtained from the HS package as

$$\nabla T = -q''/k_{air} \qquad (2.37)$$

is used with an interpolated coefficient (see Section 2.4.2.3) to calculate the actual diffusion velocity. The thermal conductivity of air, k_{air}, is evaluated at the surface temperature of the heat structure using the properties of air for consistency with the evaluation of the aerosol coefficients with air properties.

Diffusiophoresis

When water condenses on (evaporates from) a structure surface, composition gradients will exist in the adjacent gas which will affect aerosol deposition on the surface. Two related mechanisms produce these gradients. First, a net molar flux of gas toward (away from) the condensing (evaporating) surface will exist, and this net flux, commonly called the Stefan flow [20], will tend to move aerosol particles with it. Second, differences in the momentum transferred by molecular impacts on opposite sides of the particle will tend to drive the particle in the direction of decreasing concentration of the heavier constituent. By some definitions, only this second component constitutes diffusiophoresis; however, in this discussion the term "diffusiophoresis" will be used to represent the net result of both effects and the equations given include both effects. Note that when the noncondensible gas is heavier than steam, as in air-steam mixtures, the differential molecular impact effect opposes the Stefan flow (which dominates the net result); the effects are in the same direction if the noncondensible gas is lighter than steam.

The treatment in MELCOR is valid for particle sizes large compared with molecular mean free paths, a condition which will generally apply for accident analyses. A diffusiophoretic deposition velocity (including the Stefan flow) $v_{diffusio}$ is calculated from

$$v_{diffusio} = \left(\frac{\sqrt{M_s}}{X_s \sqrt{M_s} + X_{NC} \sqrt{M_{NC}}} \right) \left(\frac{W_{cond}}{\rho_b} \right) \quad \text{if } W_{cond} \geq 0 \text{ (condensation)} \qquad (2.38)$$

$$v_{diffusio} = W_{cond} / \rho_s \quad \text{if } W_{cond} < 0 \text{ (evaporation)} \qquad (2.39)$$

where

M_s = molecular weight of water (kg/mole)

M_{NC} = molecular weight of noncondensible gases (air

W_{cond} = condensation mass flux to the surface (kg/s-m^2)

ρ_b = density of bulk gas (kg/m^3)

ρ_s = saturation density of water vapor (kg/m^3)

X_s = mole fraction of water vapor in the bulk gas

X_{NC} = mole fraction of noncondensible gases in the bulk gas

The condensation mass flux is obtained from the HS package. Note that the differential molecular impact effect is ignored in MELCOR for evaporation ($W_{cond} < 0$). The velocity

calculated is toward the surface for condensation and away from the surface for evaporation.

MELCOR calculates these four velocities, representing deposition by gravity, diffusion, thermophoresis, and diffusiophoresis, for each surface. The sum gives the aerosol removal rate term $\overline{\Re}_{\ell,k}$ (kg/m^3·s) in Equation (2.28) in the form

$$\overline{\Re}_{\ell,k} = \sum_{j=1}^{N_{str}} K_{j,\ell} K_{\ell,k} \tag{2.40}$$

where

N_{str} = total number of heat structure surfaces and/or pool surfaces for aerosol deposition in the control volume

$K_{j,\ell}$ = deposition rate for the heat structure j for aerosol section ℓ (s^{-1})

$Q_{\ell,k}$ = aerosol density for section ℓ of component k (kg/m^3)

$K_{j,\ell}$ in Equation (2.41) is defined as

$$K_{j,\ell} = \frac{A_j}{V}\left(v_{grav} + v_{diff} + v_{therm} + v_{diffusio}\right) \tag{2.41}$$

where

A_j = area of heat structure surface j (m^2)

V = control volume atmosphere volume (m^3)

The total component mass that deposits on all surfaces from each section is calculated by MAEROS. The fraction $Fr_{j,\ell}$ of the mass in each section that deposits on surface j in the control volume is given by the simple expression

$$Fr_{j,\ell} = \frac{A_j K_{j,\ell}}{\sum_{j}^{N_{sur}} A_j K_{j,\ell}} \tag{2.42}$$

For fallout aerosols the procedure is similar except that the areas are summed for the floor heat structures, pool, and flowthrough areas; no kernels are involved since any kernel would be common to all surfaces involved. The total fallout mass calculated by agglomeration in MAEROS is then distributed over the floor heat structures, pools, and passes through flowthrough areas proportional to the area of each as follows:

$$Fr_i = A_i \Big/ \sum_i^{N_{sur}} A_i \qquad (2.43)$$

where N_{sur} is the total number of surfaces and flowthrough areas.

If part or all of a water film drains from a surface of a heat structure to the pool in the associated control volume, any fission products deposited on that surface or in the water film are normally relocated with the water, in proportion to the fraction of the film that is drained. However, the user may change this for any class by resetting the corresponding value in sensitivity coefficient array 7136 to the fraction of the class assumed to be dissolved in, and therefore to relocate with, the film.

When a phase (pool or atmosphere) in a control volume ceases to exist, the aerosols it contains must be relocated. If the pool in a volume completely evaporates, any aerosols in the pool are distributed between the floor heat structures and the flowthrough areas according to Equation (2.43). If the atmosphere in a control volume that is almost completely filled with water completely condenses, all the suspended aerosol mass is added to the aerosol mass in the pool because it is assumed that the pool will then completely fill the control volume.

2.4.2.3 Numerical Implementation

In stand-alone MAEROS, the full aerosol dynamics equations are integrated using a conventional Runge-Kutta integration routine [21]. Because the integration is stopped and restarted only at times when an edit is desired, this approach is both accurate and efficient. However, in MELCOR the integration must be stopped at the end of each system timestep and restarted at the beginning of the next to account for the continuous coupling with other MELCOR models, most of which must be exercised outside the MAEROS framework. These include aerosol release from fuel in the Core package, aerosol generation during core-concrete interactions by the MELCOR implementation of VANESA, fog condensation or evaporation calculated by CVH package thermodynamics, simultaneous condensation or evaporation of fission product vapors on heat structure and aerosol particle surfaces, and advection of aerosols between control volumes as controlled by CVH flow rates. Because of this, the Runge-Kutta solver can be very inefficient (the startup costs become excessive) and, for very short steps, there is little or no increase in accuracy over an explicit (forward Euler) integration.

Therefore, in MELCOR appropriate rates of change are evaluated at the beginning of each system timestep and, if an explicit step will produce only small changes in the sectional densities, the distribution is updated using this explicit Euler step. Otherwise, the Runge-Kutta solver is used to advance the equations. The criteria for "small change in the sectional densities" and the error tolerances for the Runge-Kutta solution are controlled by the sensitivity coefficients in array 7000 (see Appendix A). If the Runge-Kutta solver does not converge within the requested tolerances, the RN package will reduce the timestep to one-half the current value and write a message to the output and diagnostic files informing the user.

Whether the new aerosol distribution is calculated by an explicit step or by the Runge-Kutta solver, a check is performed to ensure that component masses are conserved within a suitable tolerance (given by a sensitivity coefficient in array 7000; see Appendix A). If this check fails, the RN package will reduce the timestep to one-half the current value and write a message to the output and diagnostic file informing the user.

The calculation of the MAEROS coefficients is somewhat costly; a full calculation for 20 sections requires about 10 s processing time on a CRAY 1S computer. Therefore, the coefficients are calculated on the first call to the aerosol model for use throughout the entire problem. Input records describing these coefficients (the RNCFXXX series) are written to a file automatically and may be read in from this file on a subsequent restart if called for on the RNACOEF record, but this practice is not recommended because of the possibility of user file handling errors. Sensitivity coefficient array 7001 contains error tolerances for numerical integration of the MAEROS coefficients.

Using a constant set of coefficients imposes some modeling constraints however, because various parameters embedded in the coefficients, such as material properties for the CVH atmosphere, are also effectively held fixed despite the fact that they should vary with changing conditions during the problem. Several of the terms in Equation (2.28) also contain driving forces. The coefficients of these forces are calculated and stored.

The following constraints pertain to the current coefficient set:

a	The aerosol material density is assumed to be the same for all components (specified by the user on Input Record RN1100).
b	The aerosol shape, as modeled by the dynamic and agglomeration shape factors (specified by the user on Input Record RNMS000), is independent of aerosol composition.
c	The medium in which the aerosol processes are assumed to occur has fixed properties, taken as those for air.
d	The degree of turbulent agglomeration is fixed throughout the problem, specified by the user on Input Record RNMS000.

e	Other parameters that control deposition rates do not depend on particle composition. For example, the ratio of the thermal conductivity of air to that of the aerosol material is fixed.

The pressure and temperature of the atmosphere are embedded in these coefficients and are fixed for a single set of coefficients. However, the aerosol module actually calculates four sets of coefficients at points given by combinations of two temperatures (T_{min} and T_{max}) and two pressures (P_{min} and P_{max}), all of which may be specified by the user. The effects of changing thermal-hydraulic conditions during the problem are approximated by interpolating between these sets of coefficients. The T_{min}, T_{max}, P_{min}, and P_{max} parameters are chosen to bound the temperatures and pressures expected in the calculation, and are specified on user Input Record RNPT000.

The interpolated sectional coefficients CF_i for agglomeration or deposition mechanism i are given by

$$CF_i = (1-F_T)\left[(1-F_p)AC_{11,i} + F_p AC_{12,i}\right] + F_T\left[(1-F_p)AC_{21,i} + F_p AC_{22,i}\right] \quad (2.44)$$

where

$AC_{11,i}$ = the aerosol coefficient for mechanism i for the lower atmospheric temperature (T_{min}) and pressure (P_{min})

$AC_{12,i}$ = the aerosol coefficient for mechanism i for the lower atmospheric temperature (T_{min}) and higher pressure (P_{max})

$AC_{21,i}$ = the aerosol coefficient for mechanism i for the higher atmospheric temperature (T_{max}) and lower pressure (P_{min})

$AC_{22,i}$ = the aerosol coefficient for mechanism i for the higher atmospheric temperature (T_{max}) and pressure (P_{max})

and F_T and F_p in Equation (2.45) are defined as

$$F_T = \left(\frac{T_{gas} - T_{\min}}{T_{\max} - T_{\min}}\right) \quad (2.45)$$

and

$$F_p = \left(\frac{P_{gas} - P_{\min}}{P_{\max} - P_{\min}} \right) \tag{2.46}$$

where

T_{gas} = cell temperature (K), and

P_{gas} = cell pressure (Pa).

At the expense of larger sets of coefficients, some of the constraints above could be removed by interpolating to accommodate other changing parameters or by separating the coefficients so that a relevant parameter is not embedded, but this is not currently allowed through user input.

2.4.3 Sources

In stand-alone MAEROS, sources of aerosols are included in the differential equation solution at a constant source rate over that timestep. In MELCOR, however, only user-defined sources are treated in this way; sources generated by models in other packages are currently added as a single increment because of the explicit coupling of these packages. Since masses that are added to the aerosol scheme could be from the previous timestep or the present timestep, depending on the calling sequence of the various packages, all masses to be added from other models are lumped together and added to the aerosol size distribution at the start of the timestep.

Sources of aerosols are calculated in-vessel by the fuel-cladding gap release model and the CORSOR release models, as described in Section 2.3.1. Aerosols generated by these models are put into the smallest aerosol section, consistent with the production of small particles by gas-to-particle conversion. Sources of aerosols are also calculated ex-vessel by the VANESA model, as described in Section 2.3.2. The size distribution for these aerosols is assumed to be log-normal, with median diameter and standard deviation given by VANESA.

A number of time-dependent aerosol sources (specified on record RN1001) can also be specified for a control volume by the user (see the RNASXXX input record series). The aerosols can be put in either the control volume pool or atmosphere, with the time rate of the source specified by a tabular function. The mass added is determined by multiplying the mass addition rate (an input constant times the value of the tabular function at the midpoint of the current timestep) by the timestep, or

$$M_{added} = \left[\frac{dM}{dt}\right] \Delta t = \left[C \times TF(t + \Delta t / 2)\right] \Delta t \qquad (2.47)$$

where C is the mass addition constant *XM* on the RNASXXX input records, *TF* is the tabular function value, and t and Δt are the time and timestep, respectively. The size distribution of the source can be uniform, log-normal with respect to log diameter, or user specified, and is constant with time.

2.4.4 Resuspension

The resuspension model in MELCOR depends on other packages for activation. A package can call for an arbitrary fraction of deposited aerosols in a control volume to be resuspended at any time. However, no package at present has a model to calculate the fraction of deposited mass to be resuspended. User input is not available to activate resuspension. **Therefore, resuspension is currently not calculated.** When implemented, however, the user will be allowed to specify the size distribution of resuspended mass on the RNARXXX input records.

2.5 Condensation/Evaporation

Fission products and water can condense onto or evaporate from aerosols, heat structure surfaces, and water pools. Aerosol water is identified with “fog” in the CVH package. The change in fog mass is determined by thermodynamics calculated within the CVH package and is distributed over aerosol sections by the RN package as described below in Section 2.5.1. Water condensation and evaporation for heat structure and water pool surfaces are treated solely in the HS and CVH packages, respectively. The calculation of fission product vapor condensation and evaporation in the RN package is described in Section 2.5.2.

2.5.1 Water

The stand-alone version of MAEROS includes terms, given in Equation (2.28), for particle growth resulting from condensation of water onto (and shrinkage from evaporation of water from) aerosols. In MELCOR, these terms are not included with the MAEROS numerical solution for agglomeration and deposition. The reason is that inclusion of these terms makes the MAEROS equations “stiff” and therefore computationally difficult to solve, because the characteristic time for mass transfer is small compared to other characteristic times in the problem.

There are two approaches available in MELCOR to deal with condensation and evaporation of aerosol water. The original model, which neglects hygroscopic, surface

tension, and molecular free path effects, is described in this section. The user has the option to specify (as part of RN package input) the use of a more detailed model that includes these effects, as described in Section 2.10. The original model is used by default.

In addition to neglect of hygroscopic and surface tension effects, the original MELCOR model assumes that both the temperature difference between gas and aerosols and the characteristic time for mass transfer to and from aerosols may also be neglected. Under these assumptions, the atmosphere can never become significantly supersaturated, and can be significantly subsaturated only if there is no water available to evaporate from the aerosols. In short, the system of atmosphere plus aerosol water must be in thermodynamic equilibrium.

This makes the aerosol assumptions consistent with the equation of state as described in the Control Volume Thermodynamics (CVT) Package Reference Manual, and avoids the need to estimate the disequilibrium between liquid and vapor within a basically equilibrium formulation of thermodynamics or to reconcile calculations including rate effects in the RN package with calculations based on equilibrium thermodynamics within the CVT package. It also allows the water on aerosols to be identified with “fog” in the CVT package.

This reduces the task of the RN package to one of distributing the total change in fog mass, as calculated by equilibrium thermodynamics in the CVT package, among the aerosol sections. In general, this is done with changes in sectional water masses proportional to the appropriate relative rates, which are all proportional to the same super- or sub-saturation driving force, and the actual driving force need not be calculated. However, in a few cases (e.g., a sudden decompression in a volume with little or no initial aerosol content) the condensation rate necessary to maintain equilibrium may exceed that possible on existing aerosols. In such cases, a very rough estimate of the limiting condensation rate is made (as described below), and the excess water is assumed to form new aerosols in the smallest aerosol section by spontaneous nucleation.

The MAEROS equations do not account for the distribution of *composition* of particles within a single section. This major simplification of the general equations resulted from approximating all material densities as equal, rendering the agglomeration and deposition coefficients independent of composition. Thus the evolution of particle composition and size distribution is independent of composition for these two processes. The composition distribution can be important in cases of water condensation or evaporation, where a change in water mass can carry a wet aerosol particle from one size section to another. A full treatment would require both the tracking of a more general size-and-composition distribution, and the inclusion of models to account for the differing rates of condensation of water on particles of differing composition.

In MELCOR, two assumptions are permitted for condensation/evaporation of water. The first is equivalent to assuming that all particles within a section have the same composition, and allows changes in water mass to freely carry particles of other materials from one size section to another. If water condenses on and then evaporates from a dry aerosol, the

final distribution calculated using this treatment will not match the initial one—even in the absence of agglomeration or deposition—and may contain particles smaller than any initially present. The alternative assumption is that condensation and evaporation of water are ineffective in moving other materials from section to section. This is sometimes described as "allowing water to condense only on water." The errors in this treatment are different from—but no less serious than—those in the first treatment. The two options, while not necessarily representing limiting cases, allow a user to investigate the potential importance of the effects modeled.

Condensation within a section is evaluated explicitly. The total change in water mass is taken as proportional to the sum over sections of the ${}^1\overline{G}$ term in Equation (2.28) for water, using start-of-step aerosol masses (the ${}^2\overline{G}$ growth terms cancel when summed over all sections, while the ${}^3\overline{G}$ terms are infinitesimal contributors in the differential limit and are ignored). Since the new total water mass on aerosols is equal to the new fog mass calculated by the CVH package, the normalization constant, *A*, can therefore be determined from the equation

$$\Delta m_w = A\ \Delta t\ \sum_{\ell} {}^1\overline{G}_{\ell,w} Q_{\ell} \tag{2.48}$$

where Δm_w is the total mass of water which must be condensed, as required by the CVH package.

The rate of growth of an individual aerosol particle as a result of condensation is given by the Mason equation [9] as

$$\begin{aligned} \frac{dm}{dt} &= \rho_1 4\pi r \left(r \frac{dr}{dt} \right) \\ &= \frac{4\pi r (S-1)}{a+b} \end{aligned} \tag{2.49}$$

where *a* and *b* are heat flux and vapor diffusion terms, respectively,

$$a = \frac{M_w\ i_{fg}^2}{k_v\ R\ T^2} \tag{2.50}$$

$$b = \frac{R\ T}{P_{sat}\ D\ M_w} \tag{2.51}$$

and where

m = particle mass

ρ_1 = particle density

S = ambient saturation ratio

r = mean aerosol particle radius of section i

M_w = molecular weight of water

i_{fg} = latent heat of water

k_v = vapor thermal conductivity

R = gas constant

T = ambient temperature

P_{sat} = saturation pressure at T

D = diffusivity of water vapor in air

Equations (2.48) through (2.51) can be combined to relate the normalization constant A and the ${}^1\overline{G}_{\ell,w}$ term to the Mason equation:

$$\frac{dm_w}{dt} = \sum_\ell N_\ell \left\langle \frac{dm}{dt} \right\rangle = \sum_\ell Q_\ell \left\langle \frac{1}{m}\frac{dm}{dt} \right\rangle = \sum_\ell Q_\ell \left\langle \frac{4\pi r}{m} \right\rangle \frac{(S-1)}{a+b} = \sum_\ell Q_\ell \, {}^1\overline{G}_{\ell,w} \, A \tag{2.52}$$

where N_ℓ is the number of particles in section ℓ and the angle brackets denote an appropriate sectional average. Therefore, the MAEROS coefficient ${}^1\overline{G}_{\ell,w}$ can be evaluated as an appropriate sectional average of $4\pi r/m$ and A can be taken as the term $(S - 1)/(a + b)$, which is independent of size. Equations (2.49) and (2.52) are consistent if an effective value of the saturation ratio S, which varies through the timestep, is chosen appropriately. A limiting rate on condensation can be estimated from Equation (2.52), using an upper bound on the saturation ratio based on the assumption that all vapor destined to condense exists in the vapor phase at the start of the step. That is,

$$S_{\max} = 1 + \Delta m_w \; / \; m_{v,sat} \tag{2.53}$$

where Δm_w is again the mass of water to be condensed and $m_{v,sat}$ is the mass of water vapor at saturation in the atmosphere. If the required condensation exceeds this limiting rate, A in Equation (2.48) is set to the limiting value, $(S_{max} - 1)/(a + b)$, and the excess water is simply put into the smallest aerosol section, consistent with the assumption that excess water that cannot condense on existing aerosol, structures, or pools condenses by homogeneous nucleation, forming small fog droplets.

Transfer from section to section by growth of aerosols is evaluated implicitly; that is, the ${}^2\overline{G}_{1,w}$ terms are evaluated using end-of-step masses. For condensation, aerosols can only grow, and by definition there can be no growth into the smallest section. This allows the new masses to be evaluated in a single pass from the smallest section to the largest by forward substitution,

$$Q_{1,k}^{n} = \frac{Q_{1,k}^{o+}}{1 + A\,\Delta t\ {}^2\overline{G}_{1,w}} \tag{2.54}$$

$$Q_{\ell,k}^{n} = \frac{Q_{\ell,k}^{o+} + A\ \Delta t\ {}^2\overline{G}_{\ell-1,w} Q_{\ell-1,k}^{n}}{1 + A\,\Delta t\ {}^2\overline{G}_{\ell,w}} \tag{2.55}$$

where $Q_{\ell,k}^{o+}$ is the start-of-step mass for all classes but water, in which case it includes the explicitly calculated condensation. Note that, from a strictly numerical standpoint, no negative masses can be predicted by this equation if there were none at the start of the step.

The treatment of evaporation is very similar to that for condensation. Evaporation within a section is calculated explicitly, and the total is normalized to the change in water mass required by the CVH package, but no rate limit is considered. If one or more explicitly calculated water masses would be negative, they are set to zero and the remaining (positive) masses renormalized to the correct total.

As in condensation, the section-to-section transfers are evaluated implicitly in a single pass, this time from the largest to the smallest. Experience has shown that one further modification is necessary. If the limit and renormalize procedure just mentioned is used, the value of A used for section-to-section transfers out of each section must be made to agree with the effective value of A used for evaporation from that section. This is easily done by defining

$$A_s \Delta t = \frac{Q_{\ell,w}^{o+} - Q_{\ell,w}^{o}}{{}^1G_{\ell,w} Q_{\ell}} \tag{2.56}$$

where A_s is simply the normalization constant A in cases where no dryout occurred.

2.5.2 Fission Product Vapors

The condensation and evaporation of fission product vapors to and from heat structures, pool surfaces, and aerosols is evaluated by the same equations as in the TRAP-MELT2 code [8]. The fission product vapor masses in the control volume atmosphere and condensed on the aerosol and heat structure surfaces are determined by rate equations based on the surface areas, mass transfer coefficients, atmosphere concentration, and the saturation concentrations corresponding to the temperatures of the surfaces:

$$\frac{dM_a}{dt} + \sum_i \frac{dM_i}{dt} = 0 \tag{2.57}$$

$$\frac{dM_i}{dt} = A_i k_i \left(C_a - C_i^s\right) \tag{2.58}$$

where

C_a = M_a / V = concentration of vapor in atmosphere

C_i^s = saturation concentration of vapor in atmosphere at temperature of surface i

M_i = condensed mass of vapor on surface i

V = volume of atmosphere

A_i = area of surface i

k_i = mass transfer coefficient for surface i

and subscript i denotes any heat structure surface, pool surface, or aerosol section.

These differential equations can be solved as in TRAP-MELT2 to yield the following algebraic equations:

$$C_a = M_a / V = \frac{\beta}{\alpha} - \left(\frac{\beta}{\alpha} - C_{a0}\right) e^{-\alpha \Delta t} \tag{2.59}$$

$$M_i = M_{i0} + A_i k_i \left(\frac{\beta}{\alpha} - C_i^s \right) \Delta t - A_i k_i \left(\frac{\beta}{\alpha} - C_{a0} \right) \left(\frac{1 - e^{-\alpha \Delta t}}{\alpha} \right) \tag{2.60}$$

where

$$\alpha = \sum_i A_i k_i / V \tag{2.61}$$

$$\frac{\beta}{\alpha} = \frac{\sum_i A_i k_i C_i^s}{\sum_i A_i k_i} \tag{2.62}$$

and subscript 0 denotes the value at start of the timestep, Δt .

Total sectional areas A_p for aerosols are calculated from the average particle in each section, as derived in Appendix C:

$$A_p = 12\pi \left(\frac{3}{4\pi} \right)^{2/3} \frac{M}{\ln(m_2/m_1)} \left(m_1^{-1/3} - m_2^{-1/3} \right) \tag{2.63}$$

The mass transfer coefficient k_p for aerosols is based on zero slip flow, or Sherwood number = 2.0.

All HS package heat structures are automatically included for condensation and evaporation of fission product vapors unless made inactive through user input on RNDSXXX records. The area of the heat structure in the atmosphere A_w is used to define the net area for fission product vapor interactions. This area is the total heat structure area times the fraction of the heat structure in the atmosphere as determined by the HS package.

Although fission products may condense on pool surfaces, evaporation of fission products residing in control volume pools is not permitted. The fission product vapor location within a phase in a control volume (pool or atmosphere) may change when one phase is no longer present. Any vapor mass associated with a disappearing phase is added to the remaining phase in that control volume.

The mass transfer coefficient for condensation of fission product vapors onto heat structure surfaces, k_w, is calculated based on the mass transfer coefficient, k_{HS}, for water condensation onto a heat structure surface calculated by the HS package, which uses the steam-air diffusivity, $D_{st,a}$:

$$k_w = k_{HS}\, D_{k,g} / D_{st,a} \tag{2.64}$$

The vapor diffusivity for the fission product vapors in the bulk gas, $D_{k,g}$, is calculated from the following equation as presented in Welty, Wicks, and Wilson [22]:

$$D_{k,g} = \frac{1 - y_k}{\sum_n \left(y_n / D_{k,n} \right)} \tag{2.65}$$

where

y_k = mole fraction of trace vapor k

y_n = mole fraction of bulk gas n

$D_{k,n}$ = binary diffusivity of vapor k in gas n

The binary diffusivities are evaluated from the following expression from Bird, Stewart, and Lightfoot [23]:

$$D_{A,B} = 0.0018583 \; \frac{\left[T^3 \left(M_A^{-1} + M_B^{-1} \right) \right]^{1/2}}{P \sigma_{AB}^2 \Omega_{D,AB}} \tag{2.66}$$

with

$D_{A,B}$ = binary diffusivity in cm^2/s

T = temperature in K

P = pressure in atmospheres

M_i = molecular weight in kg/kg-mole

σ_{AB} = collision diameter in Angstroms = $0.5 \left(\sigma_A + \sigma_B \right)$

$\Omega_{D,AB}$ = collision integral = function of kT/ε (see Table B-2 of Reference [23])

The actual calculation of D_{AB} is performed by a model in the Material Properties (MP) package, using data for the collision integral contained in the MP database. Values for the Lennard-Jones potential parameters σ and ε/k for the bulk gases are obtained from the MP database, while values for some of the fission product vapors, obtained from

Reference [23], are stored in RN sensitivity coefficient array 7111 (see Appendix A). Actual values are used for Xe and I_2; other classes are defaulted to values for air due to a lack of information. (The values for the bulk gases are the same ones used for calculation of viscosity in the absence of tabular data; they may be changed through MP input if desired.)

In addition to being used to determine the amount of each material class present as aerosol and as fission product vapor, the vapor pressure is used in the model for condensation and evaporation to determine the saturation concentrations, C_i^s, calculated from the perfect gas law,

$$C_i^s = \frac{P(T_i)M_w}{RT_i} \tag{2.67}$$

The expression for the vapor pressure is

$$\log_{10}(P) = -A/T + B + C\ \log_{10}(T) \tag{2.68}$$

with P and T in units of mm of Hg and K, respectively. The coefficients A, B, and C for each class are stored in sensitivity coefficient array 7110 for different temperature ranges (see Appendix A). Classes for which there are no data are assumed to have a default vapor pressure curve characteristic of a nonvolatile ceramic (zero vapor pressure below 3000 K and the vapor pressure of UO_2 above 3000 K); nondefault vapor pressure coefficients are defined for classes 2 (Cs), 3 (Ba), 4 (I), 5 (Te), 6 (Ru), 7 (Mo), 8 (Ce), 9 (La), 10 (UO_2), 11 (Ag), 12 (Sn), 13 (B_2O_3), and 16 (normally CsI), and class 1 (Xe) is always a vapor. (See the RN Package Users' Guide for details on defining temperature ranges and forcing classes to always be an aerosol or always a vapor.)

For temperatures above a maximum temperature value, T_{max}, the correlation is extrapolated. However, direct use of the correlation outside its range of applicability can return a pressure that decreases with increasing temperature, because C is negative and $C\ \log_{10}(T)$ can dominate $-A/T$. Therefore, the extrapolation uses

$$\log_{10}(P) = -A'/T + B' \tag{2.69}$$

The coefficients A' and B' are derived from the last range coefficient values A, B, and C by demanding that P and dP/dT be continuous at the matching temperature T_{max}. This requires

$$A' = A + C\ \log_{10}(e)T_{\max} \tag{2.70}$$

$$B' = B + C\ \left[\log_{10}(e) + \log_{10}(T_{\max})\right] \qquad (2.71)$$

2.6 Decay Heat Distribution

All decay heat released by radionuclides in a control volume pool is assumed to be absorbed by that pool. None of this decay heat is added directly to any heat structure surface or to the atmosphere of the control volume.

The decay heat released by radionuclides in the control volume atmosphere and from those deposited on the various heat structure surfaces can be apportioned according to user specifications among the volume atmosphere, the surfaces of heat structures in that volume, and the pool surface (if a pool is present). Fractions may also be specified as going to the atmosphere and surfaces of other volumes to simulate decay radiation transmitted through flow paths. Defaults are provided, as discussed below.

Approximately one half of decay heat is generated as gamma radiation and one half as beta radiation. Because typical gaseous atmospheres are nearly transparent to typical gammas and fairly opaque to typical betas, deposition of decay heat in a volume atmosphere results primarily from absorption of beta radiation. (The split and the characteristic energies are not explicitly modeled by MELCOR.) These observations and solid angle considerations led to the default splits suggested by Reference [3]:

Decay Heat from Radionuclides in the Atmosphere	
Atmosphere of current CV	50%
Surfaces of current CV	50%
Atmosphere of other CVs	0%
Surfaces of other CVs	0%
Decay Heat from Radionuclides on Heat Structure Surfaces	
Current Heat Structure	50%
Atmosphere of current CV	25%
Other surfaces of current CV	25%
Atmosphere of other CVs	0%
Surfaces of other CVs	0%

All fractions are independent of the RN class. Those for airborne radionuclides can be changed on a volume-by-volume basis using the RNDHVXXX and RNDHVSXXX input record series. Those for radionuclides on surfaces can be modified similarly, on a surface-by-surface basis, using the RNDHSXXX and RNDHSSXXX input record series.

Decay heat from airborne or deposited radionuclides that is absorbed by surfaces in the same control volume is allocated among the surfaces in proportion to their areas. (Note that for deposited radionuclides the bearing surface is not included.) The areas considered are the portions of heat structure surfaces exposed to the atmosphere, and the surface of

the pool (if a pool is present). If there are no such surfaces, the fraction of decay heat allocated to the surfaces of a control volume is deposited instead in the atmosphere of that control volume.

The fractions specified as going to the local control volume atmosphere (by default or user input) are interpreted as the values appropriate for complete absorption of beta radiation. They must be reduced for small volumes or low densities, where the thickness of the atmosphere is insufficient to permit complete absorption of beta rays. This reduction is by a factor

$$\min\left(\rho_A\, D_{CV}/R_\beta, 1.0\right)$$

where ρ_A is the atmosphere density, D_{CV} is the characteristic dimension for absorption in the control volume, and R_β is the range of a typical beta particle (given in sensitivity coefficient array 7002, with a default value of 1.2 kg/m^2; see Appendix A). D_{CV} has a default value given by the minimum of the cube root of the volume and the square root of the flow area from the CVH database (so as to be reasonable for both tanks and pipes). It can be modified using the RNDHLENXXX input record series.

Any reduction in deposition to the local atmosphere is compensated by proportionate increase in energy distributed to other surfaces in the volume and to the atmosphere and surfaces of other control volumes. (The calculation is bypassed if the sum of these other split coefficients is zero.)

2.7 ESF Models

Models are currently available for the removal of radionuclides by pool scrubbing, filter trapping, and spray scrubbing. These models are described in the following subsections. The normal RN deposition and condensation models described in Sections 2.4 and 2.5 are applied to heat structures used to model ice condensers; see the HS Package Reference Manual for a detailed description of methods used to model ice condensers, including a surface area enhancement factor for radionuclide deposition.

2.7.1 Pool Scrubbing

The pool scrubbing model in the RN package is based on the SPARC-90 code [10]. (The thermal-hydraulic aspects of pool scrubbing are modeled in the CVH package.) Aerosols and iodine vapor are removed by pool scrubbing; the model will also treat organic iodine vapor (CH_3I) but currently it is not included in the MELCOR RN class structure. Decontamination is calculated for those flow paths activated on the FLnnn02 input record (see the FL Package Users' Guide) and for gases evolved from core-concrete interactions

in cavities activated on the CAVnn00 input record (see the CAV Package Users' Guide). By default, the model treats these cases by using the horizontal vent scrubbing option from SPARC-90 along with the flow area provided by the FL package (FLARA on input record FLnnn01) or the flow area calculated by the CAV package. However, the user may override the default venting treatment by providing appropriate input on the RN2PLSXX records. For consistency with the CVH package, pool scrubbing is only calculated if the submerged depth of the flow path is greater than the zero efficiency bubble rise height given in CVH sensitivity coefficient array 4405. The gases evolved from the core-concrete interactions calculated by VANESA are supplemented by an inferred steam flux generated by boiling at the cavity/pool interface. This flux is evaluated by dividing the cavity/pool interfacial heat flux calculated by CORCON by the latent heat of vaporization for water in the pool.

The decontamination factor (DF) is defined as the ratio of the radionuclide mass entering the pool to that leaving, and has a value greater than or equal to unity. However, when the iodine concentration in the pool divided by the equilibrium partition coefficient (discussed in Appendix F) exceeds the concentration of iodine vapor in the gas entering the pool, then iodine vapor scrubbing cannot occur and the corresponding decontamination factor must be equal to unity. (Furthermore, MELCOR is not structured to calculate iodine stripping from the pool under these conditions, so iodine removal from the pool is not considered.) If the iodine concentration in the bubbles is significant (i.e., exceeds a threshold value implemented in sensitivity coefficient array 7159 with a default value of 10^{-6} moles/cm^3), a message is issued once per calculation by the scrubbing routine to inform the user of this condition.

The gas flow through the pool is described in two overlapping regions. In the vent exit region, the injected gas forms large, unstable globules. The initial size of the globule depends on the vent type and the noncondensible gas flow rate. As the globules rise they begin to break up into swarms of smaller bubbles. It is assumed that break-up is complete by the time the globule rises a distance equal to twelve times its initial diameter. In the swarm rise region, bubbles continually coalesce and redisperse during their erratic ascent. On average, however, it is assumed that they can be represented by oblate spheroids of a constant, stable size with the flatness given by a correlation depending on bubble size. The rise velocity of individual bubbles in the swarm relative to the liquid is given by a correlation depending on bubble size, also, and remains constant since the size remains constant. The swarm rise velocity represents the volumetric average velocity on a cross section of the swarm. Bubbles in the center rise faster than swarm periphery bubbles, and the swarm rise velocity increases as the swarm ascends because the volumetric flow rate of the swarm increases as the gas expands under a decreasing static head. In the SPARC-90 model, however, the swarm rise velocity is assumed to remain constant with a value given by the average of the value at the vent exit depth and the value at the pool surface. The bubbles in the swarm multiply (i.e., the number density increases) as the expanding bubbles split to preserve their stable size. The viscous shear of the liquid in

relative motion past the bubble causes the bubble surface and interior to move in a top-to-bottom rotation.

It is assumed that the inlet gas comes into thermal equilibrium with the pool almost instantaneously in the vent exit region. When this results in steam condensation in the inlet gas, aerosol particles and iodine vapors are removed in proportion to the reduction in the volumetric flow rate. Particle capture also occurs when the injection velocity is large because inertia forces the particles into the front boundary of the rapidly decelerating globules. For multihole vents with small orifices, centrifugal, diffusional and gravitational deposition are evaluated during gas injection because they are significant at the large velocities achieved. Details of globule formation and vent exit region scrubbing are given in Appendix D.

Scrubbing in the swarm rise region is evaluated by numerically marching through the region in several discrete spatial steps. At the beginning of each step, the fraction of the inlet gas that is still contained in the initial globule is determined. The remainder is assumed to be contained in bubbles. During each step the thermal hydraulic conditions within the bubbles are updated and used to evaluate the incremental removal of particles and iodine vapors during the step. The particle removal mechanisms modeled in the bubble include centrifugal and diffusional deposition and gravitational sedimentation. These mechanisms generate a flux of particles toward the bubble surface, where they are removed by absorption into the pool. The particle flux may be hindered by a flux of water vapor into the bubble, if evaporation is occurring at the bubble surface. Conversely, condensation onto the particles within the bubble because of supersaturation from bubble expansion will enhance particle removal. The vapor removal mechanism is diffusion, which also may be hindered if there is an evaporative flux into the bubble. The removal factor for each particle size and iodine vapors during the step is given by:

$$DF_{SR,i} = \frac{1}{f_{gl} + \left(1 - f_{gl}\right) / DF_{BB,i}} \tag{2.72}$$

where

$DF_{BB,i}$ = removal factor inside the bubble

f_{gl} = fraction of inlet gas still in the inital globule

The cumulative removal factors for each particle size and iodine vapors in the swarm rise region are given by the product of the incremental removal factors at each step. Details of transient bubble behavior and particle scrubbing in the bubbles are given in Appendix E. Details of iodine scrubbing in the bubbles are given in Appendix F.

The overall removal factor for each particle size and iodine vapors in the vent exit and swarm rise regions is given by:

$$DF_{OV,i} = DF_{EC} \bullet DF_{II,i} \bullet DF_{ER,i} \bullet DF_{SR,i} \tag{2.73}$$

where

DF_{EC} = DF from steam condensation in the vent exit region

$DF_{II,i}$ = DF from inertial impaction (of particles only) in the vent exit region

$DF_{ER,i}$ = DF from centrifugal, diffusional and gravitational capture (of particles only) in the vent exit region

$DF_{SR,i}$ = cumulative DF in swarm rise region

The overall removal factor for all particle sizes is obtained by dividing the sum of the inlet mass rates over all sizes by the sum of the outlet mass rates (the inlet rates for each size divided by the overall removal factor for that size) over all sizes:

$$DF_{OV,part} = \frac{\sum_{i=1}^{NBINS} \dot{m}_{part,i}}{\sum_{i=1}^{NBINS} \left(\frac{\dot{m}_{part,i}}{DF_{OV,i}} \right)} \tag{2.74}$$

2.7.2 Filters

The MELCOR RN package contains a simple filter model. When aerosols and vapors are transported through flow paths with the bulk fluid flow of pool and/or atmosphere calculated by the CVH package, some fraction of the transported RN materials may be removed by the action of filters in the flow path. A single filter can remove either aerosols or fission product vapors, but not both. However, a flow path can contain more than one filter. The efficiency of each filter is defined by decontamination factors, specified by user input. By default, a single decontamination factor is applied to all RN classes *except* water, for which the default DF is 1.0. Additional user input may be used to modify the DF on a class-by-class basis, *including the water class*. The parameters for the filter characteristics are specified on the RN2FLTXXYY input record series.

A maximum loading may be specified for each filter; when this loading is reached, no further RN materials will be removed (i.e., the DF is set to unity).

The effect of filter loading on the flow resistance of the associated flow path may be modeled through user input. This requires construction of a control function to link the laminar loss coefficient for the flow path (SLAM, input on segment record FLnnnSk; see the FL Package Users' Guide) to the filter loading. The filter loading may be obtained from one or more of the RN2-AMFLT or RN2-VMFLT control function arguments described in Section 5 of the RN Package Users' Guide.

The decay heat energy from radionuclides deposited on filters is given to the downstream control volume according to the vapor flow direction.

2.7.3 Sprays

The containment spray model used in MELCOR is the same as that in the HECTR code. The MELCOR Containment Sprays (SPR) package, which calculates the thermal-hydraulic behavior associated with spray systems, is coupled to the RadioNuclide package for the calculation of aerosol washout and atmosphere decontamination by the sprays.

The SPR Package Reference Manual describes the thermal-hydraulic modeling of the spray systems. To summarize here, the spray droplets are assumed to be spherical and isothermal and to fall through containment at their terminal velocity without a horizontal velocity component. Droplet heatup and cooldown in a steam environment are modeled using a correlation for forced convection heat transfer coefficients. Similarly, evaporation and condensation are modeled using a correlation for mass transfer coefficients. A standard integrator is used to integrate these transfer rates over the fall height of the spray droplet to obtain the final droplet mass and temperature. By comparing the droplet mass and temperature at the bottom of the compartment to the inlet conditions, the heat and mass transfer to a given droplet is computed. Total heat and mass transfer rates are calculated by multiplying the rates for one droplet by the total number of droplets of that size and summing over all droplet sizes.

The SPR-RN interface may produce nonphysical results if the SPR package is required to make multiple passes (numerically) through the same control volume on a given timestep. Therefore, the user is strongly encouraged to avoid this situation by limiting the spray activity to a single drop size in each spray train. The user must also ensure that only one spray train passes through each control volume. These restrictions are necessary only when the SPR and RN packages are used at the same time.

The particulate removal by sprays is a mechanistic treatment of removal processes, closely coupled to the thermal-hydraulic behavior calculated by the spray package. The user is cautioned to use a single drop size and a single spray train per volume because of the method by which the RN removal calculation is "piggybacked" onto the Spray Package thermal-hydraulic calculations. Specifically, the thermal-hydraulic stepwise integration over the spray train height is made first, then the RN removal processes are calculated by a simple trapezoidal integration over the step, using the appropriate end-of-interval values.

Because each droplet size is integrated over the full height of fall separately, there exists the possibility of competing radionuclide removal by differing drop sizes and competing removal by different spray trains.

The particulate removal from sprays is modeled as a first-order rate process,

$$\frac{dM_k}{dt} = -\lambda_{k,i} M_k \tag{2.75}$$

where

M_k = mass of class k

$\lambda_{k,i}$ = rate constant, class k, droplet size i

The actual physical removal processes for vapors and aerosols are different and therefore different rate constants, λ, are associated with each process.

Vapor removal by adsorption is calculated using a stagnant film model for the adsorption efficiency. The vapor removal is calculated as an injection spray removal rate; no recirculation of spray liquid is considered. The expression for the rate constant is [24, 25, 26]:

$$\lambda_{k,i} = \frac{F_i E_{k,i} H}{V} \tag{2.76}$$

where

F_i = volumetric flow rate for droplets of size i

$E_{k,i}$ = adsorption efficiency for vapor class k

H = partition coefficient for partition of the vapor between spray water and gas

V = volume of control volume

The vapor absorption efficiency is given by the expression [27]

$$E_{k,i} = 1 - \exp\left[-\frac{6\ k_g\ t_e}{2 r_i \left(H + k_g / k_\ell\right)} \right] \tag{2.77}$$

where k_g, the gas boundary layer mass transfer coefficient, is calculated using the Ranz and Marshall approximation [28] to the Frossling equation [29],

$$k_g = \frac{D_{k,gas}}{2 r_i} \left(2.0 + 0.060\ \mathrm{Re}^{1/2}\, Sc^{1/3}\right) \tag{2.78}$$

and k_ℓ, the liquid boundary layer mass transfer coefficient, is calculated using Griffith's approximation for diffusion in a rigid drop [30],

$$k_\ell = \frac{\pi^2\ D_{k,\mathrm{H_2O}}}{3 r_i} \tag{2.79}$$

In these equations,

r_i = drop radius

t_e = drop exposure time

$D_{k,gas}$ = diffusivity of vapor *k* through bulk gas

$D_{k,\mathrm{H_2O}}$ = diffusion constant for vapor *k* in liquid water

Re = Reynolds number, $2 \rho_g v_d r_i / \mu_g$

Sc = Schmidt number, $\mu_g / \rho_g D_{k,gas}$

v_d = drop velocity

Under LWR accident conditions, iodine may exist as a vapor over relatively long time periods in containment pressure/temperature conditions. Other materials have low vapor pressures at accident conditions that preclude their extended existence as vapors; that is, they will condense to aerosol forms quickly. The RN input record series RN2SPRXX allows the user to specify a limit on iodine adsorption by spray droplets using a partition coefficient. The partition coefficient for iodine, defined as the equilibrium ratio of the iodine density in the liquid to its density in the gas,

$$H = \rho_{\ell,eq} / \rho_{g,eq} \tag{2.80}$$

is specified by the user for sprays containing different additives, with various recommended values ranging from 500 to 100,000 [31] listed in the RN Package Users' Guide.

Aerosol removal is calculated primarily by inertial impaction and interception; diffusiophoresis and diffusion effects are also included. No droplet interactions are considered. Impaction and interception are the primary removal mechanisms as long as droplet radii are in the 10 – 100 micron size range. From 1 – 10 microns diffusiophoresis becomes an important contributor; diffusion only becomes important for droplets with radii < 0.1 micron. The expression for the rate constant is [31]

$$\lambda_{k,i} = \frac{3F_i h E_{i,j}}{4Vr_i} \tag{2.81}$$

where F_i, V, and r_i are as defined before, h is the fall height of the drops, and $E_{i,j}$ is the efficiency of collection of aerosol particles in size section j by drops of size i.

For viscous flow around a sphere, the collection efficiency for interception (denoted by subscript *In*) is given by the expression [32]

$$\varepsilon_{In,vis} = (1+I)^2 \left[1 - \frac{3}{2(1+I)} + \frac{1}{2(1+I)^3} \right] \tag{2.82}$$

where $I = r_p / r_d$ and r_p and r_d are the radii of the particle and the drop, respectively.

For potential flow around a sphere, the collection efficiency for interception is given by the expression [32]

$$\varepsilon_{In,Pot} = (1 + I)^2 - (1 + I)^1 \tag{2.83}$$

For potential flow around a sphere, the collection efficiency for inertial impaction (denoted by subscript *Im*) is given by the expression [33]

$$\varepsilon_{Im,Pot} = \left[\frac{Stk}{Stk + 0.5} \right]^2 \tag{2.84}$$

for $Stk \geq 0.2$, is zero for $Stk \leq 0.0834$, and is given by interpolation for $0.0834 < Stk < 0.2$. For viscous flow around a sphere, the collection efficiency for inertial impaction is given by the expression [32]

$$\varepsilon_{Im,Vis} = \left[1 + \frac{0.75 \log_e (2\ Stk)}{Stk - 1.214}\right]^{-2} \tag{2.85}$$

for *Stk* > 1.214, and is zero otherwise. *Stk* is the Stokes number,

$$Stk = \frac{2 r_p^2 \rho_p (v_d - v_p)}{9 \mu r_d} \tag{2.86}$$

where v_d and v_p are the terminal settling velocities of the drop and particle, respectively, and μ is the bulk gas viscosity. An interpolation scheme from Reference [33] is used to combine the potential and viscous efficiencies for both interception and inertial impaction:

$$\varepsilon_x = \frac{\varepsilon_{x,Vis} + \varepsilon_{x,Pot}(\mathrm{Re}/60)}{1 + (\mathrm{Re}/60)} \tag{2.87}$$

where Re is the drop Reynolds number and subscript *x* is either *In* (interception) or *Im* (inertial impaction).

The collection efficiency due to diffusion is given by the expression [25]

$$\varepsilon_{diff} = 3.02\,\mathrm{Re}^{1/6} Pe^{-2/3} + 1.14\,(\mathrm{Re}/Pe)^{1/3} I + 0.57\,\mathrm{Re}^{1/3} I^2 \tag{2.88}$$

where *Pe* is the Peclet number, $2r_d(v_d - v_p)/D$.

The collection efficiency due to diffusiophoresis is given by the expression

$$\varepsilon_{diffusio} = \frac{4}{3} \frac{r_d}{F\ h} \left[\frac{M_s^{1/2}}{X_s\ M_s^{1/2} + X_g M_g^{1/2}}\right] \frac{W_s}{c M_s} \tag{2.89}$$

where W_s is the mass condensation rate of steam on drops, *M* is molecular weight, *X* is mole fraction, *c* is the molar concentration of bulk gases, and subscripts *s* and *g* refer to steam and noncondensible bulk gases, respectively.

Finally, the collection efficiencies for different processes are combined using the following expression

$$E_{i,j} = 1 - \prod_k \left(1 - \varepsilon_{ijk}\right) \tag{2.90}$$

where subscript *k* refers to the collection process.

2.8 Fission Product Chemistry

Chemistry effects can be simulated in MELCOR through the use of *class reactions* and *class transfers*. The class reaction process uses a first-order reaction equation with forward and reverse paths. The class transfer process, which can change the material class or location of a radionuclide mass, can be used to simulate fast chemical reactions. With these two processes, phenomena including adsorption, chemisorption, and chemical reactions can be simulated.

Note: Only fission product vapors are considered in the chemistry models.

2.8.1 Class Reactions

The reaction process model in MELCOR is a first-order reversible reaction for a class going from state *C* in the gas-phase to state C_1 on a surface, or

$$\frac{dM_c}{dt} = -\left(\frac{k_m \ A \ / V}{k_m A \ / V + k_f} \right) \left(k_f M_C - k_r M_{C1} \right) \tag{2.91}$$

where

k_m = mass transfer rate constant for the process, based on the mass transfer coefficient calculated by the HS Package, (m/s)

k_f = forward reaction rate constant from user input, (s^{-1})

k_r = reverse reaction rate constant from user input, (s^{-1})

A / V = surface-to-volume ratio, where the surface area is that for the reaction and the volume is that of the control volume (m^{-1}).

The mass transfer rate constant is calculated in the same manner as the vapor condensation/evaporation diffusivity given in Section 2.5.

The solution technique is the same as for vapor condensation/evaporation under the assumption that the mass of *C*1 does not change during the timestep. This assumption

avoids solving a differential equation and allows the use of the same algebraic solution given in Section 2.5.

Alternatively, if the user specifies the use of a deposition velocity instead of the forward and reverse reaction rate constants,

$$\frac{dM_C}{dt} = -V_d (A / V) C = -\frac{dM_{C1}}{dt} \tag{2.92}$$

where V_d is the user input reaction deposition velocity in m/sec.

The reaction only occurs in user-specified control volumes and depends on the availability of the various classes as determined by the user input reaction stoichiometry. The first "from" class in the reaction must be in the vapor phase, while all the other specified classes must be deposited on the surface when the reaction occurs. Surfaces that can undergo reactions include heat structures, the pool surface, and aerosol surfaces as specified by the user. A flag to specify whether the reaction still occurs when a water film is present is also available. At the present time, water mass should not be used in the class reaction model.

In addition to the masses, reaction energy can also be specified for both the forward and reverse directions. The energy is in terms of the mass of the first "from" reacting class. This energy is added to the atmosphere in the case of reaction with aerosols, to the pool for a pool reaction, and to the heat structure if a surface reaction occurs.

2.8.2 Class Transfers

Mass transfers between classes may be accomplished by the transfer mechanisms. The user may change the class and location of aerosols and/or vapors in an arbitrary fashion. Therefore, this feature must be carefully used.

A stoichiometric reaction is specified, and the permitted control volumes and "from" and "to" states are given. The permitted states are aerosols or condensed vapors on a given surface of a heat structure, or aerosols or vapors in either the atmosphere or pool. A flag to determine if the transfer will proceed with a water film present is also available. Water should not be used in the class transfer model.

The mass transfer rate is given by the user as is the energy transfer information. The masses are changed as follows:

$$M_{from,\,t+\Delta t} = M_{from,\,t} - \frac{dM}{dt}\Delta t \tag{2.93}$$

$$M_{to,\ t+\Delta t} = M_{to,t} + \frac{dM}{dt}\Delta t \qquad (2.94)$$

where *dM*/*dt* is the user-specified mass transfer rate. Thus, with this option, aerosols of Class A in the pool may be, for example, changed into condensed vapors of Class B on a heat structure. This model is used for fast reactions with the "from" and "to" state generally the same.

2.8.3 Example

As an example of both class reactions and class transfers, consider the adsorption of CsI on a surface with a known deposition velocity which is then transformed immediately to CsOH plus HI when adsorbed water is present. After the transformation, the revaporization of CsOH is delayed until the surface temperature reaches T_1 while the HI revaporization is simply mass transfer limited. In this case, CsI, CsOH, and HI are separate material classes, and the reaction diagram can be written as

$$\begin{array}{rcl} CsI(g) & \rightarrow & CsI(ad) \\ & & \downarrow\ H2O \\ CsOH(g) & \leftrightarrow & CsOH(ad) \\ & & +\ (\text{depends on } T_1) \\ HI(g) & \leftrightarrow & HI(s) \end{array}$$

where (*g*), (*ad*), and (*s*) are gaseous, adsorbed, and solid states, respectively.

This reaction can be simulated by the RN package by the following sequential class reactions and transfers:

CsI(g) → CsI(ad)	rate constant for adsorption is supplied through input
CsI(ad) → CsOH(ad) + HI(s)	instantaneous and complete transfer between classes when water is present. **Note that the water mass is not included in the model; water mass is not explicitly conserved.**
CsOH(g) → CsOH(ad)	rate constant for adsorption supplied or condensation limited
CsOH(ad) → CsOH(g)	reaction with zero rate constant below T_1
	positive value or instantaneous above T_1
HI(s) ↔ HI(g)	controlled by condensation/evaporation

2.9 Chemisorption on Surfaces

The chemisorption model is implemented as a finite-difference version of the equations in [34]. The relevant radionuclide classes that are chemisorbed are removed from the vapor mass arrays and stored in chemisorption arrays. The chemisorption arrays correspond to six chemisorption classes. In accounting for radionuclide mass and decay power, the chemisorption classes are mapped back to the corresponding radionuclide class, so chemisorption output edits are ordered by the radionuclide class rather than by chemisorption class. Chemisorption shows up in the output edits as an additional column in the radionuclide mass edits.

2.9.1 Implementation

There are six chemisorption classes corresponding to the first six chemisorption equations in Table 1 of [34]. There is a mapping array that establishes the correspondence between the chemisorption classes and the radionuclide classes. The radionuclide classes are CsOH (2), I_2 (4), and the user-defined class used to model CsI (usually 16). There is no HI radionuclide class, and hence chemisorption class 5 is mapped to radionuclide class 4. There also is an array that establishes the type of surface material for the chemisorption class; at present, this only contains mapping for stainless steel and Zircaloy, although this could be extended by adding more materials to the database or by implementing a method of mapping between user-defined materials and the chemisorption classes.

The chemisorption rate equation is

$$\frac{dM_{ij}}{dt} = A_i k_{ij} C_j \tag{2.95}$$

M_{ij} = mass of species j chemisorbed on surface i (kg)

A_i = area of surface i (m^2)

k_{ij} = chemisorption coefficient of species j on surface i (m/s)

C_j = concentration of species j in atmosphere (kg/m^3)

The mass chemisorption coefficient k_{ij} is temperature dependent and is given as

$$k_{ij} = a_{ij} e^{-E_{ij}/RT_i} \tag{2.96}$$

where

a_{ij} = chemisorption coefficient for species j on surface type i (m/s)

E_{ij} = activation energy for species *j* on surface type *i* (J/kg)

T_i = temperature of surface *i* (K)

R = universal gas constant (8314 J/kg-K)

As implemented, a finite-difference equation of the form

$$M_{ij}^{n} = M_{ij}^{0} + \Delta t\ A_i k_i(T_i) C_j \tag{2.97}$$

is used to advance the chemisorption equations in time. These equations are applied sequentially in each control volume, for each surface, for each chemisorption class. After all equations are applied in a given volume, the total chemisorbed for each vapor radionuclide class is checked to ensure that the total is not greater than the total vapor mass; the chemisorbed masses for the current timestep are reduced by the ratio of vapor mass to chemisorbed mass if this occurs. The chemisorbed masses are then subtracted from the corresponding radionuclide vapor mass to complete the timestep.

2.9.2 Comparison to Exact Solution

An exact solution to the chemisorption equations can be found over a timestep for comparison to the numerical solution given above. Briefly, noting that the change in mass of a given species chemisorbed on a given surface is the same as the negative change in the species in the vapor phase, that the vapor concentration is the vapor mass divided by the component volume, and that the sum of the changes over all surfaces is the total change in vapor mass, the chemisorption equations can be summed and written in terms of the vapor species mass as

$$\frac{dM_j}{dt} = -\frac{M_j}{V} \sum\nolimits_i k_{ij} A_i \tag{2.98}$$

Defining an effective chemisorption rate for species *j* as

$$(kA)_j = \frac{1}{V} \sum\nolimits_i k_{ij} A_i \tag{2.99}$$

The solution to the above equation is

$$M_j(t) = M_j^0 e^{-(kA)_j} \tag{2.100}$$

where

M_j^0 = vapor mass at time zero (kg).

If we apply the exact equation over a timestep and expand in a Taylor series about the beginning of the timestep,we have

$$M_j = M_j^0\left[1-\Delta t(k\,A)_j + \ ...\right] \tag{2.101}$$

after dropping higher powers of the timestep. This can be compared to the result of applying the finite-difference equations, which can be written as the sum also:

$$M_j = M_j^0\left(1-\Delta t\frac{1}{V}\sum\nolimits_i k_{ij}A_j\right) = M_j^0\left[1 - \Delta t(kA)_j\right] \tag{2.102}$$

Comparison of the two above equations shows that the finite-difference result is the same as the Taylor series expansion of the exact solution carried out through linear terms of the timestep. At this point, it might be asked, why not use the exact solution? This is not done because this is an exact solution for the change in the vapor mass, not the change in chemisorbed mass for each surface. The change in chemisorbed mass for each surface in the control volume cannot be backed out of the vapor solution.

An exact solution for each surface could be formed, given the assumption that the vapor mass remains constant over the timestep; these could then be summed, leading to an equation for vapor mass involving the sum of the exponents, rather that the exponential of the sum. When expanded in a Taylor series, this results in the same equation as the above equation.

The above expansion in Taylor series gives a criterion for the accuracy of the solution:

$$\frac{k_{ij}A_i}{V}\Delta t << 1 \tag{2.103}$$

The chemisorption coefficients are much less than 1, barring user input error (the largest coefficient, CsOH on stainless steel, is about 0.01 at 2500 K). The ratio A_j/V is less than 1 provided $V > 1$ m^3; for typical MELCOR timesteps of 1 to 5 s, the lower limit on V for the above inequality to hold is about 1 cc, so it appears that the above will be true except for very small volumes.

2.9.3 Implementation Restrictions

As implemented, there is no provision for revaporization of chemisorbed species. Chemisorbed species will thus stay on the absorbing surface. The first six chemisorption equations listed in the design report, Table 1, are implemented as the default classes in the model, because the deposition coefficients for tellurium, rows 7 and 8 in Table 1, are zero. Also, the model is set up to use the materials in the MELCOR material properties database as surface materials. As presently coded, surfaces consisting of user-defined materials cannot be made active for chemisorption because there is no method to relate them to the chemisorption classes. Also, the database does not contain Inconel, which means that only chemisorption of CsI, CsOH, HI, and I_2 on stainless steel and Zircaloy can occur. The coding framework is set up to use Inconel if it is added to the database in the future.

As noted in [39], there was no trace of iodine when CsI was chemisorbed on stainless steel. This means that, realistically, the iodine mass from the CsI should be transferred to the HI or I_2 class when chemisorbing. In the present model, the iodine from the chemisorbed CsI is transferred to the condensed iodine class, so that it will be released on the next timestep. Because the CsI chemisorbed class is mapped to the CsI vapor class, and this class is treated separately in MELCOR from the Cs and iodine element classes, the chemisorbed Cs is transferred to the corresponding chemisorbed CsOH class (there currently are two each, for stainless steel and Inconel surfaces). This has two consequences: the CsI chemisorbed class is always zero, with the Cs showing up in the CsOH class, and the CsOH class must be active if the CsI class is active (this is the default).

2.10 Hygroscopic Aerosols

Aerosol particles that are soluble in water exhibit hygroscopic properties such that they can absorb moisture from an atmosphere with relative humidity less than 100%. This effect will lead to a growth of the particle size as water vapor condenses onto the soluble particle. An important consequence of this growth in size (and mass) is an increase in the gravitational settling rate, and the subsequent depletion of airborne fission product aerosols.

The hygroscopic model in MELCOR is based on the Mason equation describing the diffusion of water vapor molecules to the surface of an aerosol particle, and the conduction of the latent heat of vaporization away from the particle and to the bulk atmosphere. The model presented here includes the solubility (hygroscopic) effect. In addition, the Kelvin effect, (surface tension) as well as noncontinuum (free molecule) effects, both of which are important for very small particle sizes, are considered.

In MELCOR 1.8.5, some improvements to the earlier MELCOR 1.8.4 implementation of the hygroscopic effect are included. Principally these include an updated and generalized method for calculating the chemical activity of the soluble particle, and a means of

calculating a mean hygroscopic effect that considers the fact that not all aerosol materials are soluble and that multi-component aerosols can be comprised of varying proportions of soluble and non-soluble materials.

2.10.1 The Mason Equation for Particle Growth

The Mason equation [35] describes the rate of condensation or evaporation of water on an aerosol particle of radius *r* as:

$$\frac{dr}{dt} = \frac{1}{r}\frac{(S - S_r)}{a + b} \tag{2.104}$$

where,

$$S_r = A_r \cdot \exp\left(\frac{2M_w\sigma}{RT_\infty\rho_w r}\right). \tag{2.105}$$

In the Mason equation, S is the atmosphere saturation ratio, or relative humidity and S_r is the effective saturation ratio at the particle surface. *(Note to reader: a subscript "r" from here on indicates that the quantity is size or radius dependent.)* The term (S -S_r) is the driving potential for condensation or evaporation. If the difference is positive, condensation will occur and if the difference is negative, evaporation takes place. The S_r term is a function of the chemical activity of the solution, A_r, which varies with the concentration of the solute (dissolved solid) within the solvent (water). The exponential term represents the Kelvin effect which resists condensation for small particles due to surface tension effects.

In Eq. (2.104), the terms *a* and *b* determine the time constant for the particle growth rate and are defined as:

$$a = \left(\frac{\Delta h_f^2 M_w \rho_w}{RT_\infty k_a^*}\right) \tag{2.106}$$

$$b = \left(\frac{RT_\infty \rho_w}{D_v^* M_v p_{sat}(T_\infty)}\right). \tag{2.107}$$

The term *a* accounts for the thermal conduction of the latent heat associated with condensation from the particle to the atmosphere, and the term *b* accounts for the diffusion of water vapor from the atmosphere to the particle surface. The other terms are defined in the following list of variables.

D^*_v = effective vapor diffusion coefficient

k^*_a = effective thermal conductivity of atmosphere
M_w = molecular weight of water
T_∞ = bulk atmosphere temperature
$P_{sat}(T_\infty)$= saturation pressure of bulk atmosphere gas
R = gas constant
r = particle radius
S = atmosphere saturation ratio (RH/100)
S_r = saturation ratio at particle surface
ρ_w = density of water
Δh_f = heat of vaporization of water
σ = water surface tension

The activity, A_r, is a function of the concentration of the solute and is the dominant term in the driving potential for condensation or evaporation, S_r. In the MELCOR 1.8.4 [36] implementation, the activity was estimated using the van't Hoff formula as follows:

$$A_r = \frac{1}{1+\sum_i \frac{I_i n_i}{n_w}} \tag{2.108}$$

where n_i is the moles of solute i, n_w is moles of water, and I_i is the van't Hoff ionization constant for solute i. An important limitation in the 1.8.4 model was the fact that the sum in Eq. (2.108) in effect was "simplified" by assuming that all aerosols were soluble and all had the same ionization factor. Hence, the effective form for calculating activity in MELCOR 1.8.4 was:

$$A_r = \frac{1}{1+\frac{I_s n_s}{n_w}} \tag{2.109}$$

where the subscript "s" refers to soluble aerosol (and all aerosols were considered soluble). In the present MELCOR 1.8.5 model, a generalized and more contemporary form for the activity is used as follows:

$$A_r = \exp\left[-\sum_i \frac{\nu_i n_i}{n_w}\right] \tag{2.110}$$

where,

n_s, n_i = moles of dissolved solute in wet particle (may be less than total)

n_w = moles of water on wet particle

v_i = ionization factor for solute molecule (usually 2).

Note that Eq. (2.108) constitutes a linear approximation of Eq. (2.110) for dilute solutions. The van't Hoff factors provided some correction to the linearization for concentrated solutions. In Eq. (2.110) the term ν_i represents the number of ions formed when the solute becomes dissolved. This value is normally 2. The form for activity in Eq. (2.110) is more commonly encountered in chemistry texts describing the solute effect and is similar to that used in the CONTAIN [37] model for hygroscopic growth. Additionally, the present activity form estimates a *net* activity that is a mole weighted average of all aerosol materials within a given size range - soluble and insoluble. Finally, the value of n_i in the present model is limited by the saturation solubility of the aerosol component *i*. The importance of the revised activity formula is as follows. If the aerosol materials are insoluble or of low solubility, the aerosol will exhibit low hygroscopic behavior, and if the proportion of soluble materials in the aerosol composition is large, then a proportionally larger hygroscopic effect will result. This replaces the "all or none" treatment that was present in the MELCOR 1.8.4 model.

The activity term, A_r, is a function of the wet particle radius since, as the particle grows by condensation of water, the concentration of the solute decreases. When the soluble particle is virtually dry, any water on the drop acquires a concentration of dissolved solute that is limited to the maximum solubility of the solute (that is, the solution is saturated with solute). At this point the chemical activity is at its lowest value, and as a result, the driving potential, S-S_r, is at it's highest value. Until sufficient water is acquired to completely dissolve the aerosol solid material, the activity remains at this minimum value. However, after this point the concentration of the solute begins to drop below the saturation value, resulting in an increase in the activity. When infinitely dilute, the activity approaches 1. In general, the value of S_r is dominated by the activity. As the particle acquires more water, the value of S_r increases thereby increasing the atmospheric humidity necessary to drive further condensation.

2.10.2 Transition Regime Corrections to the Mason Equation

The particle growth rate equations (2.104) - (2.107), make use of *effective* values for the air thermal conductivity and the diffusion coefficient for water vapor molecules in moist air. These effective values approach the nominal conductivity and diffusion coefficient values when the aerosol particle radius is large in comparison to the mean free path of the water vapor molecules. However, when the aerosol particle radius is on the order of the vapor molecule mean free path, these factors introduce correction terms to the otherwise continuum regime Mason model. Based on the derivation presented in Prupracher and Klett [35], the effective values of thermal conductivity and diffusion coefficient are determined by:

$$k_a^* = \frac{k_a}{\left(\frac{r}{r+\Delta_T}\right)+\left(\frac{k_a}{r\,\alpha_T\,\rho_a\,c_{p,a}}\left(\frac{2\pi\,M_a}{R\,T_a}\right)^{1/2}\right)} \quad (2.111)$$

$$D_v^* = \frac{D_V}{\left(\frac{r}{r+\Delta_V}\right)+\frac{D_V}{r\,\alpha_C}\left(\frac{2\pi M_a}{RT_a}\right)^{1/2}} \quad (2.112)$$

where

α_c	=	0.036, the condensation coefficient,
α_T	=	0.7, thermal accommodation coefficient,
$c_{p,a}$	=	atmosphere constant pressure specific heat,
λ	=	vapor molecular mean free path,
Δ_V	=	vapor jump distance $\approx 1.32\lambda$,
Δ_T	=	thermal jump distance $\approx \lambda$, and
M_a	=	atmosphere molecular weight.

2.10.3 MELCOR Solution to the Mason Equation

In the MELCOR implementation of the Mason expression, Eq.(2.104) is rewritten as

$$\frac{dr^2}{dt} = \frac{2\cdot(S - S_r)}{a+b} \quad (2.113)$$

which, when expressed in an implicit backwards difference form becomes:

$$\left(r_{new}^2 - r_{old}^2\right) = \frac{2\cdot(S - S_r)}{a+b}\cdot\left(t_{new} - t_{old}\right) \quad (2.114)$$

where all of the right hand side terms are evaluated at the end of time step conditions. A zero-finder routine is used to solve for the new value of r^2 that results in a value for S_r satisfying Eq. (2.114). This numerical method is fast, stable and the small amount of "undershooting" that results from the backward difference is inconsequential in that the characteristic time associated with Eq.(2.113) attaining steady state is short in comparison to a typical MELCOR time step.

2.10.4 User Suggestions Concerning Use of the Hygroscopic Model

MELCOR uses Eq.(2.114) to predict the growth of a representative particle in each of the size sections, and from this determines a section to section mass transfer that reflects this growth. MELCOR uses MAEROS to perform other aerosol dynamics calculations including agglomeration and deposition. Understanding the overall model requires understanding a little about MAEROS. The user is encouraged to review the sections in this manual pertaining to the MAEROS model. For convenience, the following review is given. MELCOR of course uses a ***Class*** grouping to represent fission product species which have common physical/chemical characteristics such as volatility. MELCOR's aerosol mechanics model (MAEROS) recognizes and operates on the aerosol portions of these fission product (radioactive and non-radioactive) classes. For the purposes of performing more economic aerosol mechanics calculations, MELCOR allows the user to define aerosol ***Components***, which are groupings of one or more fission product ***Classes***. These components are allowed to have distinct size distributions. The size distributions are characterized by the amount of aerosol mass within a range of aerosol particle sizes. These size ranges are referred to as ***Sections***, or sometimes as size bins. MAEROS homogenizes the section populations of aerosol *classes* that are members of the same aerosol *component*, even if the user sources in the classes with different size distributions.

The hygroscopic growth model operates on the section populations without any consideration of the component definition. That is to say that all particles of all RN classes within a given *section* (regardless of their component assignment) are used to determine the mean activity using Eq. (2.110), which in turn is used to determine particle growth by condensation. As a result, all aerosol mass associated with all radionuclide *classes* that reside in a given size *section* are transferred to larger (or smaller) size sections proportionally by the hygroscopic growth routines.

This means that non-hygroscopic particles residing in a size section that is dominated by hygroscopic particles will be moved to different size sections along with their hygroscopic companions, and conversely, hygroscopic particles residing in a size section that is dominated by non-hygroscopic particles will be retained in the section to the extent determined by their non-hygroscopic companions. However, if hygroscopic and non-hygroscopic particles reside in different size sections (which can only be represented by MAEROS if they are assigned to different aerosol components), the two particle populations will behave independently. The hygroscopic particles will grow or shrink, depending on the relative humidity, while the non-hygroscopic ones will remain the same size (after losing any water that they may have contained). This makes it important that water and non-water aerosol components be assigned to different aerosol classes. The MELCOR 1.8.5 code release has a default configuration of 2 aerosol components, one for water class aerosol which will subsume fog droplets formed as a results of thermodynamic conditions in the atmosphere into the smallest size section, and one for non-water class aerosols. Three aerosol components are recommended if it is desired to track hygroscopic and non-hygroscopic aerosols that have different size distributions.

2.11 Iodine Pool Model

2.11.1 Introduction

The potential release of radioactive iodine as a result of a core damage accident in a nuclear power plant has long been a principal concern of reactor safety and consequence analyses. Iodine in particular is a concern because of its major contribution to the radiological hazard to the environment. A specific model devoted to the chemistry of iodine in reactor containments under accident conditions is needed in the MELCOR computer code because of the unique chemical properties of iodine and the severe consequence attributed to the release of the radioactive isotopes of iodine to the environment. Possible release of iodine has always played a significant role in the regulation of nuclear reactors. In early assessments of iodine consequences, it was assumed that iodine would be released to the reactor containment as a gaseous species. About one quarter of the initial core inventory was assumed to remain in the containment atmosphere, available for release to the environment. However, research over the last 15 years has shown it to be more likely that most of the iodine will be released to the containment atmosphere as aerosol particles, principally CsI. The Revised Accident Source Term (NUREG-1465) [38] assumes that at least 95% of the iodine reaching the containment is in aerosol form. Iodine within the containment atmosphere is able to pass through containment leak paths to the environment, thereby resulting in a dose to the public with ensuing consequences. Reduction of releases therefore requires control of atmospheric iodine concentration. This can be accomplished by causing the iodine to remain confined in aqueous forms in pools and sumps. Advanced reactor designs may incorporate chemical systems to keep the atmospheric concentration of iodine low by trapping iodine in aqueous forms and hence limit risk. An important use for MELCOR will be to assess the adequacy of these designs and identify processes and mechanisms that may defeat the intent of these systems.

Light water reactor containment temperatures can be expected to condense any residual cesium iodide vapors and form aerosols. These containments will also contain substantial quantities of water that can trap aerosol particles during severe accidents. For example, the condensation of steam formed during the core degradation processes will take place to a large extent within the containment. Trapping of most radionuclides in water effectively removes these radionuclides from further consideration in the analysis of the public consequences of reactor accidents by removing them from the containment atmosphere. However, radioactive iodine may not remain trapped in water because of its relatively dynamic chemical behavior. Engineered safety systems, such as sprays and suppression pools, are still effective mechanisms for scrubbing particulate iodine from the system and trapping it in the aqueous phase. However, there are important processes that can regenerate gaseous forms of iodine that release into the containment atmosphere from the water, thus becoming available for release to the environment for long times after the accident initiation.

The chemical and radiolytic oxidation of iodine in the pool can lead to the formation of a variety of chemical forms of iodine, such as elemental iodine and volatile organic iodides. The formation of volatile iodine in the pool is followed by a "partitioning" of the iodine between the pool and the atmosphere. This partitioning is important primarily in the longer term phases of the accident after the natural and engineered safety features have removed the other radioactive aerosols released during the accident. The formation of volatile forms of iodine in solution is dependent not only upon the dose rate to the aqueous phase but also on temperature, the hydrogen ion concentration (conventionally expressed as pH), and the total iodine concentration. It has been shown experimentally that large fractions of the iodine released from the reactor core can be expected to reside within the containment atmosphere in a volatile form when pH is not controlled to an alkalinity level greater than 7 [38]. It has also been observed that irradiation induced release of acids from the wall surface coatings, cable insulation, and the containment air lowers the pH [39]. However, the combination of high pH and high irradiation has not been thoroughly tested. In addition, the effect of other materials on the pool chemistry is not well established. Consequently, any model must be adaptable to the results of ongoing research. This fact is considered in the design of the MELCOR model, and provision is made to accommodate new information as it becomes available.

2.11.2 Features of Iodine Pool Model

The iodine pool model addresses these concerns. It embodies the current state of knowledge in a form that can be easily modified as current research yields results. It uses the known chemistry to predict what factors affect the iodine concentration in the atmosphere, while allowing for additional chemical reactions. In the containment atmosphere, where gas-phase behavior is important, there are submodels relating the radiolysis of the air and cable insulation to the generation of nitric acid and hydrochloric acid, respectively. On the structural surfaces, provision is made to account for the type of surface, thus allowing the extension to treat the effects of different paints and other surface coatings on iodine behavior. In the water pool, where liquid phase behavior is important, the model determines the pH based upon the user controlled boric acid and phosphate buffering, the effects of cesium hydroxide, cesium iodide and control rod silver released by the accident scenario chosen, and the effects of the acids introduced from the containment atmosphere due to radiolysis. The aqueous pool chemistry model then determines the speciation of iodine, particularly the important elemental, molecular, and organic forms, over the full range of pH. Thus, chemical systems that control pool pH can be examined as well as pools and films on surfaces that have no pH controls. With this combination of features, the iodine pool model allows for the ability to conduct sensitivity studies and incorporate new effects found in the course of ongoing research.

2.11.3 Criteria for Application of the Model

A MELCOR calculation typically involves several volumes with differing properties. When the model is invoked, it will be applied everywhere. The full model is used only in volumes with a pool, atmosphere, and iodine. Acid generation by radiolysis is still calculated in volumes with only an atmosphere, as these acids can be transported by MELCOR to other connected volumes. However, the aqueous chemistry model was designed for volumes where the pressure is less than 10 atm and the liquid temperature is less than 423 K, corresponding to conditions in a commercial reactor containment. If these limits are exceeded, the pool model becomes invalid. In such cases, the aqueous chemistry model is not used.

The effects of partitioning of iodine between the aqueous and gaseous phases is typically only important in the late term phases of an accident (after about 10 hours for the NUREG-1465 severe accident [38]). By this time, most of the iodine in a MELCOR calculation will have been transported to volumes where the pool model is valid. At earlier times, radionuclide behavior will be dominated by other phenomena. Thus, the limitations on the applicability of the aqueous chemistry model should have little impact on the ability to calculate the important phenomena in reactor accident sequences.

2.11.4 Detailed Description of the Model

The model involves four areas of modeling as shown schematically in Figure 2.2. The area labeled as one (1) indicates the transport of iodine species among the walls, the bulk gas, and the pool. This part of the model interacts directly with the MELCOR intra-cell mass transport coefficient (TRAP-MELT like) solution, and contributes to determining the structural surface concentration of the chemically and physically bound iodine species by using kinetic reactions to determine a transport rate. The change in pool depth from timestep to timestep changes in heat structure surface area, and transfer of iodine between pools and films is handled by existing MELCOR coding. The area labeled as two (2) is the containment atmosphere part of the model. It determines the radiolytic formation of acids and the gas-phase destruction and formation of iodine species. Species of iodine added to the cell atmosphere come from the pool, the structural surfaces, and adjacent cells (e.g., the reactor coolant system break location.) The area labeled as three (3) is concerned with the hydrogen ion concentration (i.e., pH), and accounts for the effects of the acids and bases introduced into the pool as well as the removal of iodine due to silver. The pH solution is typically dominated by the effect from the initial buffering of the pool. Thus, the model does not currently account for the hydrolysis of the other materials that may be in the pool, for example, cadmium, sludge, iron, and uranium. The area labeled as four (4) is the aqueous iodine chemistry model where the iodine, hydrogen, oxygen, carbon, iron, and electron balance equations are solved.

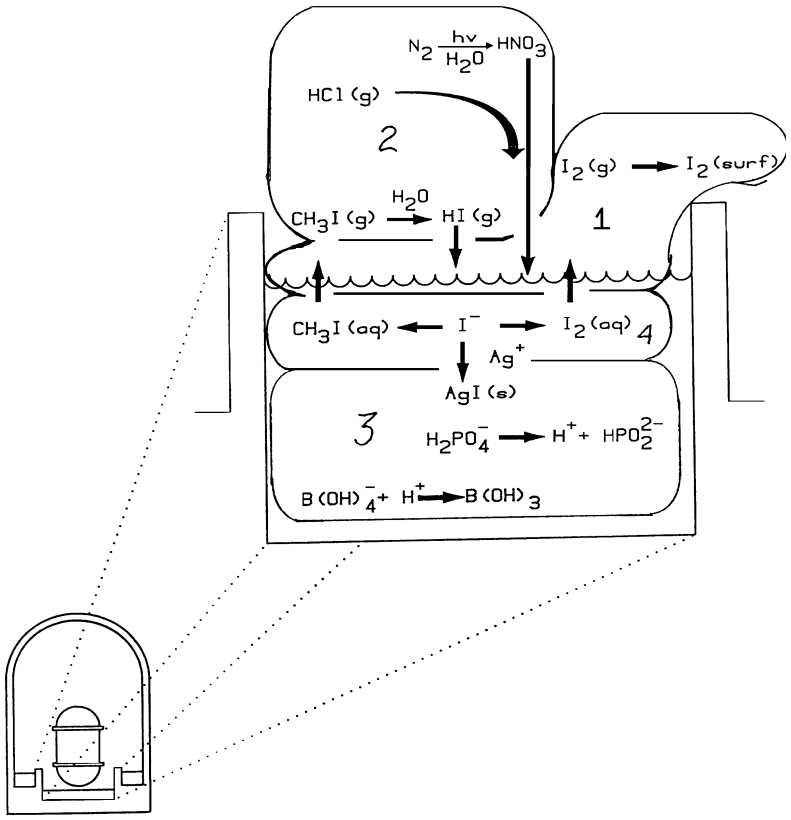

Figure 2.2 Schematic Representation of the Iodine Transformations Considered

The formulation chosen uses a dilute solution approximation that allows the effect of water radiolysis and radiolytic reactions to be explicitly included and should allow the results of current experimental studies to be compared. The approach adopted by Weber et al. [40] is modified here to include a more comprehensive set of chemical reactions and to explicitly include dose rate effects for the radiolysis while retaining the quasi-steady approximations for the dynamic equations.

2.11.5 Interaction with MELCOR

In MELCOR, intra-cell transport processes, for example condensation and aerosol deposition in a volume, is followed by inter-cell transport of material, for example silver and iodine moving from the reactor coolant system to the containment. The iodine chemistry model can be thought of in terms of intra-cell transport. The iodine model processes affect the distribution of iodine among the pool, the atmosphere, and the heat structures in

various control volumes. Thus, for a PWR, after a mix of water and radionuclides has been removed from the containment by deposition or through the action of the sprays and placed into the sump, this model allows MELCOR to distribute the iodine among the sump, the containment open volume, and the walls. Similarly, in a BWR, after the radionuclides have been placed in the wetwell, this model allows MELCOR to distribute the iodine among the suppression pool, the vapor space above it, and the wetwell walls.

Figure 2.3 shows the relationship between the iodine models and the balance of the MELCOR code. Volumes 1 and 2 are typical MELCOR hydrodynamic control volumes where a variety of processes take place. As shown for volume 1, these include scrubbing of aerosols from the atmosphere by sprays, deposition of aerosols onto structural surfaces with water films draining into the pool, and interface transport between pool and atmosphere. MELCOR also accounts for the transport of material between volumes. Not all MELCOR processes are shown; for example, the heat transfer processes are not indicated. None of these MELCOR processes will be affected by adding the iodine model. The iodine model performs aqueous chemistry calculations within existing pool regions of MELCOR control volumes. That is, based upon a species distribution and the radiation environment it determines the local pH and the quantity of elemental and organic iodine available at the pool-atmosphere interface. The model also performs vapor chemistry calculations within the existing atmosphere regions of MELCOR control volumes. That is, based upon a species distribution and the radiation environment, it determines the radiolytic formation of acids and destruction of iodine. These submodels are shown as the two add-on boxes above and below volume 1 in Figure 2.3. The model determines the transport and partitioning of the iodine species between the pool and atmosphere regions, allowing MELCOR to determine the late phase concentration of iodine in the atmosphere.

MELCOR determines the flux of important species into and out of all volumes within the inter-volume transport calculation. For the purposes of this model, important transported species include: the original thirteen (13) MELCOR radionuclide classes, used to determine the distribution of radiation sources in the control volume (xenon, cesium hydroxide, barium, elemental iodine, tellurium, ruthenium, molybdenum, cerium, lanthanum, uranium dioxide, cadmium, tin, and boron classes), four (4) species to control the hydrogen ion concentration in the pool (boric acid, cesium iodide, and phosphate are new; cesium hydroxide can be represented by existing class 2), four (4) in the atmosphere (methyl iodine, hydrochloric acid, and nitric acid are new; iodine is represented as class 4), two (2) deposited species (non-volatile form of iodine and methyl iodine to allow for surface chemistry), one (1) pool species which acts as a sink for iodine (silver, represented as existing class 12), and three (3) water pool chemistry species (silver iodine and methyl iodine are new; aqueous iodine is represented as class 4). There are many more species included in the aqueous pool chemistry model, including the two main species, elemental and molecular iodine; however, due to the equilibrium nature of the chemistry model, these species do not all need to be transported—the model is initialized at the beginning of a timestep by a small subset of the species, principally iodine, and creates the speciation for the conditions existing in the pool during that timestep. Obviously, these new species are

not all radionuclides and do not need to be examined in all code modules, i.e., they do not all need to be full RN classes. Table 2.5 shows some of the main and secondary species available from the model.

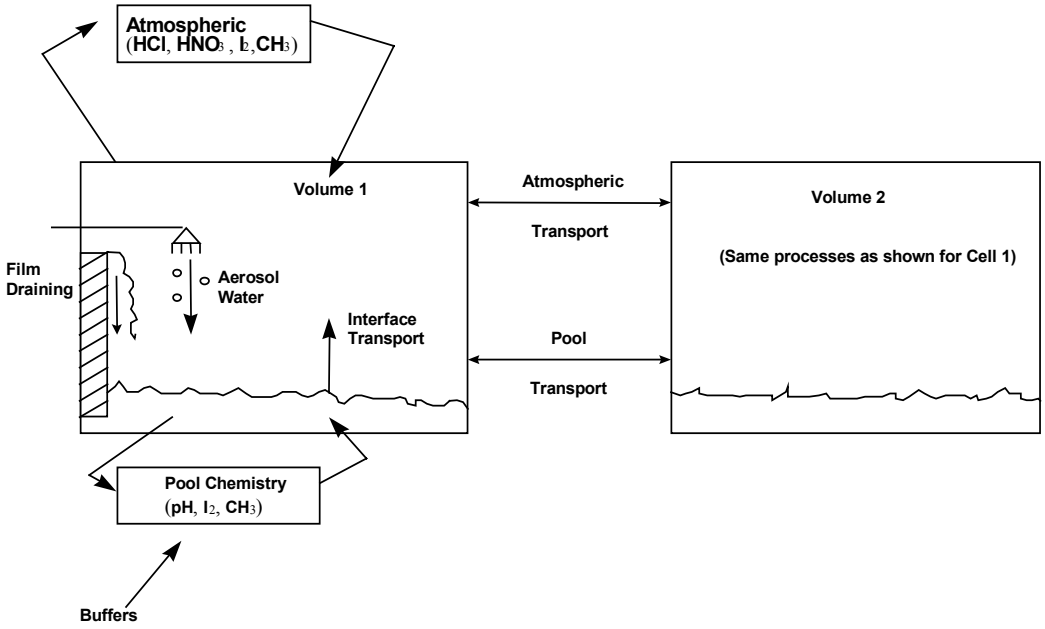

Figure 2.3 Interface between MELCOR and Iodine Pool Model

Table 2.5 Representative Species in Iodine Pool Model

Species	RN Class (Y/N)?	Species	RN Class (Y/N)?
I2	Y (4)	HOI-	N
I-	Y (4 or 16)	H2O2	N
I3-	N	O2-	N
IO-	N	HO2-	N
IO3-	N	CH3I	Y
I2OH	N		

Classes 14 (water) and 15 (concrete) are included in the original RN list—even though they are not “radionuclides”—because they form aerosols. Many current calculations include cesium iodide as a user-defined 16th class. CsI has been changed as part of the iodine pool model update to be a default RN class.

Transport of air and water, also used by the iodine pool model, is done by the MELCOR hydrodynamics module CVH. To use the pool model, it is necessary that the atmosphere components hydrogen, methane, and carbon dioxide be initialized in MELCOR input, as well as the usual atmosphere constituents (nitrogen, oxygen, and steam).

MELCOR determines the liquid, vapor, and heat structure surface temperatures and vapor pressure within the volume, within the energy transport calculation. With this information, the iodine models determine the intra-cell transport coefficients for the iodine species, that is, those coefficients determining the transport of elemental and organic iodine between the pool and the vapor space and between the vapor space and the heat structures. The model also determines the change from volatile to non-volatile iodine species on the surfaces, the change from one iodine species to another in the pool (including silver iodide), and the homogeneous destruction of iodine species in the atmosphere.

2.11.6 Order of Calculation of Model

The order of calculation in a control volume for the model is shown in Figure 2.4. This figure shows that the main functions of the model are carried out in a simple consecutive order, starting with the check for atmosphere volume in the upper left corner (Block 1) and continuing to the output block in the lower right corner (Block 14). Starting with the check for atmosphere volume, Block 1 in Figure 2.4, the calculation proceeds as follows:

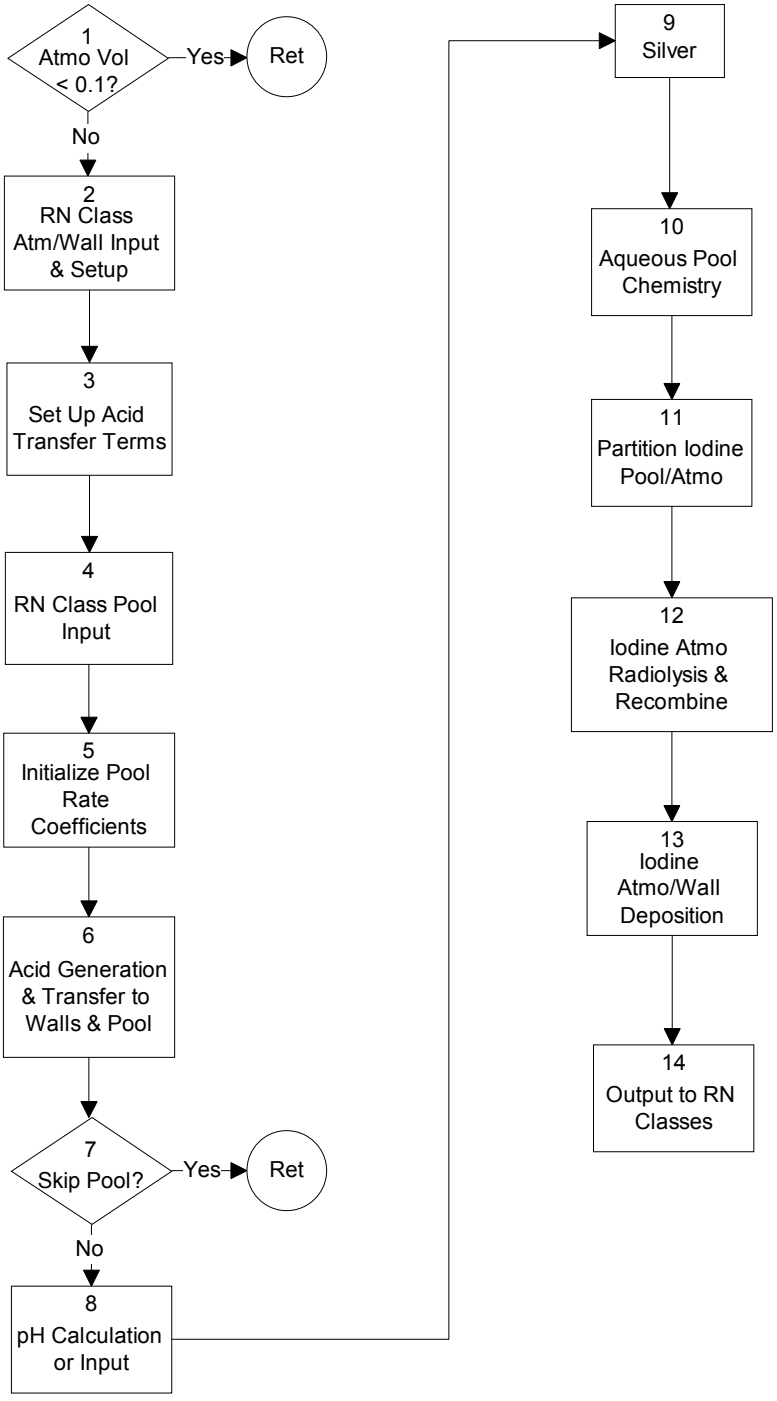

Figure 2.4 Calculation Flow of MELCOR Iodine Pool Model

(1) The atmosphere volume in the control volume is checked against a limit with a default of 0.1 m^3. If this test is not satisfied, the rest of the model is skipped for this control volume.

(2) RN class input and atmosphere/pool setup: the atmosphere and pool driver species are initialized at the beginning of the timestep from the MELCOR RN classes. This is only done for the atmosphere and walls at this point in the calculation. In the atmosphere, these are iodine (class 4), methyl iodine (class 17), hydrochloric and nitric acid (classes 18 and 19), and nitrogen, steam, oxygen, hydrogen, carbon dioxide, and methane (hydrodynamic materials). Atmosphere, pool, and wall areas and volumes are set up. Wall species for physically and chemically bound iodine and methyl iodide, and deposited nitric and hydrochloric acid on wet walls, are initialized from extended MELCOR chemisorption classes.

(3) The terms in the ordinary differential equations describing mass transport of hydrochloric and nitric acid from the atmosphere to the walls are set up, as are the radiolysis generation terms.

(4) The pool species are initialized from the MELCOR RN classes. These are iodine (class 4 and 16, CsI), the buffers boric acid (class 20) and phosphate (class 22), hydrochloric and nitric acid (classes 18 and 19), cations (CsI, class 16), silver (class 12), and iron (class 7). Although silver iodide is also transported as an RN class, the pool silver iodide does not need to be initialized, as silver acts only as a sink for iodine, not a source, and hence silver iodide (once formed) plays no further role in the pool chemistry.

(5) The rate coefficients for the pool chemistry calculation are initialized. These will be used later in the aqueous chemistry routine.

(6) The calculation of mass transport for hydrochloric and nitric acid is done. This includes the radiolysis generation rates, transport between the atmosphere and wall surfaces, and transport between atmosphere and pool. This last step is necessary to have the updated pool acid concentrations available for the pH calculation.

(7) The conditions for using the full iodine pool model are checked against limits here. These include the presence of iodine, atmospheric pressure less than 1 MPa, pool present, and pool temperature less than 425 K. If these conditions are not satisfied, then the rest of the pool calculation is skipped. There is a user input flag that will override the iodine criterion, allowing pool hydrolysis calculations to be done.

(8) The pH calculation is performed based on the relative molar concentrations of acids and bases in the pool. Alternatively, the pH can be directly entered in user input via tabular or control functions, or an external data file.

(9) A fraction of the silver present (set to 10^{-6}) is assumed chemically active and can remove some of the iodine in the pool as silver iodide, acting as a sink.

(10) The aqueous pool chemistry solver is called. This is a quasi-equilibrium solver and assumes steady-state conditions. The iodine from the MELCOR RN classes 4 (I_2) and 16 (I^-) is treated as an initial inventory of I^-. The aqueous chemistry model performs the speciation of the iodine each timestep, based on the pH and radiolysis in the pool (see Table 2.5 for major and secondary species available for output in MELCOR).

(11) The molar concentrations of iodine and methyl iodide in the pool are used to determine a pool surface concentration. This is used together with atmosphere conditions to partition the iodine and methyl iodide between the pool and atmosphere, giving new concentrations in the pool and atmosphere.

(12) The atmospheric iodine and methyl iodide concentrations are further modified by atmospheric radiolysis and thermal and concentration-dependent destruction rates to form free iodine; the final concentrations are determined by a recombination step using equilibrium coefficients.

(13) The atmosphere iodine and methyl iodide concentrations are used together with the wall concentrations to determine mass transport between the atmosphere and dry wall surfaces. Radiolysis at painted walls is included.

(14) Results of the pool model calculation are output. The relevant RN classes are updated, (see block 2 and 4 descriptions), including the silver iodine class. The silver iodide class is necessary to maintain mass conservation. On output, available cations (Cs) is combined with available I^- in the pool to form the new CsI (class 16) mass, and uncombined Cs or I^- are added to the CsOH (class 2) or I_2 (class 4) masses, respectively. The main iodine species, I_2 and I^-, are otherwise output as class 4. Other secondary species are also added into class 4 to maintain mass conservation. Updated wall concentrations are also output. The pH of the pool is available as a MELCOR plot variable. The masses and concentrations of the RN classes for the pool and atmosphere (transported species) are likewise available via control functions. A list of main and secondary species available via control function is shown in Table 2.5.

2.11.7 Submodels in the Iodine Pool Model

There are seven main submodels in the iodine pool model. These are detailed below, starting with the acid generation and transport models.

2.11.7.1 Acid Generation and Transfer to Walls and Pool

Formation of nitric acid in the atmosphere by radiolysis is calculated using the rate

$$\dot{S}_{HNO_3} = 5.45 \times 10^{-7} M_{N_2} \dot{D}_{atm} \tag{2.115}$$

where

$\dot{S}_{HNO_3}$ = formation rate of nitric acid by radiolysis (kg-mole/s)

M_{N_2} = mass of nitrogen in the atmosphere (kg)

$\dot{D}_{atm}$ = atmosphere dose rate (MRad/hr)

and the constant has the appropriate units

Formation of hydrochloric acid is assumed to occur via radiolysis of plastic wire insulation in a control volume and go into the atmosphere instantly. The rate is given as

$$\dot{S}_{HCL} = 2.88 \times 10^{-7} M_{cable} \dot{D}_{cable} \tag{2.116}$$

where

$\dot{S}_{HCL}$ = rate of formation of HCl by radiolysis of wire cable insulation (kg-mole/s)

M_{cable} = mass of cable insulation in control volume (kg)

$\dot{D}_{cable}$ = cable dose rate (MRad/hr)

and the constant has the appropriate units.

Nitric and hydrochloric acids in the atmosphere can be deposited in the water films on wet walls via a non-reversible mass transport equation of the form

$$\frac{dC_{w,acid,n}}{dt} = k_{w,acid,n} C_{atm,acid} \tag{2.117}$$

where

$C_{w,acid,n}$ = moles of acid on wall surface n (kg-mole)

$k_{w,acid,n}$ = transport coefficient from atmosphere to wall *n* for acid (m/s)

$C_{atm,acid}$ = atmospheric moles of acid (kg-mole)

and the subscript *acid* refers either to nitric or hydrochloric acid. A similar equation is used for transport from the atmosphere to the pool. The new amount of acid in the atmosphere is determined by summing up the transport to all the wet walls in a control volume and the pool (if present) to get

$$\frac{dC_{atm,acid}}{dt} = -C_{atm,acid}\frac{1}{V_{atm}}\left(\sum_n k_{w,acid,n}A_{w,n} + k_{p,acid}A_{pool}\right) + \dot{S}_{acid} \qquad (2.118)$$

where

$k_{w,acid,n}$ = transport coefficient from atmosphere to wall surface *n* for acid (m/s)

$A_{w,n}$ = wall *n* surface area (m^2)

$k_{p,acid}$ = transport coefficient from atmosphere to pool for acid (m/s)

A_{pool} = pool-atmosphere surface area (m^2)

V_{atm} = atmospheric volume (m^3)

$\dot{S}_{acid}$ = formation rate of acid (kg-mole/s).

This can be solved analytically over the timestep as

$$C_{atm,acid}(t) = C_{atm,acid}(t_0)\exp(-k_{eff,acid}t) + \frac{\dot{S}_{acid}}{V_{atm}k_{eff,acid}}(1-\exp(-k_{eff,acid}t)) \qquad (2.119)$$

where $k_{eff,acid}$ is defined by

$$k_{eff,acid} = \frac{1}{V_{atm}}\left(\sum_n k_{w,acid,n}A_n + k_{p,acid}A_{pool}\right). \qquad (2.120)$$

The change in amount of wall acid can be expressed in terms of the change in atmospheric acid as

$$C_{w,acid,n}(t) = C_{w,acid,n}(t_0) + \frac{k_{w,acid,n}}{k_{eff,acid}}\left([C_{atm,acid}(t) - C_{atm,acid}(t_0)] + \dot{S}_{acid}(t - t_0)\right), \quad (2.121)$$

and a similar equation applies for the change in pool acid,

$$C_{p,acid}(t) = C_{p,acid}(t_0) + \frac{k_{p,acid}}{k_{eff,acid}}\left([C_{atm,acid}(t) - C_{atm,acid}(t_0)] + \dot{S}_{acid}(t - t_0)\right). \quad (2.122)$$

Acids deposited in wall films are transported to the pool or other surfaces using the MELCOR film transport model.

2.11.7.2 Pool pH Calculation

The pool pH is determined either from an acid-base balance or set via user input. The pH calculation is done by first performing a charge balance of the acids and bases to estimate pH, and then performing an iteration over the species and charge balance to get the final pH.

The first step is to estimate the hydrogen ion concentration (or pH) from a charge balance on the phosphate (Na_3PO_4), cation (Cs), nitric and hydrochloric acid concentrations, as

$$\Delta Z = 3x_{NaP} + x_{Cs} - x_{HNO_3} - x_{HCl}$$

where (kmole=10^3 mole)

ΔZ = charge balance (kmole/m^3)

x_{NaP} = phosphate concentration (Na_3PO_4), (kmole/m^3)

x_{Cs} = cation concentration (cesium), (kmole/m^3)

x_{HNO_3} = nitric acid concentration (kmole/m^3)

x_{HCl} = hydrochloric acid concentration (kmole/m^3)

If ΔZ is greater than 0, then the pH is estimated as

x_{OH^-} = $\min(0.0001, \Delta Z)$

$$x_{H^+} = \frac{K_{eq,H_2O}}{x_{OH^-}}$$

$$pH = \log_{10}\left(x_{OH^-}\right).$$

If ΔZ equals 0, then

$$x_{H^+} = 10^{-7}$$

$$pH = 7$$

If ΔZ is less than 0, then

$$x_{H^+} = \min\left(0.0001, \left|\Delta Z\right|\right)$$

$$pH = \log_{10}\left(x_{H^+}\right)$$

The activities are then initialized. Activities are calculated using Davies modification of the Debye-Huckel equation [41],

$$\log_{10}\gamma(i) = -A\,Z(i)^2\left[\frac{\sqrt{I}}{1+\sqrt{I}} - b\ I\right]$$

where

$\gamma(i)$ = activity coefficient for ion *i*

$Z(i)$ = absolute value of the charge on ion *i*

b = empirical constant = 0.2

I = ionic strength, defined as

$$I = \tfrac{1}{2}\sum_{all\ ions} C(j)Z(j)^2$$

$C(j)$ = concentration of the j^{th} ion in solution

A = $1.825\times10^6\,\rho_w^{1/2}/\left(\varepsilon\,T\right)^{3/2}$

ρ_w = density of water (g/cm^3)

ε = dielectric constant of water.

The initial strength is estimated using the initial buffer species along with the OH^- and H^+ concentrations

$$I = 0.5\left(3x_{NaP} + x_{Cs} + x_{HNO_3} + x_{HCl} + x_{OH^-} + x_{H^+}\right).$$

The equations to be solved are:

(1) the phosphate mole balance:

$$M(P) = [H_3PO_4] + [H_2PO_4^-] + [HPO_4^{2-}] + [PO_4^{3-}],$$

where $M(P)$ is the total kmoles of phosphate per m^3 of water and is user input,

(2) the borate mole balance:

$$M(B) = [B(OH)_4^-] + [B(OH)_3]$$

where M(B) is the input kmoles of borate per m^3 of water,

(3) the CO_2 hydrolysis balance:

$$M(C) = [HCO_3^-] + [CO_3^{2-}]$$

where *M(C)* is the moles of dissolved CO_2 per m^3 of water, and

(4) the charge balance:

$$[NO_3^-] + [Cl^-] + [OH^-] + [H_2PO_4^-] + 2[HPO_4^{2-}] + 3[PO_4^{3-}] + [B(OH)_4^-] + [HCO_3^-] + 2[CO_3^{2-}] = [H^+] + [A^+] + 3M(P)$$

where $[A^+]$ is the kmoles of alkali per m^3 added to adjust for boric acid and the kmoles/m^3 of phosphate added is assumed to be in the form Na_3PO_4. Also needed is the ionization constant for water, written in the form:

$$K_w = [H^+]\gamma(1)[OH^-]\gamma(1)$$

where the activity coefficients have been included. The ionization constant is determined from the formula

$$\log_{10} K_{w,p} = 2(7.2 + 2.5\rho_w)\log_{10} \rho_w - \frac{3108}{T} - 3.55$$

where

$K_{w,p}$ = ionization constant of water in units of (moles/kg)^2

ρ_w = density of water in g/cm^3.

To get the ionization constant in units of (kmole/m^3)^2, multiply by the density of water squared:

$$K_w = K_{w,p}\rho_w^2 .$$

The concentrations of the derived species are determined from equilibrium constants:

$$k_4 = \frac{[H^+][B(OH)_4^-]}{[B(OH)_3]}\gamma(1)^2$$

$$\log_{10} k_4 = \frac{1573}{T} + 28.8397 + 0.11748T - 13.2258 \log_{10} T + \log_{10} K_w$$

$$k_5 = \frac{[HPO_4^{2-}]}{[H^+][PO_4^{3-}]}\frac{\gamma(2)}{\gamma(1)\gamma(3)}$$

$$\log_{10} k_5 = \frac{-675}{T} + 1.793 + \log_{10} K_w$$

$$k_6 = \frac{[OH^-][H_2PO_4^-]}{[HPO_4^{2-}]}\frac{\gamma(1)^2}{\gamma(2)}$$

$$\log_{10} k_6 = \frac{-17156.9}{T} - 37.7345 \ln T + 0.0322082\, T + \frac{8.97579 \times 10^5}{T^2} + 246.045$$

$$k_7 = \frac{[OH^-][H_3PO_4]}{[H_2PO_4^-]}\gamma(n)$$

$$\log_{10} k_7 = \frac{-17655.8}{T} - 39.4277 \ln T + 0.0325405\ T + \frac{810134}{T^2} + 253.198$$

$$k_2 = \frac{[H^+][HCO_3^-]}{[CO_{2aq}]}\gamma(1)^2$$

$$\log_{10} k_2 = \frac{2518}{T} - 0.7566 + \log_{10} K_w$$

$$k_3 = \frac{[H^+][CO_3^{2-}]}{[HCO_3^-]}\gamma(2)$$

$$\log_{10} k_3 = \frac{2142}{T} - 3.523 + \log_{10} K_w$$

The iteration proceeds by

(1) setting the activities, and mass ratios of the acid and CO_2 total masses to the principal species,

(2) get new species concentrations from the ratios and mole balances,

(3) recalculate the strength and activities including all species in the charge balance, and

(4) use the charge balance to calculate the pH. This process is repeated until the pH converges to within 0.0001. The iteration is accelerated by using the gradient of the change in pH after the first 5 iterations.

2.11.7.3 Silver-Iodine Model

Silver in the pool can act to trap iodine. This is modeled in the iodine pool model by assuming a fixed fraction of the silver present in the pool (default set at 1 x 10^{-6}) is available to react with iodine, forming AgI sludge. The iodine thus reacted is assumed trapped and does not participate in the pool aqueous chemistry. The silver is assumed to be provided by RN class 12, and AgI is given its own RN class.

2.11.7.4 Iodine Aqueous Pool Chemistry

The aqueous iodine chemistry model is a semi-mechanistic model based primarily on the INSPECT equation set [42,43] plus work by Powers [44]. The model includes the effects of radiolysis, take-up of iodine by silver, metal ions (represented by iron), and acid-base buffers. Equations are included for organic iodine, represented as methyl iodine.

2.11.7.4.1 Chemical Reaction Equations

The chemical equations in the set are of the general form

$$A + B \Leftrightarrow C + D$$

with forward reaction rate k_f and reverse rate k_r. These are used to set up chemical reaction kinetic equations for each chemical species in the set. Using the above equation as an example, the reaction rate equation for species *C* would include terms from this equation plus perhaps a source from radiolysis:

$$\frac{d[C]}{dt} = k_f[A][B] - k_r[C][D] + \dot{S}$$

where the brackets [ ] indicate concentration of the species and the $\dot{S}$ is the source of *C* from radiolysis. The set of chemical reaction kinetics equations form a coupled set of nonlinear ordinary differential equations, which are solved using a standard stiff differential equation solver [45] to get the pool speciation. Initial conditions are set up by assuming some species, termed driver species, are given and constant over a calculational timestep. There are five driver species in the current equation set. These are aqueous O_2, H_2, CH_4, OH^-, and H^+. Some driver species are set by assuming equilibrium with the atmosphere via a Henry's law relationship; these are aqueous O_2, H_2, and CH_4. The OH^- and H^+ are set by determining the pool pH.

The initial total iodine concentration is specified at the beginning of the timestep as species I, and the iron ion concentration is specified as Fe^{3+}. Other species in the pool, such as silver, nitric and hydrochloric acids, and phosphate and borate buffers, do not actually participate in the calculation of speciation other than to set the initial pH and iodine level (silver, by removing some iodine). Pool pH is determined either from an acid-base balance or is read in directly via user input.

The current chemical equation set consists of 276 equations as given in Table 2.7 through Table 2.10 and includes 39 species.

Table 2.6 Kinetic Equations for Water Radiolysis

Number	Reaction	Rate Constant*
M1	$OH^O + H_2(aq) \rightarrow H^O + H_2O$	4.2×10^7
M2	$OH^O + H_2O_2 \rightarrow HO_2^O + H_2O$	2.7×10^7
M3	$OH^O + O_2^- \rightarrow O_2(aq) + OH^-$	8×10^9
M4	$H^O + O_2(aq) \rightarrow HO_2^O$	1.2×10^{10}
M5	$H^O + O_2^- \rightarrow HO_2^-$	2×10^{10}
M6	$e^- + O_2(aq) \rightarrow O_2^-$	1.9×10^{10}
M7	$e^- + H_2O_2 \rightarrow OH^O + OH^-$	1.2×10^{10}
M8	$e^- + O_2^- + H_2O \rightarrow HO_2^- + OH^-$	1.3×10^{10}
M9	$e^- + H^+ \rightarrow H^O$	2.3×10^{10}
M10	$e^- + H_2O \rightarrow H^O + OH^-$	19
M11	$e^- + HO_2^- \rightarrow O^- + OH^-$	3.5×10^9
M12	$OH^O + HO_2^O \rightarrow O_2(aq) + H_2O$	6×10^9
M13	$2\ OH^O \rightarrow H_2O_2$	5.5×10^9
M14	$H^O + HO_2^O \rightarrow H_2O_2$	2×10^{10}
M15	$H^O + H_2O_2 \rightarrow OH^O + H_2O$	5×10^7
M16	$OH^- + H^O \rightarrow e^- + H_2O$	2.5×10^7
M17	$HO_2^O + O_2^- \rightarrow O_2(aq) + HO_2^-$	9.7×10^7
M18	$2\ HO_2^O \rightarrow H_2O_2 + O_2(aq)$	2.35×10^6
M19	$H^+ + O_2^- \rightarrow HO_2^O$	5×10^7
M20	$HO_2^O \rightarrow H^+ + O_2^-$	(7.93×10^5)
M21	$H^+ + HO_2^- \rightarrow H_2O_2$	2×10^{10}
M22	$H_2O_2 \rightarrow H^+ + HO_2^-$	(0.0413)
M23	$OH^O + OH^- \rightarrow H_2O + O^-$	1.3×10^{10}
M24	$O^- + H_2O \rightarrow OH^O + OH^-$	(1.47×10^8)
M25	$HO_2^O + OH^- \rightarrow O_2^- + H_2O$	(1×10^9)
M26	$O_2^- + H_2O \rightarrow HO_2^O + OH^-$	(0.639)
M27	$H^O + OH^O \rightarrow H_2O$	7×10^9
M28	$2\ H^O \rightarrow H_2(aq)$	5×10^9
M29	$e^- + H^O + H_2O \rightarrow OH^- + H_2(aq)$	2.4×10^{10}
M30	$2e^- + 2H_2O \rightarrow 2OH^- + H_2(aq)$	5.5×10^9
M31	$e^- + OH^O \rightarrow OH^-$	3×10^{10}

Number	Reaction	Rate Constant*
M32	$O^- + O_2(aq) \rightarrow O_3^-$	3.5 x 10^9
M33	$H_2(aq) + O^- \rightarrow H^O + OH^-$	1 x 10^8
M34	$H_2O_2 + O^- \rightarrow H_2O + O_2^-$	5 x 10^8
M35	$OH^O + HO_2^- \rightarrow HO_2^O + OH^-$	7.5 x 10^9
M36	$HO_2^- + O^- \rightarrow OH^- + O_2^-$	8 x 10^8
M37	$O_3^- + H_2O_2 \rightarrow O_2^- + O_2(aq) + H_2O$	1.6 x 10^6
M38	$O_3^- + HO_2^- \rightarrow O_2^- + O_2(aq) + OH^-$	8.9 x 10^5
M40	$O_3^- + H_2 \rightarrow H^O + O_2(aq) + OH^-$	2.5 x 10^5
M102	$H_2O_2 \rightarrow 2\,OH^O$	2.33 x 10^{-7} (6.4×10^5 exp (-8540/T))
*Rate constants are in units m^3/kmole-s and s^{-1}. Most rate constants were taken from [42]. Rate constants within parentheses were estimated as part of this work.		

Table 2.7 Reactions of Iodine

Number	Reaction	Rate Constant*
M53	$I^O + e^- \rightarrow I^-$	2.4 x 10^{10}
M54	$I_2(aq) + e^- \rightarrow I_2^-$	5.1 x 10^{10}
M55	$IO_3^- + e^- \rightarrow IO_3^{2-}$	7.8 x 10^9
M56	$I_2^- + e^- \rightarrow 2I^-$	1.3 x 10^{10}
M57	$I_3^- + e^- \rightarrow I^- + I_2^-$	3.5 x 10^{10}
M59	$IO_3^O + e^- \rightarrow IO_3^-$	13.5 x 10^{10}
M60	$IO_2^- + e^- \rightarrow IO^- + O^-$	11 x 10^{10}
M61	$IO^- + e^- \rightarrow I^- + O^-$	22.9 x 10^{10}
M62	$IO^O + e^- \rightarrow IO^-$	21 x 10^{10}
M63	$HOI^- + e^- \rightarrow I^- + OH^-$	1.9 x 10^{10}
M65	$I^O + H^O \rightarrow H^+ + I^-$	2.7 x 10^{10}
M66	$I_2(aq) + H^O \rightarrow I_2^- + H^+$	3.5 x 10^{10}
M67	$I_2^- + H^O \rightarrow 2I^- + H^+$	1.8 x 10^7

1 Rate from Wren

2 Rate from Karasawa

Number	Reaction	Rate Constant*
M68	$I_3^- + H^O \rightarrow I^- + I_2^- + H^+$	8 x 10^9
M69	$I^- + H^O \rightarrow HI^-$	5.3 x 10^6
M70	$HOI^- + H^O \rightarrow I^- + H_2O$	4.4 x 10^{10}
M72	$HOI^O + H^O \rightarrow I^O + H_2O$	1 x 10^9
M73	$IO_2^- + O_2^- + H_2O \rightarrow IO^O + O_2(aq) + 2OH^-$	1 x 10^7
M74	$I_2(aq) + O_2^- \rightarrow I_2^- + O_2(aq)$	21 x 10^9
M75	$HOI^O + O_2^- \rightarrow I^O + O_2(aq) + OH^-$	1 x 10^6
M76	$I_3^- + O_2^- \rightarrow I_2^- + I^- + O_2(aq)$	22.5 x 10^8
M77	$I_2^- + O_2^- \rightarrow 2I^- + O_2(aq)$	27.5 x 10^9
M78	$IO^O + O_2^- \rightarrow IO^- + O_2(aq)$	8 x 10^7
M79	$IO_3^- + O_2^- \rightarrow IO_3^{2-} + O_2(aq)$	8 x 10^9
M80	$I_2^- + HO_2^O \rightarrow I_2(aq) + HO_2^-$	1 x 10^{10}
M81	$HOI^O + HO_2^O \rightarrow I^O + O_2(aq) + H_2O$	1 x 10^5
M82	$IO_2^- + HO_2^O \rightarrow IO^O + O_2(aq) + OH^-$	1 x 10^7
M83	$I_2(aq) + HO_2^O \rightarrow I_2^- + O_2(aq) + H^+$	1.8 x 10^7
M84	$I^O + OH^O \rightarrow HOI^O$	1.6 x 10^{10}
M85	$HOI^O + OH^O \rightarrow IO^O + H_2O$	7 x 10^9
M86	$IO^O + OH^O \rightarrow HIO_2^O$	11 x 10^{10}
M87	$IO_2^O + OH^O \rightarrow IO_3^- + H^+$	11 x 10^{10}
M88	$I^- + OH^O \rightarrow HOI^-$	1.8 x 10^{10}
M89	$I_2(aq) + OH^O \rightarrow HOI^O + I^O$	1.1 x 10^{10}
M90	$IO_3^- + OH^O \rightarrow IO_3^O + OH^-$	21 x 10^6
M91	$HOI^- + OH^O \rightarrow HOI^O + OH^-$	2.7 x 10^{10}
M92	$I_2^- + OH^O \rightarrow I_2(aq) + OH^-$	3.8 x 10^{10}
M93	$I_3^- + OH^O \rightarrow I_2(aq) + I^O + OH^-$	2 x 10^{10}
M94	$I^- + O^- + H_2O \rightarrow I^O + 2OH^-$	24.7 x 10^7
M95	$IO^- + O^- + H_2O \rightarrow IO^O + 2OH^-$	21.1 x 10^8
M96	$IO_3^- + O^- + H_2O \rightarrow IO_3^O + 2OH^-$	15.23 x 10^6
M97	$I^- + H_2O_2 \rightarrow IO^- + H_2O$	10.014
M100	$IO_3^O + H_2O_2 \rightarrow IO_3^- + HO_2^O + H^+$	1 x 10^9
M101	$I^O + H_2O_2 \rightarrow I^- + HO_2^O + H^+$	3000

Number	Reaction	Rate Constant*
M103	$HIO_2^O \rightarrow IO_2^- + H^+$	21 x 10^{10}
M104	$I^O + I^- \rightarrow I_2^-$	21.1 x 10^{10}
M105	$HOI^- \rightarrow I^- + OH^O$	2.25 x 10^6
M106	$I^- + HOI^- \rightarrow I_2^- + OH^-$	2.5 x 10^4
M107	$HOI^- \rightarrow I^O + OH^-$	1.2 x 10^8
M108	$2I_2^- \rightarrow I_3^- + I^-$	4.5 x 10^9
M109	$I_2^- + O_2(aq) + H^+ \rightarrow HO_2^O + I_2(aq)$	6 x 10^5
M110	$I_2^- + I^O \rightarrow I_3^-$	4.5 x 10^9
M111	$2I^O \rightarrow I_2(aq)$	1 x 10^{10}
M112	$I_2^- + HOI^O \rightarrow IO^O + 21^- + H^+$	1 x 10^5
M113	$IO_3^{2-} + H_2O \rightarrow HIO_3^- + OH^-$	1 x 10^8
M114	$IO_3^O + I^- \rightarrow IO_2^- + IO^O$	11 x 10^6
M115	$IO_2^O + I^- \rightarrow I_2(aq) + O_2^-$	1 x 10^{10}
M116	$HI^- + H_2O \rightarrow I^O + H_2(aq) + OH^-$	1000
M117	$HI^- + H^+ \rightarrow I^O + H_2(aq)$	11 x 10^{10}
M118	$I_2^- + HOI^- \rightarrow I_3^- + OH^-$	1.8 x 10^{10}
M119	$HOI^- + I^O \rightarrow I_2(aq) + OH^-$	2.3 x 10^{10}
M120	$2HOI^- \rightarrow I_2(aq) + 2OH^-$	2 x 10^{10}
M121	$HOI^O + e^- \rightarrow HOI^-$	2 x 10^{10}
M122	$HOI^O + O_2^- \rightarrow HOI^- + O_2(aq)$	11 x 10^9
M123	$2IO^O \rightarrow I_2O_2$	1.5 x 10^9
M124	$I_2O_2 + H_2O \rightarrow IO_2^- + HOI^O + H^+$	11000
M125	$IO^O + IO_2^- \rightarrow IO_2^O + IO^-$	11 x 10^{10}
M126	$IO_2^O + H_2O \rightarrow HIO_3^- + H^+$	11000
M127	$2HIO_3^- \rightarrow IO_3^- + IO_2^- + H_2O$	25.2 x 10^9
M128	$IO_3^O + HIO_3^- \rightarrow 2IO_3^- + H^+$	11 x 10^{10}
M129	$IO_3^O + IO_3^{2-} \rightarrow 2IO_3^-$	11 x 10^{10}
M130	$IO_2^- + H_2O_2 \rightarrow IO^- + O_2(aq) + H_2O$	1 x 10^8
M131	$I_2(aq) + H_2O \rightarrow I_2OH^- + H^+$	*
M132	$I_2OH^- + H^+ \rightarrow I_2(aq) + H_2O$	1 x10^{10}
M133	$I_2(aq) + OH^- \rightarrow I_2OH^-$	1 x 10^{10}

Number	Reaction	Rate Constant*
M134	$I_2OH^- \rightarrow I_2(aq) + OH^-$	13 x 10^5
M135	$I_2OH^- \rightarrow I^- + HOI^O$	1963
M136	$I^- + HOI^O \rightarrow I_2OH^-$	1 x 10^6
M137	$IO^- + I_2OH^- \rightarrow IO_2^- + 2I^- + H^+$	6
M138	$IO_2^- + I_2OH^- \rightarrow IO_3^- + 2I^- + H^+$	26
M139	$2HOI^O \rightarrow IO_2^- + I^- + 2H^+$	16.7
M141	$HOI^O + IO_2^- \rightarrow IO_3^- + I^- + H^+$	1 x 10^7
M144	$HOI^O + OH^- \rightarrow IO^- + H_2O$	1 x 10^9
M145	$IO^- + H_2O \rightarrow HOI^O + OH^-$	2750
M146	$2I^- + 1/2O_2(aq) + 2H^+ \rightarrow I_2(aq) + H_2O$	347
M147	$I_2(aq) + H_2O \rightarrow 2I^- + 1/2O_2(aq) + 2H^+$	1 x 10^{-10}
M148	$I_2(aq) + I^- \rightarrow I_3^-$	
M149	$I_3^- \rightarrow I_2(aq) + I^-$	*
M150	$I^- + IO_2^- + 2H^+ \rightarrow 2HOI^0$	10^{12} x R139
M151	$IO_3^- + 2I^- + 2H^+ \rightarrow H_2I_3O_3^-$	6.72 x 10^8
M152	$H_2I_3O_3^- + 3I^- + 4H^+ \rightarrow 3I_2(aq) + 3H_2O$	1 x 10^{10}
M153	$I_2^- \rightarrow I^0 + I^-$	1.1 x 10^5
M154	$HOOI + I^- \rightarrow I_2(aq) + HO_2^-$	4.5 x 10^5
M155	$I_2(aq) + HO_2^- \rightarrow HOOI + I^-$	R154 / 0.04119
M156	$HOI^0 + HO_2^0 \rightarrow HOOI + OH^0$	2.1 x 10^9
M157	$HOOI + OH^- \rightarrow I^- + O_2 + H_2O$	2 x 10^9
M158	$HOI^0 + H_2O_2 \rightarrow HOOI + H_2O$	37
M159	$HOOI \rightarrow I^- + O_2 + H^+$	0.2

Number	Reaction	Rate Constant*
Footnotes to table: *INSPECT selects a rate constant based on the equilibrium constant and the rate constant for the back reaction. **See Powers [44]. $\frac{d[I_2(aq)]}{dt} = -\frac{1}{2}\frac{d[I^-]}{dt} = -\frac{1}{2}\frac{d[H^+]}{dt} = -2\frac{d[O_2(aq)]}{dt} = 34[I^-]^2[H^+][O_2(aq)] + \frac{7.14\times10^4[I^-][B(OH)_3][H^+][O_2(aq)]}{(1+1.47\times10^8[H^+])}$ ***See Powers [44]. $\frac{d[IO_3^-]}{dt} = -\frac{d[I^-]}{dt} = -\frac{2}{3}\frac{d[O_2(aq)]}{dt} = 3.2\times10^{-5}[I^-][O_2(aq)]$		

Table 2.8 Reactions of Ferrous and Ferric Ions

Number	Reaction	Rate Constant
M259	$Fe^{2+} + O_2(aq) \rightarrow Fe^{3+} + O_2^-$	$\frac{d[Fe^{2+}]}{dt} = k[[Fe^{2+}][O_2(aq)][OH^-]^2$ $k = 3.10^{21}\exp(-3557/T)$
M260	$Fe^{3+} + H_2O_2 \rightarrow Fe^{2+} + HO_2^O + H^+$	2 x 10^{-3}/(1 + x/[H^+])
M261	$Fe^{3+} + HO_2^- \rightarrow Fe^{2+} + HO_2^O$	1.1 x 10^{24} exp(-14090/T)/(1 + x/[H^+])
M262	$Fe^{3+} + H_2^O \rightarrow Fe^{2+} + O_2(aq) + H^+$	3 x 10^5
M263	$Fe^{3+} + O_2^- \rightarrow Fe^{2+} + O_2(aq)$	5040 exp(3294/T)
M264	$Fe^{3+} + e^- \rightarrow Fe^{2+}$	2.3 x 10^{10}
M265	$Fe^{3+} + H^O \rightarrow Fe^{2+} + H^+$	9.6 x 10^7
M266	$Fe^{2+} + H^O + H^+ \rightarrow Fe^{3+} + H_2$	7.5 x 10^6
M267	$Fe^{3+} + OH^O + H_2O \rightarrow Fe^{2+} + H_2O_2 + H^+$	1.5/(1 + y/[H^+]) Ref. 184
M268	$Fe^{2+} + O^- + H_2O \rightarrow Fe^{3+} + 2OH^-$	3.8 x 10^9
M269	$Fe^{2+} + OH^O \rightarrow Fe^{3+} + OH^-$	3 x 10^8
M270	$Fe^{2+} + H_2O_2 \rightarrow Fe^{3+} + OH^- + OH^O$	77
M271	$Fe^{2+} + HO_2^O \rightarrow Fe^{3+} + HO_2^-$	3 x 10^7
M272	$Fe^{2+} + HO_2^- \rightarrow Fe^{3+} + OH^- + O^-$	770
M273	$Fe^{2+} + O_2^- \rightarrow Fe^{3+} + 2O^-$	7.2 x 10^6
M274	$Fe^{3+} + H_2O_2 \rightarrow Fe^{2+} + O_2^- + 2H^+$	2 x 10^{-3} x /([H^+] + x)
M275	$Fe^{3+} + HO_2^- \rightarrow Fe^{2+} + O_2^- + H^+$	1.1 x 10^{24} exp(-14090/T) x /([H^+] + x)

Number	Reaction	Rate Constant
M276	$Fe^{3+} + OH^O + H_2O \rightarrow Fe^{2+} + HO_2^- + 2H^+$	1.5 y/([H^+] + y) Ref. 184
x = equilibrium constant for $HO_2^O \rightarrow H^+ + O_2^- = 10^{-1431/T}$ y = equilibrium constant for $H_2O_2 \rightarrow H^+ + HO_2^- = 10^{-3484/T}$		

Table 2.9 Organic Reactions

Number	Reaction	Rate Constant
M377	$CH_4(aq) + OH^O \rightarrow CH_3 + H_2O$	1.21 x 10^8
M378	$CH_4(aq) + I_2(aq) \rightarrow CH_3I + I^- + H^+$	4
M379	$CH_4(aq) + IO^- \rightarrow CH_3I + I^- + OH^-$	1 x 10^8
M380	$CH_4(aq) + HOI^O \rightarrow CH_3I + H_2O$	1 x 10^8
M381	$2\ CH_3 \rightarrow$ products	1.24 x 10^9
M382	$CH_3 + OH^O \rightarrow CH_3OH$	1 x 10^8
M383	$CH_3 + H_2O_2 \rightarrow CH_3OH + OH^O$	3.5 x 10^7
M384	$CH_3 + O_2(aq) \rightarrow$ products	4.9 x 10^9
M385	$CH_3 + HOI^O \rightarrow CH_3I(aq) + OH^O$	1 x 10^9
M386	$CH_3 + e^- + H_2O \rightarrow CH_4 + OH^-$	1 x 10^{10}
M387	$CH_3 + H^O \rightarrow CH_4(aq)$	1 x10^{10}
M388	$CH_3 + I^O \rightarrow CH_3I(aq)$	1 x 10^{10}
M389	$CH_3 + IO_3^O \rightarrow CH_2O + HIO_2^O$	1 x 10^8
M390	$CH_3 + IO_2^O \rightarrow CH_2O + HOI^O$	1 x 10^8
M391	$CH_3 + IO^O \rightarrow CH_3OH + HOI^O$	1 x 10^8
M392	$CH_3 + HOI^O \rightarrow I^O + CH_3OH$	1 x 10^8
M393	$CH_3 + I_2(aq) \rightarrow CH_3I(aq) + I^O$	6 x 10^9
M394	$CH_3 + HIO_3^- \rightarrow CH_2O + HOI^O + OH^-$	1 x 10^8
M395	$CH_3I(aq) + OH^O \rightarrow CH_3OH + I^O$	1 x 10^8
M396	$CH_3I + H_2O \rightarrow CH_3OH + H^+ + I^-$ $\log_{10}k = 93.14585 - 9661.274/T - 24.42937 \log_{10}T$	
M397	$CH_3I + OH^- \rightarrow CH_3OH + I^-$	6.5 x 10^{-5}
M398	$CH_3I(aq) + e^- \rightarrow CH_3 + I^-$	1.6 x 10^{10}
M399	$CH_3I(aq) + H^O \rightarrow CH_3 + H^+ + I^-$	1 x 10^{10}
M400	$CH_3I(aq) + OH^O \rightarrow CH_4OI$	1.4 x 10^9

Number	Reaction	Rate Constant
M401	$CH_4OI \rightarrow CH_3I^+ + OH^-$	3.1
M402	$CH_4OI + I^- \rightarrow I_2^- + CH_3OH$	2×10^9
M403	$CH_3I^+ + OH^- \rightarrow CH_4OI$	1×10^{10}
M404	$CH_3I^+ + I^- + H_2O \rightarrow CH_3OH + I_2^- + H^+$	7.7×10^9
M405	$CH_2O + OH^O \rightarrow HCO + H_2O$	1×10^9
M406	$Fe^{3+} + 2I^- \rightarrow Fe^{2+} + I_2^-$	21
M407	$CH_3OH + OH^O \rightarrow CH_3O + H_2O$	1×10^9
M408	$2CH_3O \rightarrow$ product	1×10^9
M409	$Fe^{3+} + CH_3O \rightarrow Fe^{2+} +$ product	1×10^9
M410	$H^+ + CH_3O + Fe^{2+} \rightarrow Fe^{3+} + CH_3OH$	1×10^9
M411	$CH_3OH + H^O \rightarrow CH_3O + H_2$	5×10^8
M412	$CH_3OH + e^- \rightarrow H^O + CH_3O$	1×10^4
M413	$CH_3 + CH_3OH \rightarrow CH_4(aq) + CH_3O$	2×10^6
M414	$CH_3O + H_2O_2 \rightarrow CH_2O + OH^O + H_2O$	4×10^4
M415	$CH_3O + O_2 \rightarrow$ products	4.2×10^9
M416	$CH_2O + e^- + H_2O \rightarrow CH_3O + OH^-$	1×10^7
M417	$CH_2O + H^O \rightarrow H_2 + HCO$	5×10^6
M418	$CH_2O + CH_3 \rightarrow CH_4(aq) + HCO$	5×10^6
M419	$CH_2O + O^- \rightarrow OH^- + HCO$	1×10^9

Table 2.7 is the basic water hydrolysis set from INSPECT [42]. Table 2.7 is the iodine reaction set from INSPECT [42,43] and Powers [44]; Table 2.10 is the iron reaction set [44]. Table 2.9 is the organic iodine set [44]. The framework for the organic reactions is in place, but the equations have not been entered, due to a lack of data to compare results. When data becomes available, the organic reactions can be activated by entering the equations into the EQINIT routine. The numbers for the reactions in the first column of the tables corresponds to the reactions as labeled in Powers [44]. The column labeled "Rate Constant" in the tables gives either a constant rate or refers to a calculated rate as given in Table 2.10.

Table 2.10 Variable Rates

M10	$e^- + H_2O \rightarrow H^0 + OH^-$	$R16*K_{H2O}/K_{H0}$
M20	$HO_2^0 \rightarrow H^+ + O_2^-$	$R19*K_{HO2}$
M22	$H_2O_2 \rightarrow H^+ + HO_2^-$	$R21*K_{H2O2}$

M24	$O^- + H_2O \rightarrow OH^0 + OH^-$	R23*K_{H2O}/K_{OH0}
M26	$O_2^- + H_2O \rightarrow HO_2^0 + OH^-$	R25*R19*K_{H2O}/R20
M102	$H_2O_2 \rightarrow 2OH^0$	$6.4x10^5$ exp(-8540/T)
M134	$I_2OH^- \rightarrow I_2(aq) + OH^-$	R132*R133*K_{H2O}/R131
M145	$IO^- + H_2O \rightarrow HOI^0 + OH^-$	R144*R152*K_{H2O}/R151
M149	$I_3^- \rightarrow I_2(aq) + I^-$	R148/K_3

The K_n in the third column of Table 2.10 are equilibrium constants, and the R_n are reaction rates for equation number n. Also needed are the acid dissociation constants (Table 2.11)

Table 2.11 Acid Dissociation Constants

$OH^0 \Leftrightarrow O^- + H^+$	$\log_{10} K_{OH0}$ = -4893.6/T + 60.701 – 22.629 $\log_{10}$ T
$H_2O_2 \Leftrightarrow HO_2^- + H^+$	$\log_{10} K_{H2O2}$ = -3789.7/T + 56.284 – 16.473 $\log_{10}$ T
$HO_2^0 \Leftrightarrow O_2^- + H^+$	$\log_{10} K_{HO2}$ = -519/T – 3.06
$H^0 + OH^- \Leftrightarrow e^- + H_2O$	$\log_{10} K_{H0}$ = -2317/T – 1.816
$I_3^- \Leftrightarrow I_2 + I^-$	$\log_{10} K_{I3-}$ = 945.5/T – 0.282
$HOI \Leftrightarrow IO^- + H^+$	$\log_{10} K_{HOI}$ = -80670/T + 0.7335 T +2800 – 1115.1 $\log_{10}$ T

The solution of the equation set proceeds as follows (box 10 in Figure 2.4):

(1) If this is the initial calculation of speciation (indicated by all species being zero other than the drivers), an initialization is performed to set the initial speciation. At present, this consists of solving for the iodine ion concentration from a set of five equations; these can be reduced to a cubic equation in I^-, which is then solved for directly. The other species in the five equations (I_{2aq}, HOI, IO_3^-, and I_3^-) could also be initialized, but this does not seem to be necessary. In actuality, iodine ion is approximately equal to the total iodine concentration over most of the pH range and only differs at low pHs.

(2) If the pool speciation calculation has been done previously (on the last timestep), the speciation from the last timestep is used as the initial speciation.

(3) The set of chemical reaction equations is solved via a stiff ODE solver [45]. As implemented in MELCOR, the equations are advanced in "time" using a default "timestep" of 2.0s until equilibrium is reached, indicated by the changes in the species concentrations being less than an error criterion, or 2000 steps are taken. This result is then taken as the pool speciation. This equilibrium approach is used, rather than advancing the equations in real time, because of the uncertainty in the actual time history of the pool. That is, the pool initial conditions are set to a

simplified starting point when the pool model becomes activated. This initial starting point does not necessarily reflect the actual pool speciation at pool model activation time, and it is unknown to the pool model how long the pool has actually been in existence. Therefore, the time advancement of the pool equations is treated as an advancement in iteration time to equilibrium, rather than advancement in real time. The "iteration timestep", the number of steps, and the convergence criteria are adjustable via sensitivity coefficients 7181.

2.11.7.4.2 Aqueous Radiolysis

The radiolysis model for the pool uses a set of temperature-dependent yields based on values recommended by Buxton et al. [46] at 298 K and Elliot et al. [47] at 573 K, as listed in Table 2.12.

Table 2.12 Primary Products of Water Radiolysis

Species	G (molecules/100 ev)
$e^- = H^+$	0.9204 + 5.364 T/1000
H	0.0798 + 1.7454 T/1000
OH^0	1.3238 + 4.6182 T/1000
H_2	0.2658 + 0.6182 T/1000
H_2O_2	0.1040 + 2.000 T/1000

This set of yields is used with the user-specified pool dose to calculate the radiolysis source terms for the aqueous chemistry reaction set, as

$$\dot{S}_i = G(i)\,2.88\times10^{-7}\,\dot{D}_{pool}$$

where

$\dot{S}_i$ = radiolysis source for species *i* in pool (kmole/m^3-s)

$G(i)$ = yield factor for species *i*

$\dot{D}_{pool}$ = dose rate to pool (MRad/hr)

2.11.7.4.3 Speciation Initialization

The initialization of the pool species is done by combining a set of five iodine equations to eliminate all but the I^- concentration. This gives a cubic equation in the I^- concentration, which can be solved directly. The equation set does not include the effects of H_2O_2 on iodine, so is not a particularly good guess at high pHs.

2.11.7.5 Pool-Atmosphere Mass Transfer

Once the pool speciation is determined by the aqueous chemistry model, the mass exchange of iodine and methyl iodine with the atmosphere is calculated (see Figure 2.4). This is done via a two-film model, in which the concentration of iodine species in the pool at the pool surface is assumed to be in equilibrium via a partition coefficient with the species in the atmosphere in a film next to the pool surface at local saturation conditions. Mass transfer is then done between this surface film and the bulk atmosphere based on the surface-bulk species concentration difference and a mass transfer coefficient. Transfer rates between the bulk pool and pool surface are ignored (the pool is assumed to be well-stirred). Partition coefficients are included for I_2, CH_3I, I^0, and HOI. The mass transfer equation for iodine is written as

$$\frac{d[I_{2atm}]}{dt} = k_{pool}\frac{A_{pool}}{V_{atm}}\left([I_{2aq}] \;/\; PC_{I2} - [I_{2atm}]\right)$$

where

$[I_{2atm}]$ = atmospheric iodine concentration (kmole/m^3)

$[I_{2aq}]$ = bulk pool iodine concentration (kmole/m^3)

k_{pool} = mass transfer coefficient from pool surface to atmosphere (m/s)

PC_{I2} = partition coefficient for iodine.

The above equation can be written several ways, so care must be taken when comparing between codes.

The partition coefficient is defined as PC_I = (concentration of species *i* in aqueous phase) / (concentration of species *i* in gas-phase). The most important species released from the pool to the atmosphere is molecular iodine. The partition coefficient for iodine used in MELCOR is given as [48]

$$\log_{10} PC_{I2} = 13.5467 - 0.0605142\,T + 7.166\times10^{-5}T^2$$

where T is in °K. The partition coefficients for I^o and HOI in MELCOR are both the same and are given as

$$PC_{I0} = 0.0238\;PC_{I2}$$

This is derived by taking the ratio of the *PC* for I^0 (1.9) [43] and that for I_2 at room temperature and pressure, and assuming the same temperature dependence for I^0 as for I_2. The partition coefficients for I^0 and HOI should be used with caution, as there is little proof for the contention that either can be released from the pool. Although a number of researchers have suggested partition coefficients for HOI, researchers have failed to measure its presence [49], and the partition coefficient for HOI should be regarded as a placeholder. Likewise, release of atomic iodine is controversial. These two *PC*s are defaulted to **OFF** in the iodine model but can be turned on via user input. The *PC* for methyl iodine is [50]

$$PC_{CI} = 9.4 \times 10^{-4} \exp\left(\frac{2641}{T}\right)$$

2.11.7.6 Iodine Atmospheric Radiolysis and Recombination

The atmospheric radiolysis model considers homogeneous radiolytic decomposition of iodine species, and subsequent recombination reactions.

The atmospheric reduction of iodine is represented by reactions with hydrogen and ozone, and radiolytic reduction. The thermal reduction reaction with hydrogen is

$$\frac{d[I_{2atm}]}{dt} = -k_{TIH}[I_{2atm}][H_2]$$

where the reaction rate is [51]

$$k_{TIH} = 1 \times 10^{11} \exp\left(-\frac{20131}{T}\right)$$

And,

k_{TIH} = reaction coefficient with hydrogen (m^3/kMol-s)

T = atmospheric temperature (K).

The reaction with ozone is

$$\frac{d[I_{2atm}]}{dt} = -k_{TIO}[I_{2atm}][O_3]$$

where the reaction coefficient is [52]

$$k_{TIO} = 2.42 \times 10^{6} \exp\left(-\frac{2050}{T}\right).$$

The radiolytic reduction effect is given as [53]

$$k_{RI} = 0.028\ \dot{D}_{atm}$$

where

k_{RI} = radiolytic reduction coefficient, and

$\dot{D}_{atm}$ = atmospheric dose rate (MRad/hr).

The organic iodine is similarly reduced using an oxidation and a radiolytic reaction [54]. The oxidation reaction is

$$\frac{d[CH_3I_{atm}]}{dt} = -k_{TCIO}[CH_3I_{atm}][O_2]$$

where

$[CH_3I_{atm}]$ = atmospheric methyl iodide concentration (kmole/m^3),

k_{TCIO} = oxidation reaction rate, given as

k_{TCIO} = $10^{9} \exp\left(-\frac{13235}{T}\right)$.

The radiolytic reduction rate is

$$K_{RCL} = 0.00164\ \dot{D}_{atm}$$

where, k_{RCI} is the radiolytic reduction coefficient for CH_3I. The effect of the decomposition is to increase the amount of elemental iodine in the atmosphere, decreasing the amount of I_2 and CH_3I.

The recombination reaction is assumed to be in equilibrium, using the new concentrations of I_2 and I^0. An equilibrium coefficient,

$$K_{I2I} = \frac{p(I_2)}{p(I)^2}$$

$$K_{I2I} = 5.44 \times 10^{-6} \exp\left(\frac{18163}{T}\right)$$

and a mole balance on the iodine in the atmosphere as I_2 and I^0

$$M(I) = 2[I_2] + [I^0]$$

where *M(I)* is the molar concentration of I, is used to calculate the recombination of elemental iodine into I_2. Combining the equilibrium coefficient K_{I2I} with the mole balance gives the new concentration of I^0 as

$$[I^0] = \frac{1}{4K_{I2I}RT}\left[-1 + \sqrt{1 + 8K_{I2I}M(I)RT}\right].$$

Since I^0 is not tracked in MELCOR, the I^0 is added to the I_2 for purposes of transport. The net effect of the decomposition-recombination reactions is to deplete CH_3I from the atmosphere and form I_2.

where

$[I_{2wall}]$ = wall surface iodine concentration (kmole/m^2)

k_{ad} = adsorption coefficient (m/s)

k_{de} = desorption coefficient (s^{-1}).

Default values for steel walls were selected to match results of RTF tests [55]. The coefficients are adjustable via sensitivity coefficients 7180. If the dry wall surfaces subsequently become wet, the water film is assumed to completely dissolve the adsorbed iodine and the film can drain to other surfaces or the pool via the MELCOR film model. The same model is used for steel or painted surfaces, although there is some evidence for a second stage chemical reaction process on painted adsorbing surfaces. There is not enough data presently available to determine the terms for such a model, so the physical model is used by itself.

2.11.7.7 Iodine Atmosphere-Wall Deposition

Iodine species in the atmosphere are allowed to deposit on dry wall surfaces via a physical adsorption-desorption model similar to the one in LIRIC [55]. The model is given as

$$\frac{d[I_{2wall}]}{dt} = k_{ad}[I_{2atm}] - k_{de}[I_{2wall}]$$

where

$[I_{2wall}]$ = wall surface iodine concentration (kmole/m^2)

k_{ad} = adsorption coefficient (m/s), and

k_{de} = desorption coefficient (s^{-1}).

Default values for steel walls were selected to match results of RTF tests [55]. The coefficients are adjustable via sensitivity coefficients 7180. If the dry wall surfaces subsequently become wet, the water film is assumed to completely dissolve the adsorbed iodine and the film can drain to other surfaces or the pool via the MELCOR film model. The same model is used for steel or painted surfaces, although there is some evidence for a second stage chemical reaction process on painted adsorbing surfaces. There is not enough data presently available to determine the terms for such a model, so the physical model is used by itself.

2.11.8 Data Base Supporting Model Validation

There are three series of experiments that can be used for validating these models, the wide ranging Radioiodine Test Facility (RTF) experiments that are part of the Advanced Containment Experiments (ACE) performed at (AECL) Whiteshell Nuclear Research Establishment [56], small scale radiolysis tests performed at (CEA) Cadarache [57], and the hydrolysis experiments performed at Oak Ridge National Laboratory (ORNL) [40]. In the RTF experiments, tests 2 and 3 varied the pH over a wide range and measured the iodine partition coefficient, that is, the ratio of the aqueous iodine to the airborne iodine concentrations. Qualitatively, they were able to show that as the pH increases, the partition coefficient increases, and the atmospheric iodine concentration decreases. In the CEA tests, a solution of iodine was exposed to a 0.4 MR/hr source and the iodine speciation was measured. The present MELCOR iodine model was used in a recent participation in International Standard Problem (ISP) 41.

In the ORNL experiments, the temperature and pH of a pool was varied from 25 to 90 degrees Centigrade and from 3 to 9, respectively. In these tests, the end product iodine speciation was measured.

Development and testing of the model initial testing was based on comparison with the results from other codes, in particular radiolysis results from the INSPECT code. Testing against ISP41 results validated the iodine pool-atmosphere partitioning variation with pH and the coefficients for the wall deposition on steel walls [58]. As mentioned, sufficient data to vallidate the organic reaction set is not yet available, so the organic reactions are not implemented, although all the framework is present.

In later testing, the model will be compared with the available experimental data discussed previously, that is, the Canadian, French, and Oak Ridge data for validation. Finally, the effect of iodine chemistry on a late phase accident will be evaluated.

3. Discussion and Development Plans

3.1 RCS Deposition

The MELCOR Peer Review also placed the omission of some aerosol deposition processes, principally inertial impaction and turbulent deposition, on the list of the most important missing models in MELCOR. These processes, which are not generally important in containment and which therefore are not included in MAEROS, may assume primary importance in the reactor coolant system. As discussed in the MELCOR Peer Review, experimental data and calculations using more comprehensive aerosol deposition models indicate that the neglect of these processes may result in a significant underestimate of the retention of aerosols in the primary system, especially for low-pressure sequences in which gas velocities are high. However, the Marviken assessment calculations [59] showed good agreement with primary system retention data for both aerosols and fission product vapors, indicating the possibility of compensating processes.

3.2 Chemical Reactions with Surfaces

The MELCOR Peer Review also identified the lack of explicit modeling in MELCOR for chemical reactions between deposited fission products and structures in the primary system as one of the most important missing models. Such reactions can greatly affect deposition (chemisorption) and revaporization rates. Although a framework exists in the RN package for allowing user specification of chemical reactions, it is largely untested and unused. Because user input is basically unconstrained, the generation of errors through unexpected reactions is quite possible. The MELCOR Peer Review noted that the lack of explicit modeling applies to all accident sequences and is particularly serious for cesium hydroxide and tellurium compounds. This has been addressed in release 1.8.4 via the surface chemisorption model.

3.3 Aqueous Chemistry

The MELCOR Peer Review separately identified fission product chemistry in water pools as a less critical but still important modeling omission. The chief concern expressed in the MELCOR Peer Review was that release of iodine to the environment may be understated because MELCOR neglects processes that can occur in water pools to transform cesium iodide into more volatile forms of iodine (e.g., reaction with methane to form methyl iodide). The MELCOR 1.8.5 code release includes a detailed iodine pool chemistry model, based largely on the INSPECT code and on work by Powers. The model has received limited testing and verification against the ISP-41 test data [58]. Future assessment against other experimental data is recommended in order to further evaluate and refine other important aspects of iodine chemistry including organic compounds and silver.

Appendix A: RN Package Sensitivity Coefficients

This appendix gives the sensitivity coefficients associated with various correlations and modeling parameters described in this reference manual.

Equation or Section	Coefficient	Value	Units
Sec. 2.4.2.3	C7000(1)	1.0E-18	-
	C7000(2)	0.001	-
	C7000(3)	0.1	-
	C7000(4)	0.1	-
	C7000(5)	1.0E-12	kg/m^3

Aerosol Coefficient Criteria			
	C7001(1)	1.0E-18	-
	C7001(2)	0.001	-

Fission Product Decay Beta Range			
Sec. 2.6	C7002(1)	1.2	Kg/m^2

COR Material Release Multipliers			
Sec. 2.3.1	C7100(1)	1.0	-
	C7100(2)	0.0	-
	C7100(3)	0.0	-
	C7100(4)	0.0	-
	C7100(5)	0.0	-
	C7100(6)	0.0	-
	C7100(7)	0.0	-

CORSOR Coefficients			
2.3.1	C7101(1,1,k), $k \neq 5$	900.0	K
	C7101(2,1,k), $k \neq 5$	1400.0	K
	C7101(3,1,k), $k \neq 5$	2200.0	K
	C7101(1,1,5)	900.0	K
	C7101(2,1,5)	1600.0	K
	C7101(3,1,5)	2000.0	K
	C7101(1,2,1)	7.02E-9	min-1
	C7101(2,2,1)	2.02E-7	min-1
	C7101(3,2,1)	1.74E-5	min^{-1}
	C7101(1,3,1)	0.00886	$°C^{-1}$
	C7101(2,3,1)	0.00667	$°C^{-1}$

CORSOR Coefficients			
	C7101(3,3,1)	0.00460	$^{\circ}C^{-1}$
	C7101(1,2,2)	7.53E-12	min-1
	C7101(2,2,2)	2.02E-7	min-1
	C7101(3,2,2)	1.74E-5	min-1
	C7101(1,3,2)	0.0142	$^{\circ}C^{-1}$
	C7101(2,3,2)	0.00667	$^{\circ}C^{-1}$
	C7101(3,3,2)	0.00460	$^{\circ}C^{-1}$
	C7101(1,2,3)	7.50E-14	min-1
	C7101(2,2,3)	8.26E-9	min-1
	C7101(3,2,3)	1.38E-5	min-1
	C7101(1,3,3)	0.0144	$^{\circ}C^{-1}$
	C7101(2,3,3)	0.00631	$^{\circ}C^{-1}$
	C7101(3,3,3)	0.00290	$^{\circ}C^{-1}$
	C7101(1,2,4)	7.02E-9	min-1
	C7101(2,2,4)	2.02E-7	min-1
	C7101(3,2,4)	1.74E-5	min-1
	C7101(1,3,4)	0.00886	$^{\circ}C^{-1}$
	C7101(2,3,4)	0.00667	$^{\circ}C^{-1}$
	C7101(3,3,4)	0.00460	$^{\circ}C^{-1}$
	C7101(1,2,5)	1.62E-11	min-1
	C7101(2,2,5)	9.04E-8	min-1
	C7101(3,2,5)	6.02E-6	min-1
	C7101(1,3,5)	0.0106	$^{\circ}C^{-1}$
	C7101(2,3,5)	0.00552	$^{\circ}C^{-1}$
	C7101(3,3,5)	0.00312	$^{\circ}C^{-1}$
	C7101(1,2,6)	1.36E-11	min-1
	C7101(2,2,6)	1.36E-11	min-1
	C7101(3,2,6)	1.40E-6	min-1
	C7101(1,3,6)	0.00768	$^{\circ}C^{-1}$
	C7101(2,3,6)	0.00768	$^{\circ}C^{-1}$
	C7101(3,3,6)	0.00248	$^{\circ}C^{-1}$
	C7101(1,2,7)	5.01E012	min-1
	C7101(2,2,7)	5.93E-8	min-1
	C7101(3,2,7)	3.70E-5	min-1
	C7101(1,3,7)	0.0115	$^{\circ}C^{-1}$
	C7101(2,3,7)	0.00523	$^{\circ}C^{-1}$
	C7101(3,3,7)	0.00200	$^{\circ}C^{-1}$
	C7101(1,2,8)	6.64E-12	min-1

CORSOR Coefficients			
	C7101(2,2,8)	6.64E-12	min-1
	C7101(3,2,8)	1.48E-7	min-1
	C7101(1,3,8)	0.00631	$^{\circ}C^{-1}$
	C7101(2,3,8)	0.00631	$^{\circ}C^{-1}$
	C7101(3,3,8)	0.00177	$^{\circ}C^{-1}$
	C7101(1,2,9)	5.00E-13	min-1
	C7101(2,2,9)	5.00E-13	min-1
	C7101(3,2,9)	5.00E-13	min-1
	C7101(1,3,9)	0.00768	$^{\circ}C^{-1}$
	C7101(2,3,9)	0.00768	$^{\circ}C^{-1}$
	C7101(3,3,9)	0.00768	$^{\circ}C^{-1}$
	C7101(1,2,10)	5.00E-13	min-1
	C7101(2,2,10)	5.00E-13	min-1
	C7101(3,2,10)	5.00E-13	min-1
	C7101(1,3,10)	0.00768	$^{\circ}C^{-1}$
	C7101(2,3,10)	0.00768	$^{\circ}C^{-1}$
	C7101(3,3,10)	0.00768	$^{\circ}C^{-1}$
	C7101(1,2,11)	1.90E-12	min-1
	C7101(2,2,11)	5.88E-9	min-1
	C7101(3,2,11)	2.56E-6	min-1
	C7101(1,3,11)	0.0128	$^{\circ}C^{-1}$
	C7101(2,3,11)	0.00708	$^{\circ}C^{-1}$
	C7101(3,3,11)	0.00426	$^{\circ}C^{-1}$
	C7101(1,2,12)	1.90E-12	min-1
	C7101(2,2,12)	5.88E-9	min-1
	C7101(3,2,12)	2.56E-6	min-1
	C7101(1,3,12)	0.0128	$^{\circ}C^{-1}$
	C7101(2,3,12)	0.00708	$^{\circ}C^{-1}$
	C7101(3,3,12)	0.00426	$^{\circ}C^{-1}$
	C7101(1,2,13:20)	0.0	min-1
	C7101(2,2,13:20)	0.0	min-1
	C7101(3,2,13:20)	0.0	min-1
	C7101(1,3,13:20)	0.0	$^{\circ}C^{-1}$
	C7101(2,3,13:20)	0.0	$^{\circ}C^{-1}$
	C7101(3,3,13:20)	0.0	$^{\circ}C^{-1}$

CORSOR-M Coefficients			
2.3.2	C7102(1,1)	2.0E5	min^{-1}

CORSOR-M Coefficients			
	C7102(2,1)	63.8	kcal/mole
	C7102(1,2)	2.0E5	min^{-1}
	C7102(2,2)	63.8	kcal/mole
	C7102(1,3)	2.95E5	min^{-1}
	C7102(2,3)	100.2	kcal/mole
	C7102(1,4)	2.0E5	min^{-1}
	C7102(2,4)	63.8	kcal/mole
	C7102(1,5)	2.0E5	min^{-1}
	C7102(2,5)	63.8	kcal/mole
	C7102(1,6)	1.62E6	min^{-1}
	C7102(2,6)	152.8	kcal/mole
	C7102(1,7)*	23.15	min^{-1}
	C7102(2,7)*	44.1	kcal/mole
	C7102(1,8)	2.67E8	min^{-1}
	C7102(2,8)	188.2	kcal/mole
	C7102(1,9)**	1.46E7	min^{-1}
	C7102(2,9)**	143.1	kcal/mole
	C7102(1,10)	1.46E7	min^{-1}
	C7102(2,10)	143.1	kcal/mole
	C7102(1,11)**	5.95E3	min^{-1}
	C7102(2,11)**	70.8	kcal/mole
	C7102(1,12)	5.95E3	min^{-1}
	C7102(2,12)	70.8	kcal/mole
	C7102(1,13)	0.0	min^{-1}
	C7102(2,13)	0.0	kcal/mole

Note. The CORSOR-M model does not consider release from Class 7 (Moly), Class 9 (La) or Class 11 (Cd) to be significant. Previous versions of MELCOR used zero values for these classes when using CORSOR-M. In MELCOR 1.8.5 non-zero release coefficients are supplied as described.

* Coefficients for CORSOR-M class 7 (Moly) are based on a curve fit to the CORSOR release model for Class 7.

** Coefficients for CORSOR-M Class 7 are set identical to the CORSOR-M Class 8 values, following the same assumption as used in the CORSOR model for Class 7. Likewise for Class 11 and 12.

CORSOR-Booth Class Scaling Factors: Nominal Values			
	C7103(1)	1.0	-
	C7103(2)	1.0	-
	C7103(3)	3.33E-3	-
	C7103(4)	1.0	-
	C7103(5)	1.0	-
	C7103(6)	1.0E-4	-
	C7103(7)	1.0E-3	-
	C7103(8)	3.34E-5	-

CORSOR-Booth Class Scaling Factors: Nominal Values			
	C7103(9)	1.0E-4	-
	C7103(10)	1.0E-4	-
	C7103(11)	5.0E-2	-
	C7103(12)	5.0E-2	-
	C7103(13:20)	0.0	-

Release Surface-to-Volume Ratio			
	C7104(1)	422.5	m^{-1}

Modification of Release Rates for Tellurium			
Sec. 2.3.1	C7105(1)	5.0	-
	C7105(2)	0.7	-
	C7105(3)	0.025	-

CORSOR-Booth Coefficients for Cesium			
2.3.3	C7106(1)	5.0E-8	m^2/s
	C7106(2)	2.5E-7	m^2/s
	C7106(3)	3.0E4	MWD/MTU
	C7106(4)	3.8E5	J/kg-mole
	C7106(5)	1.0E-5	m

CORSOR-Booth Class Scaling Factors: Oxidation Modified			
	C7107(6,3)	0.05	-
	C7107(7,3)	0.05	-
	C7107(6,5)	0.70	-
	C7107(7,5)	0.025	-
	C7107(1,6)	0.75	-
	C7107(2,6)	2300.0	K
	C7107(3,6)	1.06792E-20	-
	C7107(4,6)	0.0159923	K^{-1}
	C7107(5,6)	2700.0	K
	C7107(6,9)	0.05	-
	C7107(7,9)	0.10	-
	C7107(1,11:12)	0.75	-
	C7107(2,11:12)	2000.0	K
	C7107(3,11:12)	3.194E-9	-
	C7107(4,11:12)	0.008283	K^{-1}
	C7107(5,11:12)	2300.0	K
	otherwise		

CORSOR-Booth Class Scaling Factors: Oxidation Modified			
	C7107(1,i)	1.1	-
	C7107(2,i)	0.0	K
	C7107(3,i)	0.0	-
	C7107(4,i)	0.0	K^{-1}
	C7107(5,i)	0.0	K
	C7107(6,i)	-1.0	-
	C7107(7,i)	0.0	-

Vapor Pressure			
2.5.22	C7110(1,1,1)	0.0	K
	C7110(1,2,1)	-1.0	K
	C7110(2,1,1)	10000.0	K
	C7110(1,1,2)	600.0	K
	C7110(1,2,2)	9400.0	K
	C7110(1,3,2)	21.59	-
	C7110(1,4,2)	-3.75	-
	C7110(2,1,2)	1553.0	K
	C7110(2,2,2)	6870.778	K
	C7110(2,3,2)	7.994503	-
	C7110(2,4,2)	0.	-
	C7110(1,1,3)	1000.0	K
	C7110(1,2,3)	7836.0	K
	C7110(1,3,3)	6.44	-
	C7110(1,4,3)	0.	-
	C7110(2,1,3)	10000.	K
	C7110(1,1,4)	298.0	K
	C7110(1,2,4)	3578.0	K
	C7110(1,3,4)	17.72	-
	C7110(1,4,4)	-2.51	-
	C7110(2,1,4)	387.0	K
	C7110(2,2,4)	3205.0	K
	C7110(2,3,4)	23.66536	-
	C7110(2,4,4)	-5.18	-
	C7110(3,1,4)	457.0	K
	C7710(3,2,4)	2176.912045	K
	C7110(3,3,4)	7.63735266	-
	C7110(3,4,4)	0.	-
	C7110(1,1,5)	298.0	K
	C7110(1,2,5)	13940.0	K
	C7110(1,3,5)	23.51	-

Vapor Pressure			
	C7110(1,4,5)	-3.52	-
	C7110(2,1,5)	10000.0	K
	C7110(1,1,6)	1500.0	K
	C7110(1,2,6)	33200.0	K
	C7110(1,3,6)	10.6088	-
	C7110(1,4,6)	0.0	-
	C7110(2,1,6)	10000.0	K
	C7110(1,1,7)	1500.0	K
	C7110(1,2,7)	32800.0	K
	C7110(1,3,7)	9.68	-
	C7110(1,4,7)	0.0	-
	C7110(2,1,7)	10000.0	K
	C7110(1,1,8)	1500.0	K
	C7110(1,2,8)	21570.0	K
	C7110(1,3,8)	8.74	-
	C7110(1,4,8)	0.0	-
	C7110(2,1,8)	10000.0	K
	C7110(1,1,9)	1500.0	K
	C7110(1,2,9)	21800.0	K
	C7110(1,3,9)	8.683	-
	C7110(1,4,9)	0.0	-
	C7110(2,1,9)	10000.0	K
	C7110(1,1,10)	1500.0	K
	C7110(1,2,10)	32110.0	K
	C7110(1,3,10)	11.873	-
	C7110(1,4,10)	0.0	-
	C7110(2,1,10)	10000.0	K
	C7110(1,1,11)	1000.0	K
	C7110(1,2,11)	13730.0	K
	C7110(1,3,11)	8.43	-
	C7110(1,4,11)	0.0	-
	C7110(2,1,11)	10000.0	K
	C7110(1,1,12)	1000.0	K
	C7110(1,2,12)	15400.0	K
	C7110(1,3,12)	8.15	-
	C7110(1,4,12)	0.0	-
	C7110(2,1,12)	10000.0	K
	C7110(1,1,13)	1000.0	K
	C7110(1,2,13)	19520.0	K
	C7110(1,3,13)	11.125	-

Vapor Pressure			
	C7110(1,4,13)	0.0	-
	C7110(2,1,13)	10000.0	K
	C7110(1,1,14:15)	3000.0	K
	C7110(1,2,14:15)	18000.0	K
	C7110(1,3,14:15)	8.875	-
	C7110(1,4,14:15)	0.	-
	C7110(2,1,14:15)	10000.	K
	C7110(1,1,16)	600.0	K
	C7110(1,2,16)	10420.0	K
	C7110(1,3,16)	19.70	-
	C7110(1,4,16)	-3.02	-
	C7110(2,1,16)	894.0	K
	C7110(2,2,16)	9678.0	K
	C7110(2,3,16)	20.34569	-
	C7110(2,4,16)	-3.52	-
	C7110(3,1,16)	1553.0	K
	C7110(1,1,17:20)	3000.0	K
	C7110(1,2,17:20)	18000.0	K
	C7110(1,3,17:20)	8.875	-
	C7110(1,4,17:20)	0.	-
	C7110(2,1,17:20)	10000.	K

Vapor Diffusivity Constants			
2.5.20	C7111(1,1)	4.055	Å
	C7111(2,1)	229.0	K
	C7111(1,2:3)	3.617	Å
	C7111(2,2:3)	97.0	K
	C7111(1,4)	4.982	Å
	C7111(2,4)	550.0	K
	C7111(1,5:20)	3.617	Å
	C7111(2,5:20)	97.0	K

Class Molecular Weights			
Sec. 2.1	C7120(1,1)	131.3	kg/kg-mole
	C7120(2,1)	131.3	kg/kg-mole
	C7120(1,2)	132.905	kg/kg-mole
	C7120(2,2)	149.913	kg/kg-mole
	C7120(1,3)	137.34	kg/kg-mole

Class Molecular Weights			
	C7120(2,3)	137.34	kg/kg-mole
	C7120(1,4)	253.8008	kg/kg-mole
	C7120(2,4)	253.8008	kg/kg-mole
	C7120(1,5)	127.6	kg/kg-mole
	C7120(2,5)	143.6	kg/kg-mole
	C7120(1,6)	101.07	kg/kg-mole
	C7120(2,6)	101.07	kg/kg-mole
	C7120(1,7)	95.94	kg/kg-mole
	C7120(2,7)	95.94	kg/kg-mole
	C7120(1,8)	140.12	kg/kg-mole
	C7120(2,8)	140.12	kg/kg-mole
	C7120(1,9)	138.91	kg/kg-mole
	C7120(2,9)	138.91	kg/kg-mole
	C7120(1,10)	238.03	kg/kg-mole
	C7120(2,10)	270.03	kg/kg-mole
	C7120(1,11)	112.4	kg/kg-mole
	C7120(2,11)	112.4	kg/kg-mole
	C7120(1,12)	118.69	kg/kg-mole
	C7120(2,12)	118.69	kg/kg-mole
	C7120(1,13)	69.622	kg/kg-mole
	C7120(2,13)	69.622	kg/kg-mole
	C7120(1,14)	18.016	kg/kg-mole
	C7120(2,14)	18.016	kg/kg-mole
	C7120(1,15)	28.97	kg/kg-mole
	C7120(2,15)	28.97	kg/kg-mole
	C7120(1,16)	259.8054	kg/kg-mole
	C7120(2,16)	259.8054	kg/kg-mole
	C7120(1,17:20)	28.97	kg/kg-mole
	C7120(2,17:20)	28.97	kg/kg-mole

Solubility of RN Classes in Water Films			
Sec. 2.4.2.2	C7136(1:20)	1.0	-

Not Used with LWR COR Package
7140 - Release from Molten U-Al Pools
7141 - Solubility of Classes in Al-U Alloy
7142 - Debris Particle of Average Surface Area
7143 - Molten Fraction Criterion for Release from U-Al Pools
7144 - Temperature Criterion for Release from Intact Fuel

7150 - SPARC-90 Model Parameters			
Appendix E	7150(1)	10.	-
	7150(2)	5.	-
	7150(3)	1.E-4	-
	7150(4)	25.	-
	7150(5)	1.E-4	-
	7150(6)	25.	-
	7150(7)	1.E-3	-
	7150(8)	25.	-
	7150(9)	1.E12	-
	7150(10)	1.0	-

7151 - SPARC-90 Globule Size Correlation			
Appendix D	7151(1,1)	3.45	-
	7151(2,1)	0.46	-
	7151(1,2)	0.0891	-
	7151(2,2)	0.616	-
	7151(1,3)	0.857	-
	7151(2,3)	0.73	-

7152 - SPARC-90 Bubble Size/Shape Model			
E-1	7152(1)	0.007	m
	7152(2)	-0.2265	-
	7152(3)	0.0203	-
	7152(4)	0.0313	-
	7152(5)	0.5	-
E-2	7152(6)	0.817	-
	7152(7)	1.13466	cm^{-1}
	7152(8)	-0.3795	cm^{-2}

7153 - SPARC-90 Bubble Rise Velocity Model			
E-3	7153(1)	7.876	cm/s
	7153(2)	0.5	cm
	7153(3)	1.40713	-
	7153(4)	0.49275	-

7154 - SPARC-90 Swarm Velocity Model			
E-5	7154(1)	5.33	liter/s
	7154(2)	3.011E-3	liter-s/cm^2
	7154(3)	0.5	-
	7154(4)	-3.975E-4	cm^{-1}

7154 - SPARC-90 Swarm Velocity Model			
	7154(5)	170.	cm/s

7155 - SPARC-90 Particle Impaction Model			
D-11	7155(1)	1.79182	-
	7155(2)	3.3437E-11	-
	7155(3)	5.9244E-3	-
	7155(4)	0.65868	-
D-12	7155(5)	1.13893	-
	7155(6)	1.4173E-6	-
	7155(7)	4.25973E-3	-
	7155(8)	0.99	-

7156 - SPARC-90 Solute Ionization Correlations			
E-12	7156(1)	1.79417	-
	7156(2)	-3.34363	-
	7156(3)	0.021	-
	7156(4)	1.63439	-
	7156(5)	4.30022	-
	7156(6)	1.75467	-
	7156(7)	20.7974	-
	7156(8)	-0.002321	-
	7156(9)	25.	C
	7156(10)	2.0	-

7157 - SPARC-90 Settling Velocity Correlation			
E-19	7157(1)	9.6	-
	7157(2)	27.00	-
	7157(3)	1./1.130	-
	7157(4)	93.6	-
	7157(5)	24.32	-
	7157(6)	1./1.227	-
	7157(7)	410.	-
	7157(8)	15.71	-
	7157(9)	1./1.417	-
	7157(10)	1.07E4	-
	7157(11)	6.477	-
	7157(12)	1./1.609	-
	7157(13)	2.45E5	-
	7157(14)	1.194	-
	7157(15)	1./1.867	-

7158 - SPARC-90 HOI Correlation			
F-4	7158(1)	-1388.89	K
	7158(2)	6.461	-

7159 - SPARC-90 I_2 Chemistry Model Parameters			
Appendix F	7159(1)	1.3882E-3	-
	7159(2)	3279.3	K
	7159(3)	7.7606	$moles^{-1}$
	7159(4)	1370.	K
	7159(5)	1.0423E-2	$moles^{2}$
	7159(6)	-7148.	K
	7159(7)	4.2271E-9	moles
	7159(8)	-1748.5	K
	7159(9)	1.56531E-13	$moles^{2}$
	7159(10)	5462.81	K
	7159(11)	-1.87376E6	K^{2}
	7159(12)	1.E-6	$moles/cm^{3}$
	7159(13)	1.E-3	-

7160 - Chemisorption Rate Coefficients			
2.9.2	C7160(1,1)	0.139	m/s
	C7160(2,1)	5.96e7	J/kg
	C7160(1,2)	0.035	m/s
	C7160(2,2)	5.96e7	J/kg
	C7160(1,3)	2.0e-7	m/s
	C7160(2,3)	0.0	J/kg
	C7160(1,4)	2.0e-6	m/s
	C7160(2,4)	0.0	J/kg
	C7160(1,5)	5.5e-7	m/s
	C7160(2,5)	2.49e7	J/kg
	C7160(1,6)	9.0e-10	m/s
	C7160(2,6)	3.39e7	J/kg

7170 Hygroscopic Aerosol Sensitivity Coefficients			
Reference	Coefficient	Value	Units
	C7170(1,1)	273.0	K
	C7170(2,1)	373.0	K
	C7170(3,1)	0.0	Kg/kg H_2O
	C7170(4,1)	0.0	Kg/kg H_2O
	C7170(5,1)	600.0	K
	C7170(6,1)	647.0	K

7170 Hygroscopic Aerosol Sensitivity Coefficients			
Reference	Coefficient	Value	Units
	C7170(7,1)	2	ions/molecule
	C7170(8,1)	0	Ions/molecule
	C7170(9,1)	1.0	Kg/m^3
	C7170(1,2)	273.0	K
	C7170(2,2)	373.0	K
	C7170(3,2)	3.95	Kg/kg H_2O
	C7170(4,2)	3.95	Kg/kg H_2O
	C7170(5,2)	600.0	K
	C7170(6,2)	647.0	K
	C7170(7,2)	2	ions/molecule
	C7170(8,2)	0	Ions/molecule
	C7170(9,2)	3675.0	Kg/m^3
	C7170(1,3)	273.0	K
	C7170(2,3)	373.0	K
	C7170(3,3)	0.0	Kg/kg H_2O
	C7170(4,3)	0.0	Kg/kg H_2O
	C7170(5,3)	600.0	K
	C7170(6,3)	647.0	K
	C7170(7,3)	2	ions/molecule
	C7170(8,3)	0	Ions/molecule
	C7170(9,3)	5720.0	Kg/m^3
	C7170(1,4)	273.0	K
	C7170(2,4)	373.0	K
	C7170(3,4)	0.0	Kg/kg H_2O
	C7170(4,4)	0.0	Kg/kg H_2O
	C7170(5,4)	600.0	K
	C7170(6,4)	647.0	K
	C7170(7,4)	2	ions/molecule
	C7170(8,4)	0	Ions/molecule
	C7170(9,4)	1.0	Kg/m^3
	C7170(1,5)	273.0	K
	C7170(2,5)	373.0	K
	C7170(3,5)	0.0	Kg/kg H_2O
	C7170(4,5)	0.0	Kg/kg H_2O
	C7170(5,5)	600.0	K
	C7170(6,5)	647.0	K
	C7170(7,5)	2	ions/molecule
	C7170(8,5)	0	Ions/molecule
	C7170(9,5)	5680.0	Kg/m^3
	C7170(1,6)	273.0	K

7170 Hygroscopic Aerosol Sensitivity Coefficients			
Reference	Coefficient	Value	Units
	C7170(2,6)	373.0	K
	C7170(3,6)	0.0	Kg/kg H_2O
	C7170(4,6)	0.0	Kg/kg H_2O
	C7170(5,6)	600.0	K
	C7170(6,6)	647.0	K
	C7170(7,6)	2	ions/molecule
	C7170(8,6)	0	Ions/molecule
	C7170(9,6)	6970.0	Kg/m^3
	C7170(1,7)	273.0	K
	C7170(2,7)	373.0	K
	C7170(3,7)	0.0	Kg/kg H_2O
	C7170(4,7)	0.0	Kg/kg H_2O
	C7170(5,7)	600.0	K
	C7170(6,7)	647.0	K
	C7170(7,7)	2	ions/molecule
	C7170(8,7)	0	Ions/molecule
	C7170(9,7)	7440.0	Kg/m^3
	C7170(1,8)	273.0	K
	C7170(2,8)	373.0	K
	C7170(3,8)	0.0	Kg/kg H_2O
	C7170(4,8)	0.0	Kg/kg H_2O
	C7170(5,8)	600.0	K
	C7170(6,8)	647.0	K
	C7170(7,8)	2	ions/molecule
	C7170(8,8)	0	Ions/molecule
	C7170(9,8)	7000.0	Kg/m^3
	C7170(1,9)	273.0	K
	C7170(2,9)	373.0	K
	C7170(3,9)	0.0	Kg/kg H_2O
	C7170(4,9)	0.0	Kg/kg H_2O
	C7170(5,9)	600.0	K
	C7170(6,9)	647.0	K
	C7170(7,9)	2	ions/molecule
	C7170(8,9)	0	Ions/molecule
	C7170(9,9)	6510.0	Kg/m^3
	C7170(1,10)	273.0	K
	C7170(2,10)	373.0	K
	C7170(3,10)	0.0	Kg/kg H_2O
	C7170(4,10)	0.0	Kg/kg H_2O
	C7170(5,10)	600.0	K

7170 Hygroscopic Aerosol Sensitivity Coefficients			
Reference	Coefficient	Value	Units
	C7170(6,10)	647.0	K
	C7170(7,10)	2	ions/molecule
	C7170(8,10)	0	Ions/molecule
	C7170(9,10)	10960.0	Kg/m^3
	C7170(1,11)	273.0	K
	C7170(2,11)	373.0	K
	C7170(3,11)	0.0	Kg/kg H_2O
	C7170(4,11)	0.0	Kg/kg H_2O
	C7170(5,11)	600.0	K
	C7170(6,11)	647.0	K
	C7170(7,11)	2	ions/molecule
	C7170(8,11)	0	Ions/molecule
	C7170(9,11)	8150.0	Kg/m^3
	C7170(1,12)	273.0	K
	C7170(2,12)	373.0	K
	C7170(3,12)	0.0	Kg/kg H_2O
	C7170(4,12)	0.0	Kg/kg H_2O
	C7170(5,12)	600.0	K
	C7170(6,12)	647.0	K
	C7170(7,12)	2	ions/molecule
	C7170(8,12)	0	Ions/molecule
	C7170(9,12)	6446.0	Kg/m^3
	C7170(1,13)	273.0	K
	C7170(2,13)	373.0	K
	C7170(3,13)	0.0	Kg/kg H_2O
	C7170(4,13)	0.0	Kg/kg H_2O
	C7170(5,13)	600.0	K
	C7170(6,13)	647.0	K
	C7170(7,13)	2	ions/molecule
	C7170(8,13)	0	Ions/molecule
	C7170(9,13)	2520.0	Kg/m^3
	C7170(1,14)	273.0	K
	C7170(2,14)	373.0	K
	C7170(3,14)	0.0	Kg/kg H_2O
	C7170(4,14)	0.0	Kg/kg H_2O
	C7170(5,14)	600.0	K
	C7170(6,14)	647.0	K
	C7170(7,14)	2	ions/molecule
	C7170(8,14)	0	Ions/molecule
	C7170(9,14)	1000.0	Kg/m^3

7170 Hygroscopic Aerosol Sensitivity Coefficients			
Reference	Coefficient	Value	Units
	C7170(1,15)	273.0	K
	C7170(2,15)	373.0	K
	C7170(3,15)	0.0	Kg/kg H_2O
	C7170(4,15)	0.0	Kg/kg H_2O
	C7170(5,15)	600.0	K
	C7170(6,15)	647.0	K
	C7170(7,15)	2	ions/molecule
	C7170(8,15)	0	Ions/molecule
	C7170(9,15)	2250.0	Kg/m^3
	C7170(1,16)	273.0	K
	C7170(2,16)	373.0	K
	C7170(3,16)	0.44	Kg/kg H_2O
	C7170(4,16)	2.25	Kg/kg H_2O
	C7170(5,16)	600.0	K
	C7170(6,16)	647.0	K
	C7170(7,16)	2	ions/molecule
	C7170(8,16)	0	Ions/molecule
	C7170(9,16)	4510.0	Kg/m^3

Appendix B: Agglomeration Kernels

The agglomeration kernels currently implemented in the MELCOR implementation of MAEROS are summarized in this appendix. These kernels are those that are recommended by Powers, Sprung, and Leigh [**1**].

Brownian

$$\beta = 2\pi \left(D_i + D_j \right)\left(\gamma_i d_i + \gamma_j d_j\right)/F \tag{B.1}$$

$$D_i = \frac{kT}{3\pi d_i \mu \chi_i} C_i \tag{B.2}$$

$$C_i = 1 + Kn_i \left[c_m + 0.4 \ \exp\left(-1.1 / Kn_i\right)\right] \tag{B.3}$$

$$F = \frac{d_i + d_j}{d_i + d_j + 2g_{ij}} + \frac{8\left(D_i + D_j\right)}{v_{i,j}\left(d_i + d_j\right)c_s} \tag{B.4}$$

$$g_{i,j} = \left(g_i^2 + g_j^2\right)^{1/2} \tag{B.5}$$

$$v_{i,j} = \left(v_i^2 + v_j^2\right)^{1/2} \tag{B.6}$$

$$g = \frac{1}{3\, d_i\, l_i}\left[\left(d_i + l_i\right)^3 - \left(d_i^2 + l_i^2\right)^{3/2}\right] - d_i \tag{B.7}$$

$$l = \frac{8D_i}{\pi v_i} \tag{B.8}$$

$$v = \left(\frac{8kT}{\pi m_i}\right)^{1/2} \tag{B.9}$$

$$Kn_i = 2\lambda / d_i \tag{B.10}$$

$$\lambda = \frac{\mu}{\rho_g}\left(1.89\times10^{-4}\, M_{w,g}/T\right)^{1/2} \tag{B.11}$$

$$\rho_g = 1.21\times10^{-4} P\, M_{w,g} / T \tag{B.12}$$

μ = values for air; from the Material Properties (MP) package

Gravitational

$$\beta = \varepsilon_g \tfrac{\pi}{4} c_s \left(\gamma_i d_i + \gamma_j d_j\right)^2 \left|V_{Ti} - V_{Tj}\right| \tag{B.13}$$

$$V_{Ti} = \frac{\rho_{pi}\, g d_i^2 C_i}{18\mu\chi_i} \tag{B.14}$$

$$\varepsilon_g = 1.5\left[\frac{\min\ (d_i, d_j)}{(d_i + d_j)}\right]^2 \tag{B.15}$$

Turbulent

$$\beta = c_s\left(\ \beta_{T1}^2 + \beta_{T2}^2\ \right)^{1/2} \tag{B.16}$$

$$\beta_{T1} = \left(\frac{\pi\varepsilon_T\ \rho_g}{120\mu}\right)^{1/2}\left(\gamma_i d_i + \gamma_j d_j\right)^3 \tag{B.17}$$

$$\beta_{T2} = \frac{0.04029\ \rho_g^{1/4}\ \varepsilon_T^{3/4}}{\mu^{5/4}}\left(\gamma_i d_i + \gamma_j d_j\right)^2\left|\frac{\rho_{p1} C_1 d_1^2}{\chi_1} - \frac{\rho_{p2} C_2 d_2^2}{\chi_2}\right| \tag{B.18}$$

Nomenclature	
c_m	particle slip coefficient
c_s	particle sticking coefficient
c_t	thermal accommodation coefficient
C	particle mobility
d	particle diameter
D	diffusion coefficient
k	Boltzmann constant
k_g/k_s	ratio of thermal conductivity of the gas over that for the particle
Kn	Knudsen number
m	particle mass
M_w	molecular weight
P	pressure
T	temperature
V	volume

Greek:	
β	coagulation kernel (m^3/s)
ε_T	turbulence dissipation density
ρ	density
μ	viscosity
λ	mean free path

Greek:	
γ	agglomeration shape factor
χ	dynamic shape factor

Subscripts	
b	bulk
g	gas (air assumed)
i,j	particle identifier
p	particle
s	steam

Appendix C: Aerosol Surface Area

The aerosol surface area is used for fission product vapor condensation and evaporation of aerosols. The general equation for the surface area is:

$$A_T = \int_{x_1}^{x_2} n(x)A(x)dx \tag{C.1}$$

where

A_T	total surface area
$A(x)$	area of a particle as a function of x
$n(x)$	number of particles as a function of x

MAEROS assumes that the aerosol size distribution in each section is constant with respect to the natural log of the mass, so the number density can be expressed as (Gelbard [**7**]):

$$n(x) = \frac{M}{m\ \left(\ln m_2 - \ln m_1\right)}\ d\left(\ln m\right) \tag{C.2}$$

A and m can be expressed in terms of ln m as follows:

$$m = e^{\ln m} \tag{C.3}$$

$$A = 4\pi\, r^2 \tag{C.4}$$

$$= 4\pi\left(\frac{3m}{4\pi\rho}\right)^{2/3} \tag{C.5}$$

$$= 4\pi\left(\frac{3e^{\ln m}}{4\pi\rho}\right)^{2/3} \tag{C.6}$$

Equation (C.1) becomes

$$A_T = 4\ \pi \left(\frac{3}{4\pi\rho}\right)^{2/3} \frac{M}{\ln\ (m_2/m_1)} \int_{\ln m_1}^{\ln m_2} \exp\left(-\tfrac{1}{3}\ \ln m\right) d(\ln m) \qquad \text{(C.7)}$$

and, after integration,

$$A_T = 12\pi \left(\frac{3}{4\pi\rho}\right)^{2/3} \frac{M}{\ln(m_2/m_1)} \left[m_1^{-1/3} - m_2^{-1/3}\right] \qquad \text{(C.8)}$$

Appendix D: Pool Scrubbing Vent Exit Region Modeling

D.1 Globule Formation

The initial globules formed have a unique size given by a correlation relating the normalized globule volume to the Weber number for each vent type considered. The correlation is

$$v_n = a \cdot We^b \tag{D.1}$$

$$D_{g,o}^3 = \frac{3}{2} v_n D_o^2 \left(\frac{\sigma}{\rho_l g} \right)^{1/2} \tag{D.2}$$

where

$$We = \frac{\rho_l D_o V_o^2}{\sigma} \tag{D.3}$$

and

ρ_l	pool liquid density,
σ	pool liquid surface tension,
D_o	vent equivalent diameter, and
V_o	exit velocity of the gas.

It is assumed that $Q = V_o(\pi/4)D_o^2$, where Q is the gas volumetric flow rate at the vent in equilibrium with the pool conditions at the vent depth. The default correlation constants implemented in sensitivity coefficient array 7151 are:

Vent	a	b	Source
Multiple small holes	3.45	0.46	EPRI program
Downcomer	0.0891	0.616	PNL with EPRI data
Horizontal vent	0.857	0.73	EPRI program

These correlations only apply to inlet gases containing noncondensible gases. Very high steam fractions provide for residual bubbles. High steam fractions have a “cone”-shaped region that does not detach from the vent.

The globule diameter decreases linearly to zero over a distance of twelve times its initial value:

$$D_g = D_{g,o}\left[1 - \frac{x}{12D_{g,o}}\right] \tag{D.4}$$

where x has a value of zero at the elevation of the vent exit.

D.2 Vent Exit Region Scrubbing Models

In the vent exit region, aerosol capture occurs because of:

(1) Stefan flow from steam condensation during gas equilibration to pool conditions,

(2) inertial impaction of aerosol particles in rapidly decelerating gas flow, and

(3) centrifugal, diffusional and gravitational particle deposition during gas injection through small orifice, multihole vents.

D.2.1 Steam Condensation

It is assumed that the fraction of particles removed by steam condensation during globule breakup at the vent exit is simply equal to the fractional loss in gas volume caused by condensation at the temperature and pressure of the pool at the vent depth:

$$DF_{EC} = \frac{X_o}{X_i} \tag{D.5}$$

where X_i is the mole fraction of noncondensible gas in the inlet gas and X_o is the mole fraction of noncondensible gas in the gas after equilibration. X_i is determined from the flow composition in the vent provided by the FL package, and X_o is given by

$$X_o = 1 - \frac{P_{sat}\left(T_p\right)}{P_{surf} + \rho_l g h_p} \tag{D.6}$$

where T_p, P_{surf} and h_p are the pool temperature, pressure at the pool surface and pool depth at the vent exit, respectively. DF_{EC} is limited to a minimum value of one.

For iodine vapor scrubbing the value of DF_{EC} calculated above may need to be reduced significantly. The concentration of iodine in the condensate may not exceed the product of the equilibrium partition coefficient and the concentration of iodine in the vapor state remaining in the bubbles. Hence, if the concentration of iodine in the condensate would exceed the equilibrium value consistent with the partition coefficient when iodine removal is assumed to be proportional to the volumetric reduction factor (DF_{EC}), then iodine vapor scrubbing will not occur to the extent given by DF_{EC}. Rather, the decontamination factor for vapor scrubbing will be given by

$$DF_{EC,vap} = 1 + \min\left[H_{vap}\left(\frac{\rho_v}{\rho_l} \right), 1 \right] (DF_{EC} - 1) \qquad \text{(D.7)}$$

so that $DF_{EC,vap}$ is less than DF_{EC} if $H_{vap}(\rho_v / \rho_l) < 1$, and equal to DF_{EC} otherwise. (Additional vapor diffusion into the aqueous phase is considered to be too slow with respect to the time scale of steam condensation to increase $DF_{EC,vap}$ above DF_{EC} in those cases where $H_{vap}(\rho_v / \rho_l)$ exceeds unity.)

D.2.2 Inertial Impaction

If gas leaves the vent exit at a high velocity, the initial globules rapidly lose that velocity. The forward globular interface, as it slows and stops, can capture particles if they have sufficient inertia. Inertia of particle size *i* is represented by the Stokes number

$$Stk_i = \frac{\rho_i V_e d_i^2}{9 \mu D_o} \qquad \text{(D.8)}$$

where

d_i	particle diameter
ρ_i	particle density
V_e	vent exit gas velocity (before equilibration with pool)
μ	gas viscosity
D_o	vent exit orifice diameter

The *DF* for this impaction process is

$$DF_{II,i} = \frac{1}{1 - \alpha_i} \qquad \text{(D.9)}$$

where

$$\alpha_i = 1.79182\left(3.3437\times10^{-11}\right)^{\left(5.9244\cdot10^{-3}\right)\sqrt{Stk_i}} \quad \text{if } \sqrt{Stk_i} \le 0.65868 \tag{D.10}$$

and

$$\alpha_i = 1.13893\left(1.4173\times10^{-6}\right)^{\left(4.25973\cdot10^{-3}\right)\sqrt{Stk_i}} \quad \text{if } 0.65868 < \sqrt{Stk_i} \tag{D.11}$$

The constants in these correlations have been implemented in sensitivity coefficient array 7155, and the maximum value of α_i permitted is constrained to 0.99, which is also included in sensitivity coefficient array 7155. The importance of inertial impaction is minimal unless near-sonic values of V_e occur.

D.2.3 Centrifugal, Diffusional and Gravitational Deposition

Centrifugal, diffusional and gravitational particle deposition are only evaluated in the vent exit region for small orifice, multihole vents (MVENT=1 on input record RN2PLSXX). The bases for the model are assumptions about the vent injection bubble geometry and velocity relative to pool liquid.

Particle scrubbing is evaluated in two connected time intervals. The injection interval is defined as the time it takes to fill the globule and is given by

$$\tau_{fill} = \frac{\frac{\pi}{6}D_g^3}{\frac{\pi}{4}D_o^2 V_o} \tag{D.12}$$

During the detached globule interval, which follows the injection interval, the globule is slowed by drag forces. This interval is assumed to be three times the characteristic stopping time, which is the time required for the drag force to nullify the bubble momentum

$$\tau_{stop} = \frac{4\rho_g D_g}{3f\rho_l V_o} \tag{D.13}$$

where *f*, the friction factor, has a hard-wired value of 0.2. It is assumed that the final detached injection globule is spherical (of diameter D_g) and during globule formation, the

forming globule is elongated with a hemispherical front of diameter D_o (orifice diameter) moving at velocity V_o relative to the bulk liquid.

For each particle size, denoted by subscript *i*, the centrifugal deposition velocity is calculated by scaling the gravitational settling velocity by the ratio of the centrifugal acceleration to the gravitational acceleration. The gas circulation velocity is assumed to equal the injection velocity and the radius of curvature is equal to the circular vent radius. The decontamination factors during the injection and detached globule periods are proportional to the ratio of the volumes swept to the globule surface by centrifugal velocity to the total globule volume. The values are given by

$$DF_{C,i} = \exp\left(V_{C,i}/V_o\right) \quad \text{during injection}$$

$$DF_{C,i} = \exp\left(\frac{V_o V_{g,i}\rho_g}{9D_o fg\rho_l}\right) \quad \text{after detachment} \tag{D.14}$$

where $V_{c,i}$ is given by Equation (E.20) with $r_c = D_o/2$ and $V_s = V_o$. The method used to determine the settling velocity, $V_{g,i}$, is also described in Section E.3 below.

Particle deposition from Brownian diffusion during the injection and detached globule periods is modeled using film penetration theory, which is discussed in Section E.2 below. The decontamination factor during each period is proportional to the ratio of the volume swept to the globule surface by Brownian diffusion to the total globule volume. For each particle size, the decontamination factors are given by

$$DF_{D,i} = \exp\left[\frac{16\tau_{fill}}{3D_o}\left(\frac{D_i}{\pi\tau_{fill}}\right)^{1/2}\right] \quad \text{during injection}$$

$$DF_{D,i} = \exp\left[\frac{12\tau_{stop}}{D_o}\left(\frac{V_o D_i}{\pi D_o}\right)^{1/2}\right] \quad \text{after detachment} \tag{D.15}$$

Particle deposition from gravitational settling during the injection and detached globule periods both use a settling velocity based on Stokes's law for small particles and an empirical correlation based on the Reynolds number for larger particles. These correlations are presented in Section E.3 below. For each particle size, the decontamination factors are given by

$$DF_{g,i} = \exp\left(\frac{\overline{A}_s V_{g,i} \tau_{fill}}{(\pi/6) D_{g,o}^3}\right) \quad \text{during injection}$$

$$DF_{g,i} = \exp\left(\frac{3V_{g,i}(3\tau_{stop})}{2D_{g,o}}\right) \quad \text{after detachment} \tag{D.16}$$

where the average settling area, $\overline{A}_s$, during injection is equal to one half the final settling area of the horizontally oriented bullet-shaped globule given by

$$A_{s,o} = \frac{2D_{g,o}^3}{3D_o} + D_o^2\left(\frac{\pi}{8} - \frac{1}{3}\right) \tag{D.17}$$

The overall decontamination factor resulting from centrifugal, diffusional and gravitational deposition, $DF_{ER,i}$, which is used in Equation 2.7.3 in Section 2.7.1, is given by

$$DF_{ER,i} = DF_{c,i} \cdot DF_{D,i} \cdot DF_{g,i} \tag{D.18}$$

Appendix E: Pool Scrubbing Swarm Rise Region Modeling

The primary modeling objective in the swarm rise region is to determine how evolving thermal-hydraulic conditions within the bubbles affect the removal of particulate aerosols and iodine vapors from the bubble. This is achieved by dividing the total rise height (the distance between the vent exit and the pool surface) into several equal sections (given by XNRISE implemented in sensitivity coefficient array 7150 with a default value of 10.), and then marching upward to update the thermal-hydraulic conditions in each section to evaluate the incremental removal in each section. In this procedure it is assumed that the swarm velocity is constant, so that the bubbles spend the same amount of time in each section.

E.1 Bubble Characteristics

The bubbles are modeled as oblate spheroids with an equivalent spherical diameter, d_{vm}, of 0.7 cm (this default value can be adjusted through sensitivity coefficient array C7152), if they contain no steam initially. The presence of steam reduces d_{vm} as follows

$$d_{vm} = 0.7 \cdot 10^{-0.2265+(0.0203+0.0313\,x_{nc})^{1/2}} \qquad \text{(E.1)}$$

The constants in Equation (E.1) re implemented in sensitivity coefficient array 7152. The shape of the bubble is calculated using the following correlation

$$\frac{a}{b} = 0.84107 + 1.13466\ d_{vm} - 0.3795\ d_{vm}^2 \qquad \text{(E.2)}$$

where *a* and *b* are the lengths of the major and minor axes of the oblate spheroid, respectively. (NOTE: The SPARC-90 documentation erroneously had *a/b* inverted as *b/a*.) This correlation was established for $0.15 \le d_{vm} \le 1.3$ cm. All bubbles smaller than 0.15 cm are spheres (*a/b* = 1), and bubbles larger than 1.3 cm have *a/b* = 1.675. The constants in Equation (E.2) are implemented in sensitivity coefficient array 7152.

The bubble rise velocity relative to the liquid is given by the following correlation

$$V_r = 7.876\left(\sigma/\rho_l\right)^{1/4}\text{(cm/s)} \ \text{ for } d_{vm} \le 0.5\,\text{cm}$$

$$V_r = 1.40713\ d_{vm}^{0.49275}\ V_r\left(d_{vm} = 0.5\right)\text{(cm/s) otherwise} \qquad \text{(E.3)}$$

The constants in Equation (E.3) have been implemented as sensitivity coefficient array 7153. The swarm rise velocity is given by the average of the correlation value at the depth of the vent exit and at the pool surface

$$\overline{V_s} = 0.5 \cdot \left[V_s(x=0) + V_s\left(x=h_p\right) \right] \tag{E.4}$$

where

$$V_s(x) = \left[\left(\dot{Q}_s + 5.33 \right) / 3.011 \cdot 10^{-3} \right]^{1/2} \left[1 - 3.975 \cdot 10^{-4} x \right] \quad \text{(cm/s)} \tag{E.5}$$

where $\dot{Q}_s$ is the total gas volumetric flow rate (liter/s) at depth $h_p/2$, and the depth, x, is measured in cm. (NOTE: In the SPARC-90 documentation, Equation (E.4) is erroneous.) $\overline{V_s}$ is limited to a maximum value of 170. cm/s, which is implemented in sensitivity coefficient array 7154 along with the constants that appear in Equation (E.5).

E.2 Bubble Heat and Mass Transfer

During each spatial step the change in the internal energy of the gas in the bubbles is tracked by evaluating iteratively the work performed by bubble expansion and the heat and mass transfer from the pool to the bubble across the bubble boundary. Because the stable size of the bubbles is assumed to remain constant, as the bubbles expand as the static pressure decreases during their ascent, they are assumed to multiply by splitting. The particle concentration (g/cm^3) in the bubbles decreases as a result of bubble multiplication to conserve mass. Bubble expansion during each step is evaluated by assuming that the bubble is isothermal and that the increase in volume is inversely proportional to the decrease in satatic head (i.e., by assuming ideal gas behavior).

The work done by the expanding bubble during each step is also evaluated by assuming ideal gas behavior and is given by

$$\begin{aligned} Pdv &= P\left[\left(\frac{\partial V}{\partial P} \right)_{\mathrm{T}} dP + \left(\frac{\partial V}{\partial T} \right)_{\mathrm{P}} dT + \Delta V_{evap} \right] \\ &= R\left[M_t\, T_1 \ln\left(\frac{P_1}{P_2} \right) + (T_2 - T_1) M_t + T_1\, \Delta M_{evap} \right] \end{aligned} \tag{E.6}$$

where ΔM_{evap} is the net increase in vapor mass from evaporation into the bubble minus condensation onto particles in the bubble during the spatial step and M_t is the sum of the steam and noncondensible mass in the bubble.

Heat and mass transfer rates between the pool and rising bubbles are based on penetration theory, in which it is assumed that the top-to-bottom gas circulation in the bubble establishes a quasi-steady boundary layer with the leading edge at the top of the bubble. The transport velocity through the boundary layer at a distance ℓ from the leading edge of the boundary layer is then given by

$$V_\phi = \left(\frac{D_\phi V_\ell}{\pi \ell} \right)^{1/2} \tag{E.7}$$

where $D_\phi = \alpha$ (thermal diffusivity of boundary layer fluid) for heat transfer, $D_\phi = D_i$ (mass diffusivity or diffusion coefficient of species *i* through the boundary layer) for mass transfer, V_ℓ is the gas circulation velocity parallel to the boundary layer and $T_e = \ell / V_\ell$ is commonly termed the "exposure" time of the surface. The heat transfer coefficients from the pool and bubble to the pool/bubble interface are

$$\begin{aligned} h_p &= \rho_l C_l (\alpha_l / \pi \tau_e)^{1/2} \\ h_b &= \rho_g C_g (\alpha_g / \pi \tau_e)^{1/2} \end{aligned} \tag{E.8}$$

respectively; and the rate of evaporation at the pool/bubble interface is

$$N_s = \left(\frac{P}{R T_s} \right) \left(\frac{D_s}{\pi \tau_e} \right)^{\frac{1}{2}} \log_e \left[\frac{P - P_{sat}(T_b)}{P - P_{sat}(T_s)} \right] \tag{E.9}$$

where the subscript *s* indicates that the term is evaluated at the pool/bubble interface.

The rates of condensation and evaporation of water on aerosol particles will be determined by using the Mason equation

$$r \frac{dr}{dt} = \frac{S - S_r}{a + b} \tag{E.10}$$

which gives the time rate of change of the radius, r, of the aerosol particle as a function of the difference between the actual saturation ratio, S (defined as $P_v/P_{sat}(T)$ inside the bubble), and its equilibrium value, S_r. a, b and S_r in Equation (E.10) are given by

$$a = \frac{\rho_l \, M_w h_{fg}^2}{k_v \, RT^2}$$

$$b = \frac{\rho \, RT}{P_{sat} D_v M_w} \qquad \text{(E.11)}$$

$$S_r = A_l \exp\left[\frac{2\sigma M_w}{r \, R \, \rho_l T}\right]$$

The heat and mass transfer equations are solved iteratively during each spatial step in the bubble's ascent. During each iteration, the heat and mass transfer rates over the bubble surface are numerically integrated by dividing the surface from 0° at the top of the bubble to 180° at the bottom of the bubble into a number (XNCIRC, with a default value of 5. implemented in sensitivity coefficient array 7150) of equally spaced latitudinal strips. The heat and mass transfer over all the strips are summed to obtain the integral values, and the exposure time, τ_e, associated with each strip is saved for use in calculating decontamination factors after the thermal-hydraulic calculations. There are actually three separate iterations to determine the end-of-step values of saturation ratio, S, and the vapor/aerosol temperature, T_b, inside the bubbles. The error tolerances and iteration limits associated with these calculations for saturation, energy and temperature are implemented in sensitivity coefficient array 7150, and have default values that normally yield reasonable accuracy with acceptable computational cost.

E.3 Particle Scrubbing in the Bubbles

Particle scrubbing in the bubbles is the result of a net flux of particles to the bubble boundary, where they are assumed to be absorbed into the pool with perfect efficiency. The decontamination factor during a time interval is defined to be the mass of particles in the bubble at the beginning of the interval divided by the mass of particles in the bubble at the end of the interval. It is assumed that particle removal in the bubble can be modeled as a first-order process as follows:

$$\frac{d \, c_i}{d \, t} = -\left[\frac{1}{v_b} \int A_{surf} V_{n,i} \, d \, A\right] c_i \qquad \text{(E.12)}$$

where c_i is the concentration of particles of size i in the bubble, v_b is the bubble volume and $V_{n,i}$ is the velocity of the particles normal to (toward) the surface of the bubble, A_{surf}. The decontamination factor during a time interval, Δt, is obtained from the solution to this equation and is given by

$$DF_{BB,i} = \exp\left[\frac{\Delta t}{v_b}\int A_{surf} V_{n,i}\, dA\right] \tag{E.13}$$

The particle velocity normal to the surface is given by the normal component of the vector sum of the velocities associated with the individual deposition mechanisms

$$V_{n,j} = V_{c,i} + V_{D,i} - V_{g,i}\ \cos\beta\ - V_v \tag{E.14}$$

where β is the angle between the normal vector and vertical. For the assumed elliptical geometry (the cross section of an oblate spheroid), β is given by

$$\beta = \tan^{-1}\left[\frac{b^2 \tan\theta}{a^2}\right] \tag{E.15}$$

where θ is the polar angle between the vertical and the ray that runs from the origin to the given point on the ellipse (θ runs from 0 to π from the top to the bottom of the bubble).

For particles with a diameter less than about 70 microns, the gravitational settling velocity, $V_{g,i}$, follows Stokes's law and is given by

$$V_{g,i} = \frac{\rho_i g S_i d_i^2}{18\,\mu} \tag{E.16}$$

where S_i is the Cunningham slip correction factor. For larger particles, a set of empirical correlations is used to determine the Reynolds number, from which $V_{g,i}$ follows

$$f(\mathrm{Re}) = \frac{4\,\rho_i\,\rho_g\,g\,d_i^3}{3\,\mu^2} \tag{E.17}$$

$$\begin{aligned}
\mathrm{Re} &= \left[f(\mathrm{Re})/27.00\ \right]^{1./1.130} \text{ if } 9.6 < f(\mathrm{Re}) < 93.6 \\
&= \left[f(\mathrm{Re})/24.32\right]^{1./1.227} \text{ if } 93.6 \le f(\mathrm{Re}) < 410. \\
&= \left[f(\mathrm{Re})/15.71\ \right]^{1./1.417} \text{ if } 410. \le f(\mathrm{Re}) < 1.07\times10^{4} \\
&= \left[f(\mathrm{Re})/6.477\right]^{1./1.609} \text{ if } 1.07\times10^{4} \le f(\mathrm{Re}) < 2.45\times10^{5} \\
&= \left[f(\mathrm{Re})/1.194\right]^{1./1.867} \text{ if } 2.45\times10^{5} \le f(\mathrm{Re})
\end{aligned} \qquad \text{(E.18)}$$

$$V_{g,i} = \frac{\mu\,\mathrm{Re}}{\rho_g d_i} \qquad \text{(E.19)}$$

The centrifugal capture velocity, $V_{c,i}$, can be obtained from the gravitational settling velocity by scaling it by the ratio of the centrifugal acceleration to the acceleration of gravity (even though the original derivation is based on the concept of particle mobility)

$$V_{c,i} = V_{gi}\left(\frac{V_s^2/r_c}{g}\right) \qquad \text{(E.20)}$$

The local surface velocity, V_s, is calculated by assuming that flow around the rising bubbles is essentially steady three-dimensional, axisymmetric, inviscid, incompressible, irrotational (potential) flow around an oblate spheroid. The stream function, ψ, for this flow can be found by solving the irrotational vorticity equation $(\nabla x\, V = 0)$ with $V = \nabla\, x\,(0, 0, \Psi/\sigma)$ chosen to satisfy the continuity equation $(\nabla \bullet V = 0)$ identically. The solution is effected by using a conformal mapping to transform the equations from cylindrical (radial coordinate σ) to elliptical coordinates. (It can be shown that the equations reduce to those for flow around a sphere as $a/b \to 1$.) V_s and the radius of curvature of the surface, r_c, which are used to calculate centrifugal acceleration in Equation (E.20) above are given by the following

$$V_s = \frac{-V_r\,(\mathrm{r}\sin\theta/\mathrm{a})}{\left[(r\cos\theta/b)^2+\sinh^2\xi_o\right]^{1/2}}\;\frac{1}{\left[\sinh\xi-\cosh^2\xi_o\cot^{-1}(\sinh\xi_o)\right]}$$

$$r_c = \frac{1}{a\,b}\left[\frac{a^4\cos^2\theta+b^4\sin^2\theta}{a^2\cos^2\theta+b^2\sin^2\theta}\right]^{\frac{3}{2}} \qquad \text{(E.21)}$$

where

$\sinh\xi_o$	$[\,(a/b)_2 - 1\,]^{-1/2}$
$\cosh\xi o$	$[\,1 - (b/a)^2\,]^{-1/2}$
r	$[\,(\sin\theta/a)^2 + (\cos\theta/b)^2\,]^{-1/2}$ (radial coordinate)
θ	spherical polar coordinate $(0 \le \theta \le \pi)$

Note that V_s is presented in spherical coordinates rather than the elliptical coordinates used in the derivation.

The local diffusional deposition velocity, $V_{D,i}$, from Brownian diffusion can be estimated from penetration theory of mass transfer

$$V_{D,i} = \left(\frac{D_i}{\pi\tau_e}\right)^{1/2} \qquad \text{(E.22)}$$

where the diffusion coefficient for the aerosol particles, D_i, can be calculated using the Stokes-Einstein equation

$$D_i = \frac{k_B T S_i}{3\pi\mu D_i} \qquad \text{(E.23)}$$

where k_B is the Boltzmann constant and T is the gas temperature in the bubble. The exposure time of the moving surface, τ_e, in Equation (E.22) is the integrated value of the arc length divided by the local surface velocity starting from $\tau_e = 0$. at the top of the bubble. When evaporation is occurring at the surface of the bubble, the diffusion velocity from Equation (E.22) is reduced as follows

$$V'_{D,i} = \xi_i\, V_{D,i} \qquad \text{(E.24)}$$

where

$$\xi_i = \frac{\exp(-\phi_i^2)}{2 - \exp(-1.85\,\phi_i)} \qquad \text{(E.25)}$$

and the parameter ϕ is equal to $V_v/V_{D,i}$.

The normal component of the deposition velocity given by Equation (E.14) is limited to a minimum value of $V_{D,i}$ and then integrated over the entire bubble surface in Equation (E.13) to get $DF_{BB,i}$, which is used in Equation 2.7.2 in Section 2.7.1.

Appendix F: Iodine Vapor Scrubbing in the Swarm Rise Region

In the swarm rise region, the scrubbing of I_2 and CH_3I is controlled by diffusion of those species. The resistance to diffusion on both sides of the pool/bubble interface is considered to evaluate effective diffusion velocities through the gas and through the liquid. As discussed in Appendix D, in the swarm rise region it is assumed that bubble circulation continually renews the bubble interface and that the film theory of mass transfer resistance holds on both sides of the interface. Because the boundary layer thickness and mass transport through it are functions of the angular position around the rising bubbles, the decontamination factors for each spatial rise step must be evaluated by numerically integrating diffusion velocity over the polar angle of the assumed spherical bubble geometry. Hence, the decontamination factors are given by Equation (E.13) with the particle deposition velocity, $V_{n,i}$, replaced by the gaseous diffusion velocities for I_2 and CH_3I, $V_{D,j}$ (j = I_2 or CH_3I), given by (brackets refer to concentrations)

$$V_{D,j} = V'_{D(g),j} \left\{ \frac{\exp\left[- \left(V_v / V'_{D(g),j}\right)^2\right]}{2 - \exp\left[- 1.85 \left(V_v / V'_{D(g),j}\right)\right]} \right\}$$

$$V'_{D(g),j} = \frac{1}{\left[I_{j(g)}\right]} \left\{ V''_{D(g),j} \left(\left[I_{j(g)}\right] - \left[I_{j(g)}\right]_i \right) \right\} \qquad \text{(F.1)}$$

$$V''_{D(g),j} = \left(\frac{D_{g,j} V_\ell}{\pi \ell} \right)^{\frac{1}{2}}$$

where the subscript i indicates the concentration is evaluated at the gas/liquid interface. $\left[I_{j(g)}\right]_i$ is determined by equating the concentration flux from the gas to the interface with the flux from the interface to the pool as follows

$$V''_{D(g),j} \left(\left[I_{j(g)}\right] - \left[I_{j(g)}\right]_i \right) = V''_{D(g),j} \left(H(I_j) \left[I_{j(g)}\right]_i - \sum \left[I_{j(aq)}\right] \right) \qquad \text{(F.2)}$$

where (g) and (l) indicate the diffusion coefficient applies to the gas and liquid phase, respectively, and $H(I_j)$is the partition coefficient for species j. Gaseous concentrations in the bubble are updated after each spatial step. However, it is assumed that the total iodine concentration in the pool does not change significantly during the transit time of bubbles (vent depth divided by average swarm velocity) so that its value is updated only at the beginning of each MELCOR system timestep.

The total liquid molar concentration of iodine is given by

$$\sum\left[I_{2(aq)}\right] = 0.5\left[I^-\right] + 1.5\left[I_3^-\right] + \left[I_{2(aq)}\right] + 0.5\left[HIO\right] + 0.5\left[H_2OI^+\right] \qquad \text{(F.3)}$$

CH_3I is the only organic iodine species considered, and its temperature-dependent partition coefficient is given by the following correlation:

$$H_{IO} = \frac{T}{10^{-1388.89/T + 6.461}} \qquad \text{(F.4)}$$

and the constants in the exponent of the denominator have been implemented as sensitivity coefficient array 7158. The partition coefficient of inorganic iodine, $H(I_2)$, is updated during each spatial step by determining the pool equilibrium inorganic iodine species concentrations and solving for $H(I_2)$ as follows

$$H(I_2) = \frac{\sum\left[I_{2(aq)}\right]_{(eq)}}{\sum\left[I_{2(aq)}\right]_{(eq)} / K_1} = \frac{\sum\left[I_{2(aq)}\right]_{(eq)}}{\left[I_{2(aq)}\right]_{(eq)}} \qquad \text{(F.5)}$$

where K_1 is the equilibrium constant for the first reaction listed in Equation (F.6) below.

Hence, in the SPARC-90 treatment of I_2 vapor scrubbing, the major task involves determining the equilibrium concentrations of inorganic iodine species, which can be used to calculate an appropriate value of $H(I_2)$ from Equation (F.5). The equilibrium concentrations of the inorganic iodine species are obtained by considering a limited set of chemical reactions involving inorganic iodine. At equilibrium, this set of reactions yields a set of simultaneous algebraic equations that relate the equilibrium concentrations of the various reactants and products to one another. The solution of this set of equations determines the required equilibrium concentrations of the inorganic iodine species.

In SPARC-90 it is assumed that the equilibrium concentration of the most important inorganic iodine species is determined by the equilibrium solution for the following set of fast reactions

$$I_{2(g)} \leftrightarrow I_{2(aq)}$$

$$I_{2(aq)} + I^{-} \leftrightarrow I_3^{-}$$

$$I_{2(aq)} + H_2O \leftrightarrow H^{+} + I^{-} + HIO \qquad \text{(F.6)}$$

$$I_{2(aq)} + H_2O \leftrightarrow H_2OI^{+} + I^{-}$$

$$H_2O \leftrightarrow H^{+} + OH^{-}$$

Slow aqueous reactions that affect the concentrations of these species, including radiation-induced pH changes, are not modeled in SPARC-90. However, if accident sequences provide excess CsOH as expected (pH remains high), the models might still be adequate.

At equilibrium the relationship between the reactants and products in Equation (F.6) is given by

$$\left[I_{2(aq)}\right]_{(eq)} = K_1 \left[I_{2(g)}\right]_{(eq)} \qquad \text{(F.7)}$$

$$\left[I_3^{-}\right]_{(eq)} = K_2 \left[I_{2(aq)}\right]_{(eq)} \left[I^{-}\right]_{(eq)} \qquad \text{(F.8)}$$

$$\left[H^{+}\right]_{(eq)} \left[I^{-}\right]_{(eq)} \left[HIO\right]_{(eq)} = K_3 \left[I_{2(aq)}\right]_{(eq)} \qquad \text{(F.9)}$$

$$\left[H_2OI^{+}\right]_{(eq)} \left[I^{-}\right]_{(eq)} = K_4 \left[I_{2(aq)}\right]_{(eq)} \qquad \text{(F.10)}$$

$$\left[H^{+}\right]_{(eq)} \left[OH^{-}\right]_{(eq)} = K_5 \qquad \text{(F.11)}$$

When Equation (F.10) is solved for $[H_2OI^{+}]_{(eq)}$ and the result is substituted into Equation (F.3) along with Equation (F.8) for $\left[I_3^{-}\right]_{(eq)}$ the result is [where subscript (eq) is henceforth suppressed]

$$\sum\left[I_{2(aq)}\right] = 0.5\,[I^-] + 1.5K_2\left[I_{2(aq)}\right][I^-] + \left[I_{2(aq)}\right] + 0.5\,[HIO] + 0.5\,\frac{K_4\left[I_{2(aq)}\right]}{[I^-]} \quad \text{(F.12)}$$

The electric charge balance between the reactants and products of Equation (F.6) can be reduced to

$$\left([I^-] - [I^-]_p\right) + [I_3^-] - [H_2OI^+] - [H^+]^* = 0 \quad \text{(F.13)}$$

where the first term in parentheses is $[I^-]$ exclusive of those ions associated with dissolved CsI particles, $[I^-]_p$ which is known and balanced by $[Cs^+]$, and $[H^+]^*$ are protons released by the third reaction in Equation (F.6) (since protons released by the fifth reaction are always balanced by the simultaneous release of $[OH^-]$). Since $[H^+]^*$ must be equal to [HIO] because of the stoichiometry of the third reaction in Equation (F.6), Equation (F.14) reduces to

$$\left([I^-] - [I^-]_p\right) + [I_3^-] - [H_2OI^+] - [HIO] = 0 \quad \text{(F.14)}$$

Equation (F.15) can be written as

$$\left([I^-] - [I^-]_p\right) + K_2\left[I_{2(aq)}\right][I^-] - \frac{K_4\left[I_{2(aq)}\right]}{[I^-]} - [HIO] = 0 \quad \text{(F.15)}$$

by using the same substitutions that were used to reduce Equation (F.3) to Equation (F.12). From Equation (F.9) [HIO] becomes

$$HIO = \frac{K_3\left[I_{2(aq)}\right]}{[H^+][I^-]} \quad \text{(F.16)}$$

where $[H^+]$ is given by

$$\left[H^+\right] = [HIO] + \left(\left[OH^-\right] - \left[OH^-\right]_p\right) \quad \text{(F.17)}$$

The first term on the right-hand side ([HIO]) are protons released by the third reaction in Equation (F.6) and the term in parentheses are protons released by the fifth reaction, which also releases that portion of $[OH^-]$ exclusive of the $[OH^-]$ associated with dissolved

CsOH ($[OH^-]_p$ which is known). Substituting Equation (F.11) into Equation (F.17) and rearranging the result yields

$$[H^+]^2 - \left([HIO] - [OH^-]_p\right)[H^+] - K_5 = 0 \qquad \text{(F.18)}$$

This quadratic equation for $[H^+]$ has the solution

$$[H^+] = \frac{1}{2}\left[\left([HIO] - [OH^-]_p\right) + \left\{\left([HIO] - [OH^-]_p\right)^2 + 4K_5\right\}\right] \qquad \text{(F.19)}$$

which may be substituted into Equation (F.16) to give

$$[HIO] = \frac{2K_3\left[I_{2(aq)}\right]/[I^-]}{\left([HIO] - [OH^-]_p\right) + \left\{\left([HIO] - [OH^-]_p\right)^2 + 4K_5\right\}^{1/2}} \qquad \text{(F.20)}$$

Equation (F.20) can be put in the form of a quadratic equation for [HIO] and solved to give

$$[HIO] = \frac{[OH^-]_p + \left\{[OH^-]_p{}^2 + 4\left(K_5 + \frac{K_3\left[I_{2(aq)}\right]}{[I^-]}\right)\right\}^{1/2}}{2\left(1 + \frac{K_5[I^-]}{K_3\left[I_{2(aq)}\right]}\right)} \qquad \text{(F.21)}$$

Equation(F.21) can be substituted into Equations (F.12) and (F.15) to yield two equations in two unknowns, $[I^-]$ and $[I_{2(aq)}]$, which may be solved iteratively to determine the desired equilibrium concentrations.

A simplification to the procedure just described arises if $[OH^-]$, including $[OH^-]_p$, is very large (pH > 9 because of large amounts of dissolved CsOH). Then $[OH^-]$ remains essentially constant so that $[H^+]$ is given from Equation(F.11) as

$$[H^+] = \frac{K_5}{[OH^-]_p} \qquad \text{(F.22)}$$

and Equation (F.15) becomes

$$\left([I^-]-[I^-]_p\right)+K_2\left[I_{2(aq)}\right][I^-]-\frac{K_4\left[I_{2(aq)}\right]}{[I^-]}-\frac{K_3\left[I_{2(aq)}\right]}{[H^+][I^-]}=0 \qquad \text{(F.23)}$$

which may be written as a quadratic in $[I^-]$ as follows

$$\left(1+K_2\left[I_{2(aq)}\right]\right)[I^-]^2-[I^-]_p[I^-]-\left(K_4+\frac{K_3}{[H^+]}\right)\left[I_{2(aq)}\right]=0 \qquad \text{(F.24)}$$

Equation (F.24) has the solution

$$[I^-]=\frac{[I^-]_p+\left\{[I^-]_p^2+4\left(1+K_2\left[I_{2(aq)}\right]\right)\left(K_4\frac{K_3}{[H^+]}\right)\left[I_{2(aq)}\right]\right\}^{1/2}}{2\left(1+K_2\left[I_{2(aq)}\right]\right)} \qquad \text{(F.25)}$$

in terms of an assumed $[I_{2(aq)}]$. Then [HIO] follows immediately from Equation (F.16) and the assumed $[I_{2(aq)}]$. Now if the resulting $[I^-]$, [HIO] and assumed $[I_{2(aq)}]$ are substituted into the right-hand side of Equation (F.12), the result may be compared to the known value of $\sum\left[I_{2(aq)}\right]$ (obtained from the MELCOR RN data base at the beginning of each system timestep). If the discrepancy is significant, then a new value of $[I_{2(aq)}]$ is assumed and the procedure is repeated until convergence is obtained.

Hence, at each spatial step in the rise of the bubbles from the vent exit region to the pool surface, the equilibrium concentrations of all the species in Equation (F.6) are updated. This is accomplished iteratively (with an error tolerance implemented in sensitivity coefficient array 7159) using the equilibrium constants for each reaction (which are temperature dependent and also implemented in sensitivity coefficient array 7159) and requiring conservation of the total iodine mass and electric charge.

References

1. D. A. Powers, J. L. Sprung, and C. D. Leigh, "Isotopes, Elements, and Chemical Classes," in Fission Product Behavior During Severe LWR Accidents: Recommendations for the MELCOR Code System, Sandia National Laboratories, Albuquerque, NM (1988).

2. D. E. Bennett, SANDIA-ORIGEN User's Manual, NUREG/CR-0987, SAND79-0299, Sandia National Laboratories, Albuquerque, NM (October 1979).

3. R. M. Ostmeyer, An Approach to Treating Radionuclide Decay Heating for Use in the MELCOR Code System, SAND84-1404, NUREG/CR-4169 (May 1985).

4. M. R. Kuhlman, D. J. Lehmicke, and R. O. Meyer, CORSOR User's Manual, BMI-2122, NUREG/CR-4173 (March 1985).

5. M. Ramamurthi and M. R. Kuhlman, Final Report on Refinement of CORSOR—An Empirical In-Vessel Fission Product Release Model, Battelle Memorial Institute (October 31, 1990).

6. D. A. Powers, J. E. Brockmann, and A. W. Shiver, Vanesa: A Mechanistic Model of Radionuclide Release and Aerosol Generation During Core Debris Interactions with Concrete, SAND85-1370, NUREG/CR-4308 (September 1985) Draft.

7. F. Gelbard, MAEROS User Manual, SAND80-0822, NUREG/CR-1391 (December 1982).

8. H. Jordan and M. R. Kuhlman, TRAP-MELT2 User's Manual, BMI-2124, NUREG/CR-4205 (May 1985).

9. B. J. Mason, The Physics of Clouds, Clarendon, Oxford, UK (1971).

10. P. C. Owczarski and K. W. Burk, SPARC-90: A Code for Calculating Fission Product Capture in Suppression Pools, NUREG/CR-5765, PNL-7723, Pacific Northwest Laboratory, Richland, WA (October 1991).

11. S. E. Dingman, A. L. Camp. C. C. Wong, D. B. King, and R. D. Gasser, HECTR Version 1.5 User's Manual, NUREG/CR-4507, SAND86-0101, Sandia National Laboratories, Albuquerque, NM (February 1986).

12. R. A. Lorenz, E. C. Beahm, and R. P. Wichner, "Review of Tellurium Release Rates from LWR Fuel Elements Under Accident Conditions," Proceedings International Meeting on Light Water Reactor Severe Accident Evaluation (1983).

13. T. Nakamura and R. A. Lorenz, “Effective Diffusion Coefficients Calculated from ORNL FP Release Test Results,” Oak Ridge National Laboratory Research Paper (April 1989).

14. T. Nakamura and R. A. Lorenz, “A Study of Cesium and Krypton Releases Observed in HI and VI Tests Using a Booth Diffusion Model,” Oak Ridge National Laboratory Research Paper (May 1987).

15. J. A. Gieseke, P. Cybulskis, R. S. Denning, M. R. Kuhlman, K. W. Lee, and H. Chen, Radionuclide Release Under Specific LWR Accident Conditions, BMI-2104 (July 1984).

16. R. K. Cole, Jr., D. P. Kelly, and M. A. Ellis, CORCON-Mod2: A Computer Program for Analysis of Molten-Core Concrete Interactions, SAND84-1246, NUREG/CR-3920, Sandia National Laboratories, Albuquerque, NM (August 1984).

17. I. H. Dunbar and S. N. Ramsdale, “Improvements in the Modeling of Sedimentation and Gravitational Agglomeration,” CSNI Specialists’ Meeting on Nuclear Aerosols in Reactor Safety, Karlsruhe, Germany (September 4-6, 1984).

18. D. C. Williams, K. D. Bergeron, P. E. Rexroth, and J. L. Tills, “Integrated Phenomenological Analysis of Containment Response to Severe Core Damage Accidents,” Progress in Nuclear Energy, Vol. 19 (1987).

19. F. Gelbard, “Modeling Aerosol Growth by Vapor Condensation,” Aerosol Science and Technology, 12, p. 399 (1990).

20. W. C. Hinds, Aerosol Technology, John Wiley & Sons, New York (1982).

21. L. F. Shampine and H. A. Watts, Practical Solution of Ordinary Differential Equations by Runge-Kutta Methods, SAND76-0585, Sandia National Laboratories, Albuquerque, NM (1976).

22. J. R. Welty, C. E. Wicks, and R. E. Wilson, Fundamentals of Momentum, Heat, and Mass Transfer, John Wiley & Sons, New York (1984).

23. R. B. Bird, W. E. Stewart, and E. N. Lightfoot, Transport Phenomena, John Wiley & Sons, New York (1960).

24. A. K. Postma, et al., Models for Predicting the Removal of Airborne Contaminants by Reactor Containment Sprays, BNWL-B-417 (1975).

25. A. K. Postma, et al., Technological Bases for Models of Spray Washout of Airborne Contaminants in Containment Vessels, NUREG/CR-0009 (1978).

26. A. E. J. Eggleton, Theoretical Examination of Iodine-Water Partition Coefficients, AERE-R-4887 (1967).

27. A. K. Postma and W. F. Pasedag, A Review of Mathematical Models for Predicting Spray Removal of Fission Products in Reactor Containment Vessels, WASH-1329 (1973).

28. A. E. J. Eggleton, Theoretical Examination of Iodine-Water Partition Coefficients, AERE-R-4887 (1967).

29. N. Frossling, Gerlands Beitr. Geophys., 52, p. 170 (1938), as cited in Ref. [23] p. 409.

30. V. Griffiths, The Removal of Iodine from the Atmosphere of Sprays, Report No. AHSB(S)R45, UKAEA, London, England (1963).

31. D. R. Grist, Spray Removal of Fission Products in PWR Containments, Report SRD R267, Safety and Reliability Directorate, UKAEA, England (1982).

32. N. A. Fuchs, The Mechanics of Aerosols, Pergamon Press, New York (1964).

33. I. Langmuir, J. Meteor, 5, 175 (1948).

34. T. J. Heames and R. M. Summers, “Fission Product Surface Chemistry Model Preliminary Design Report,” (1995).

35. Pruppacher, H.R. and J.D. Klett, *Microphysics of Clouds and Precipitation*, D. Reidel Publishing Co. Dordrecht, Holland (1980).

36. Gauntt, R.O., et al, “MELCOR Computer Code Reference Manual,” NUREG/CR-6119, Vol. 2, Rev. 1 (May 1998).

37. Murata, K.K. et al, “Code Manual for CONTAIN 2.0,” p. 7-20, NUREG/CR-6533, Dec 1997.

38. L. Soffer et al., “Accident Source Terms for Light Water Nuclear Power Plants,” NUREG-1465 (1995).

39. E. C. Beahm, R.A. Lorenz, and C.F. Weber, “Iodine Evolution and pH Control,” NUREG/CR-5950, TI93-005714 (1992).

40. C. F. Weber, E. C. Beahm, T. S. Kress, “Models of Iodine Behavior in Reactor Containments,” ORNL/TM-12202 (1992).

41. J. N. Butler, *Ionic Equilibrium, a Mathematical Approach*, Addison Wesley (1964).

42. H. Sims et al., “Iodine Code Comparison,” EUR 16507 EN, European Commission, Luxembourg (1995).

43. S. Dickinson and H. E. Sims, “Modifications to the INSPECT Model”, Proc. 4th OECD Workshop on Iodine Chemistry in Reactor Safety, Paul Scherrer Institute, Switzerland (1996).

44. D. A. Powers, R. K. Cole, and T. J. Heames, “A Simplified Model of Iodine Chemistry for MELCOR,” submitted as part of the Preliminary Design Report for Iodine Aqueous Chemistry: Task 1.2 W6203, Sandia National Laboratories, Albuquerque, NM (1998).

45. K. H. Haskell, W. H. Vandevender, and W. L. Walton, “The SLATEC Common Mathematical Subprogram Library: SNLA Implementation,” SAND80-2792, Sandia National Laboratories, Albuquerque, NM (1980).

46. G. V. Buxton et al., *J. Phys. Chem. Ref. Data*, Vol. 17, p. 513 (1988).

47. A. J. Elliott, M. P. Chenier, and D. C. Ouellette, *Canadian J. Chemistry*, Vol. 68, p. 712 (1990).

48. R. A. Barton and H. E. Sims, “A Comparison of the Predictions of the INSPECT Reaction Set with Experimental Data”, Proc. Third CSNI Workshop on Iodine Chemistry, p. 346, JAERI-M-92-012. NEA/CSNI/R(91)15, Japan Atomic Energy Research Institute, Tokai-mura, Naka-gun, Ibaraki-ken, Japan (1992).

49. L. M. Toth, K. D. Pannell, and O. L. Kirkland, “The Aqueous Chemistry of Iodine”, Proc. Fission Product Behavior and Source Term Research, NP-4113-SR, American Nuclear Society, Utah (1984).

50. M. Furrer, R. C. Cripps, and E. Frick, “Iodine Severe Accident Behavior Code IMPAIR 2”, PSI Bericht Nr. 25, Paul Scherrer Institute, CH-5232 Villigen/PSI, Switzerland.

51. A. A. Frost and R. G. Pearson, *Kinetics and Mechanism*, 2nd Edition, John Wiley & Sons (1961).

52. A. C. Vikis and R. MacFarlane, *J. Phys. Chem.*, Vol. 89, p. 812 (1985).

53. N. H. Sagert, “Radiolysis of Iodine in Moist Air: A Computer Study”, Proc. 2nd CSNI Workshop on Iodine Chemistry in Reactor Safety, AECL-9923, CSNI-149, Atomic Energy of Canada Ltd., Toronto, Canada (1989).

54. A. M. Deane, ”Organic Iodine Chemistry Relevant to Nuclear Reactors: A Review”, AERE-R-12359, Harwell, Oxfordshire, UK (1988).

55. J. C. Wren, G. A. Glowa, and J. M. Ball, “Modeling Iodine Behaviour Using LIRIC 3.0,” Proc. Fourth CSNI Workshop on the Iodine Chemistry in Reactor Safety, Wurenlingen, Switzerland, pp.507 – 530 (1996).

56. G. J. Evans et al., “Preliminary Results from the ACE/RTF Tests 1, 2, and 3”, ACE-TR-B3 (1991).

57. C. Hueber, M. Lucas, and J. Gauvain, “Validation of the IODE Code on Analytical Experiments”, in “Third CSNI Workshop on Iodine Chemistry in Reactor Safety”, JAERI-M-92-012 (1991).

58. M. F. Young, and R. O. Gauntt, “Simulation of the ISP41 Iodine Test Problem with the MELCOR Iodine Model”, in ISP-41 Containment Iodine Computer Code Exercise Based on a Radioiodine Test Facility Experiment, NEA/CSNI/R(2000)6/Vol.1 and 2 (1999).

59. L. N. Kmetyk, MELCOR 1.i.1 Assessment: Marviken-V Aerosol Transport Tests ATT-2b/ATT-4, SAND92-2243, Sandia National Laboratories, Albuquerque, NM (January 1993).